AD-A052 351 PRATT AND WHITNEY AIRCRAFT GROUP WEST PALM BEACH FL G--ETC F/G 21/5
DEVELOPMENT OF MAINSHAFT HIGH SPEED CYLINDRICAL ROLLER BEARINGS--ETC(U)
APR 77 P F BROWN, L J DOBEK, F C HSING N00140-76-C-0383
UNCLASSIFIED PWA-FR-8615 NL

1 OF 2
AD A052351

REPORT FR-8615

(6)

DEVELOPMENT OF MAINSHAFT HIGH SPEED CYLINDRICAL ROLLER BEARINGS FOR GAS TURBINE ENGINES

PRATT & WHITNEY AIRCRAFT GROUP
GOVERNMENT PRODUCTS DIVISION OF
UNITED TECHNOLOGIES CORPORATION
WEST PALM BEACH, FLORIDA 33402

(14) PWA-FR-8615

(11) APR[redacted]77

(12) 115 P.

(9) INTERIM REPORT, FOR PERIOD 1 OCT[redacted]975 — 1 APR[redacted]77

APPROVED FOR PUBLIC RELEASE: DISTRIBUTION UNLIMITED

(15) N00140-76-C-0383

(16) F41401

NAVAL AIR PROPULSION CENTER
1440 PARKWAY AVENUE
TRENTON, NEW JERSEY 08628

AND

AIR FORCE AERO PROPULSION LABORATORY
WRIGHT-PATTERSON AFB, OHIO 45433

(10) P. F. /Brown,
L. J. /Dobek,
F. C. /Hsing
J. R. /Miner

392 887 i JOB

UNCLASSIFIED

SECURITY CLASSIFICATION OF THIS PAGE *(When Data Entered)*

REPORT DOCUMENTATION PAGE

READ INSTRUCTIONS BEFORE COMPLETING FORM

1. REPORT NUMBER: FR-8615
2. GOVT ACCESSION NO.:
3. RECIPIENT'S CATALOG NUMBER:

4. TITLE *(and Subtitle)*: Mainshaft High Speed Cylindrical Roller Bearings for Gas Turbine Engines

5. TYPE OF REPORT & PERIOD COVERED: Technical Report (Interim) 1 October 1975 — 1 April 1977

6. PERFORMING ORG. REPORT NUMBER:

7. AUTHOR(s): P. F. Brown, L. J. Dobek, F. C. Hsing, J. R. Miner

8. CONTRACT OR GRANT NUMBER(s): N00140-76-C-0383 AF MIPR FY14557600623

9. PERFORMING ORGANIZATION NAME AND ADDRESS: United Technologies Corporation, Pratt & Whitney Aircraft Group, Government Products Division, West Palm Beach, Florida 33402

10. PROGRAM ELEMENT, PROJECT, TASK AREA & WORK UNIT NUMBERS: 62241N, WF41-401

11. CONTROLLING OFFICE NAME AND ADDRESS: Naval Air Propulsion Center, 1440 Parkway Avenue, Trenton, New Jersey 08628

12. REPORT DATE: April 1977

13. NUMBER OF PAGES: 110

14. MONITORING AGENCY NAME & ADDRESS *(if different from Controlling Office)*: AF

15. SECURITY CLASS. *(of this report)*: Unclassified

15a. DECLASSIFICATION/DOWNGRADING SCHEDULE:

16. DISTRIBUTION STATEMENT *(of this Report)*

Approved for public release: distribution unlimited

17. DISTRIBUTION STATEMENT *(of the abstract entered in Block 20, if different from Report)*

18. SUPPLEMENTARY NOTES

19. KEY WORDS *(Continue on reverse side if necessary and identify by block number)*

- Cylindrical Roller Bearing
- Dynamics
- Gas Turbine Mainshaft Roller Bearing
- High Speed Roller Bearing
- Roller Bearing Design and Simulating System
- Roller End Wear

20. ABSTRACT *(Continue on reverse side if necessary and identify by block number)*

This combined analytical and experimental program is aimed at generating a manual that will permit the design of 3.0 MDN cylindrical roller bearings. The roller bearing analysis will be correlated with the results from a series of bearing tests designed to determine, by statistical methods, the effect of geometrical variables on bearing performance. An existing quasi-static design optimization system has been upgraded and the basic analyses for use in developing a program to predict the dynamic behavior of roller bearing components are nearly complete. A

DD FORM 1 JAN 73 1473 EDITION OF 1 NOV 65 IS OBSOLETE

S/N 0102-LF-014-6601

UNCLASSIFIED

SECURITY CLASSIFICATION OF THIS PAGE *(When Data Entered)*

study identified a total of thirty separate bearing parameters that can influence roller skewing and skidding. Two groups of 124 mm roller bearing designs were then prepared using statistical design techniques and incorporating parameters from the list of thirty. Fabrication of full-scale bearing hardware was completed and testing was initiated on the first group of bearings.

FOREWORD

This report describes the work performed by the Pratt & Whitney Group, Government Products Division of United Technologies Corporation, West Palm Beach, Florida 33402 under U.S. Navy Contract N00140-76-C-0383 which incorporated U.S. Air Force MIPR No. FY14557600623. This is an interim report covering work conducted from 1 October 1975 to 1 April 1977.

The Government technical manager for this period was Raymond Valori of the Naval Air Propulsion Center (telephone 609-882-1414). Ronald Dayton of the Air Force Aero Propulsion Laboratory WPAFB (telephone 513-225-4939) provided the technical direction for the Air Force portion of the program.

The project was conducted at Pratt & Whitney Aircraft under the direction of John Miner, Component Technology Manager; Paul Brown, Principal Investigator; Louis Dobek, Program Manager; and Dr. Fred Hsing, Analytical Program Manager.

Appreciation is extended to the following Pratt & Whitney Aircraft personnel for their assistance on this program. Michael Carrano, Ronald Edelstein, Robert McFadden and Roger Barnsby assisted with the analytical effort. Computer programing assistance was provided by Walter Grube and James Mann. The experimental bearing testing was conducted by Edward Tobiasz who was assisted by Robert Cohen. Engine application advisory support was provided by Eugene Beverly.

Acknowledgment is also accorded both the bearing manufacturing company that provided the experimental hardware for this program, the Split Ball Bearing Division of MPB Corporation, and the consultant that provided assistance with the analytical modeling effort, Battelle Columbus Laboratories.

CONTENTS

CONTENTS (Continued)

CONTENTS (Continued)

ILLUSTRATIONS

ILLUSTRATIONS (Continued)

TABLES

SECTION I
SUMMARY

This combined analytical and experimental program is aimed at generating a manual that will permit the design of cylindrical roller bearings capable of operating reliably at 3.0 MDN speed levels. An existing quasi-static analysis will be updated in this effort and a new dynamic analysis developed and correlated with the results of extensive, statistically designed tests that are being conducted on a series of aircraft-engine-size roller bearings. The quasi-static design optimization system has been upgraded to include certain advanced treatments of fits, tolerances, clearances, misalignments, preload, moment load, structural flexibility, skew angle determination and ring flexibility. This makes the program the most advanced and powerful roller bearing design tool available to date.

The basic analyses for use in developing a program to predict the dynamic behavior of roller bearing components are essentially complete. Governing differential and algebraic equations for the interacting components and the coupled system have been formulated. The preliminary computer program has been developed and refinement of the system is underway. The finalized computer program is to be available at the conclusion of this contract.

The experimental portion of this program is aimed at evaluating the influence of geometric, tolerance, design, and operational parameters on the skidding and skewing wear characteristics of 124 mm roller bearings operating at speeds of 1.0 to 3.0 MDN. A study was completed in which a total of 30 separate bearing parameters that can influence roller skew and skid were identified. Two groups of bearing designs, labeled N and AF, were then prepared using statistical design techniques and incorporating those parameters from the list of 30 that could be varied in a sensible manner. The Group-N bearings consist of eight separate designs which will permit the quantification of the influence of seven individual bearing parameters on roller skid and skew. The Group-AF bearings consist of five bearing designs which will allow four additional parameters to be studied. A total of ten Group-N bearings were manufactured for test. One bearing for each of the eight parametric designs and two duplicates for repeat testing were procured. One each of the five Group-AF designs were produced with a duplicate of one of these designs manufactured for repeat testing. Experimental rig testing has been completed on four of the ten Group-N bearings. Three of these bearings performed in a stable manner over the entire range of conditions run in the test program. The fourth bearing failed in the course of the testing due to excessive roller wear. A wide range of wear and performance was observed during the testing of these first four bearings.

SECTION II
INTRODUCTION

A. BACKGROUND

The higher thrust-to-weight ratios required for advanced aircraft turbine engine designs demand increased rotational speeds of the turbines and compressors. The design and development of such turbomachinery is often complicated by bearing considerations. The rotor and rotor support systems are generally characterized by (1) high shaft speeds to achieve maximum gas dynamic performance, minimum size, and minimum weight; (2) flexible bearing support structures for lightweight and minimum disruption of the flowpath by interdiction of struts and vanes; and (3) large shaft diameters for high bending and torsional stiffness. These factors result in bearing specifications which require high bearing DN levels and high misalignment capability. It is anticipated that bearing DN levels to 3.0 MDN will be required for engines in the 1980-1990 time frame.

Considerable effort has been expended by various investigators on upgrading the performance of high DN ball thrust bearings. Such concentrated effort has amassed a cumulative experience level of many tens of thousands of hours in operation time at 3.0 MDN under laboratory conditions. Ball thrust-bearing technology has evolved to where material considerations determine the life limits of the design. On the other hand, the technology base needed for the design of optimum roller bearings to meet high DN requirements is not well defined. Roller bearing performance, in many cases, has been the limiting factor in the design of high speed rotor systems because of a lack of understanding in certain aspects of roller bearing behavior. There is good reason for this. The increased susceptibility of roller bearings to failure has surfaced in relatively recent times. Ever increasing engine rotational speeds have driven bearing speeds up to DN levels which serve to intensify the influence of geometric variations and certain other parameters on roller dynamics. Evidence accumulated in the field and data obtained in development tests, has indicated that bearing performance is very sensitive to roller instabilities as induced by unknown or little understood principles of roller dynamic behavior.

These instabilities occur frequently in high DN bearings resulting in roller skewing. The characteristic failure mode which identifies roller skew is rapid eccentric wear on the end surfaces of some or all of the rolling elements of a bearing. Figure 1 shows the eccentric type wear pattern on one end of a roller, with the other end having a similar pattern but 180 degrees out of phase. This condition can exist undetected until bearing failure occurs. Figure 2 shows a typical example of bearing failure precipitated by eccentric end wear of one roller element.

Related to skewing, and apparently influenced by many of the same forces which induce it, is roller skidding. When rollers skid the resulting damage is paticularly severe on the rolling contact surfaces and, subsequently, has an adverse effect on bearing durability. Currently, skidding is considered to be of secondary importance, compared to roller end wear. This conclusion is based upon considerable field service experience. Data indicates that roller end wear failures predominate. The mechanisms that cause skidding are more readily understood, and inherent to this understanding is the suggestion for its control. It is well known that roller skidding occurs when bearing radial loads are light and rotational speeds are high. A concept commonly used to supplement the external load is a two-point radial preload design. This basic preload system, which is achieved by machining the outer ring OD in an out-of-round oval shape combined with a slight interference fit in the bearing housing, adds enough load to keep the rollers "in gear" around most of the bearing's circumference. However, as speeds increase, the ability to maintain control of the internal clearance needed to ensure operation free of skidding damage becomes increasingly dependent upon accurate knowledge of the internal heat generation of the bearing. This factor, coupled with the accompanying cooling system design, determines the operating temperature level of the bearing and, more importantly, the temperature gradient from

the inner to the outer raceways. Thus, an accurate knowledge of the heat generation level is a necessity if adequate control of operating clearance is to be achieved so that roller loading is maintained to a level that successfully inhibits roller skidding.

Of course, there are other modes of engine roller bearing failure beside those attributable to end wear and skidding damage. Some of these modes are identifiable with the cage and others may be due to roller edge loading causing premature fatigue spalling. However, it appears highly likely that if the basic roller end wear problem — as influenced by skewing action — can be avoided, a large measure of the solution to other root problems can be effected. This becomes largely self-evident upon study of the long list of geometric, dimensional, tolerance, quality, and operational parameters which influence and control roller tracking forces. A design system which provides identification and regulation of these factors will provide a means for establishing the entire bearing design. For these reasons, this system must go beyond a quasi-static analysis and must address roller bearing dynamic behavior.

Figure 1. Eccentric Roller End Wear

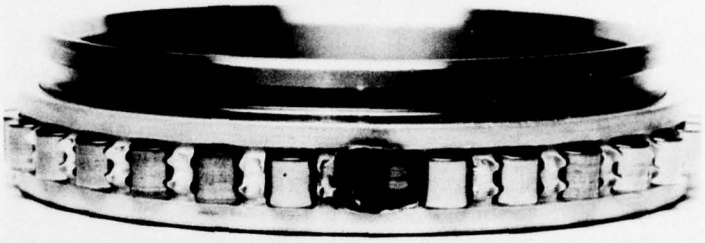

Figure 2. Typical Bearing Failure Attributable to Eccentric Roller End Wear

B. PROGRAM APPROACH

As indicated in the "Background" section, future engine design requirements dictate roller bearing DN levels to 3M. Therefore, roller bearing technology to achieve this DN level must be upgraded in time for utilization in engines slated for operation in the 1980-1990 time frame. The schedule to develop bearings to meet the 3 MDN requirement calls for an extension of the present state-of-the-art of bearing design and requires considerable analytical and experimental effort to investigate the effects of increased DN levels on many critical design parameters. In addition to the conventional parametric studies involving fatigue life, stresses, temperature, fits, clearances, alignment, lubrication and rotor dynamic response, special attention must be given to roller skidding and skewing motion which have been identified as likely problem areas for high DN operation. Proper analysis of these effects requires development of a new computer program which considers the complete dynamic motion of each element in the roller assembly.

Effort under this program is being directed toward the formulation of a viable generalized roller bearing analytical design system considering a number of geometrical and operational parameters. This development program is based on an integrated analytical/experimental effort. The resultant design system, in the form of a complete computer program, is intended to provide the bearing design engineer with a useful tool for studying the static as well as dynamic characteristics of high DN roller bearings for future aircraft engine mainshaft applications. The design system will be useful in conducting analytical experiments under simulated operating conditions. A parametric study utilizing a reliable analytical design system could establish basic design criteria, help to separate the important variables from the unimportant ones, predict the effect of each controllable design factor, and thus could substantially reduce the number of costly test programs in the early phase of new bearing development. It could also be used to assist in the diagnosis of roller bearing failures in service engines.

C. PROGRAM SCOPE

The work being performed under this contract includes both analytical and experimental activity. Under Task I, a computer program which describes the roller bearing dynamics, loads, stresses, deflections, deformations, thermal conditions, heat generation, lubrication, and operating parameters will be developed. In Task II, experimental rig tests will be conducted on a group of 124 mm bore roller bearings to define the influence of geometric and operating

variables and to verify the accuracy of the computer program. The computer program will be refined as necessary to reflect the test results. Also, certain additional results, when available from other planned experimental testing which will address a separate group of roller bearing variables, will be used to further refine the model. In Task III, the information developed under Tasks I and II will be used to design and fabricate a prototype bearing and conduct a demonstrator rig test having a goal of 60 hours operation over a range of DN values from 2.2 to 3.0 million. In Task IV, the results of Tasks I through III will be incorporated into a design manual for high-speed cylindrical roller bearings. The manual will include the computer program developed in Task I and modified during subsequent tasks. These tasks also include parametric testing on an additional group of roller bearings containing different bearing variables than those studied in Task II. The test results from this added testing will be used to further refine the analytical model developed under Task I. The work also includes installation of the computer program at the Wright-Patterson Air Force Base computer facility.

SECTION III
CONCLUSIONS AND RECOMMENDATIONS

A. CONCLUSIONS

The analytical modeling development effort has progressed smoothly thus far with no major difficulties encountered. Based on this work the following conclusions can be drawn:

- The roller bearing quasi-static optimization program, called STATIC, updated under the subject contract, is now capable of identifying the corresponding roller geometry, bearing internal clearance, outer ring out-of-round, assembly fits and lubricant flow rate, all as required to achieve maximum life. However, it is necessary with this program for the user to define certain design criteria and to use his own subprograms for generating certain structural and thermal data.

- The "modular" concept adopted in the development of the overall computer program, TRIBO I, has already proven to be a beneficial feature. Portions of the program can be run independently, which permits preliminary design of any or all of the bearing components. This feature also makes it a much simpler matter to alter the program as new techniques or data become available. Updating can thus be accomplished by changing only that module affected, thus eliminating the need to restudy the whole program in its entire length and complexity.

- The elastohydrodynamic (EHD) film thickness model chosen for use in TRIBO I is that presented by Loewenthal, Parker and Zaretsky[1] which provides the best correlation with available test data.

- The EHD traction models available from the literature were found inadequate for the needs of the high speed roller bearing program. Even the best of these gave poor agreement with existing pertinent data. The greatest need is for experimental data in the following operating regimes: high slip velocity, high temperature, high speed and moderate contact pressures.

Conclusions that can be drawn based on experience accumulated in the experimental portion of this program are as follows:

- Results obtained on repeat bearings have served to demonstrate an adequate level of repeatability for this statistically designed program.

- Although reduction of the bearing wear data by means of established statistical techniques has not yet been accomplished because testing of the Group-N bearings is not complete, it is apparent that the wide range of roller end wear levels experienced thus far will permit satisfactory application of these techniques.

- Variations in applied radial loading do not have a significant impact on bearing heat generation, based on experimental measurements.

- Increasing oil flow to the bearings tested increases basic heat generation.

- Power loss characteristics and thermal behavior of all the bearings tested thus far are very similar.

- Extreme amounts of roller slippage do not result in unusual thermal behavior of the bearing nor do they produce obvious skid damage or distress even though heavy roller end wear may occur.

B. RECOMMENDATIONS

Based upon the above conclusions the contractor makes the following recommendations:

- The statistically designed experimental program should be continued as planned. This recommendation is made on the basis of demonstrated ability of the test procedure to produce repeatable results and the discerning nature of the wear results as evidenced by the wide range experienced in tests conducted thus far.

- The roller bearing dynamics analytical model should be completed to the level planned and the results correlated with program experimental data for inclusion in the design manual which is intended to be published at the culmination of this effort.

- Some form of simplified structural and thermal modular analyses should be developed separately and incorporated into the master program as an option for the user who may not have access to any such analyses. They also would prove useful in the preliminary design process to supplement the more time-consuming sophisticated programs source users have at their disposal and which should perhaps be restricted to use in only the final design stage.

- It is advisable that separate manuals be prepared, containing design and user oriented instructions, that would allow each of the subprograms such as STATIC, SKEW, CADYN, and RODYN to be operated as individual computer analyses. Use of such programs could enhance the preliminary design process, allowing certain parametric studies to be conducted, without the encumbrance of the time-consuming main program which should be limited to use in the final design stage only.

- Additional EHD traction data should be obtained in appropriate test machines over a range of speeds, slip velocities, temperatures and contact pressures that correspond to those encountered in 3.0 MDN roller bearings. Once these data become available, an effort should be launched to develop a fully correlated analytical EHD traction model.

SECTION IV
ROLLER BEARING DESIGN TECHNOLOGY

A. GENERAL DESIGN CONSIDERATIONS

Bearing performance is influenced by the combined effects of fits, thermals, and operating conditions, as well as the structural design of the system. Ideally, the bearing internal geometry should be designed to achieve the maximum possible fatigue life under these conditions without violating any theoretical or experience-based design criteria. The oil flow level chosen for lubricating and cooling of the bearing should be such that the temperature of the bearing rings will never cause a complete loss of bearing clearance or result in a temperature level that exceeds the capability of either the ring material or the oil itself. Initial fits must also be set so that they never reduce the bearing clearances to zero, yet remain tight at speed and temperature. Since the determintion of factors such as the optimum oil flow, bearing fits, raceway out-of-roundness (OOR), and fatigue life is a laborious task involving many iterations within each and among all of the bearing performance analyses, the optimization process has usually not been fully implemented. With the development of the program described in this report, full optimization of any or all of these parameters can be more readily accomplished from a quasi-static point of view.

B. STATE-OF-THE-ART OF ROLLER-BEARING DESIGN TECHNOLOGY

The current state-of-the-art of roller bearing design technology relies primarily on various established static and quasi-static analyses. The analytical prediction system usually consists of several major analyses as shown in figure 3. A brief description of these analyses is given in this section. Throughout the text, the term "existing" is used to describe any development accomplished prior to the inception of the subject program, that is, September 1975, while the term "new" is used to identify work accomplished as a result of the new program effort as described in this report.

1. Basic Elasticity Considerations

It is a commonly accepted practice in the bearing industry to determine the fatigue life of rolling element bearings on the basis of the Lundberg-Palmgren life model[2, 3] and Weibull's statistical theory of the strength of materials[4, 5]. These theories stipulate that the fatigue life of rolling element bearings depends upon the magnitude of the stressed volume as well as upon the level and depth of the maximum shear stress. This therefore requires an accurate determination of both the load distribution among the rollers and the stress/deformation at the contact surfaces at each roller location. The basic methods used to determine the load distribution are given in this section. Also described in this section is the method used to account for the effect of interference fits on the overall bearing internal clearance.

a. Roller Load Distribution, Misalignment and Moment Load

The classical theory and procedures used to determine the basic roller load distribution are well established. The calculations are usually involved in several rather complicated iterative processes such as those reported in the literature[2, 3, 4]. The basic idea is, nonetheless, to perform an equilibrium analysis to identify the forces and corresponding deformations of the system.

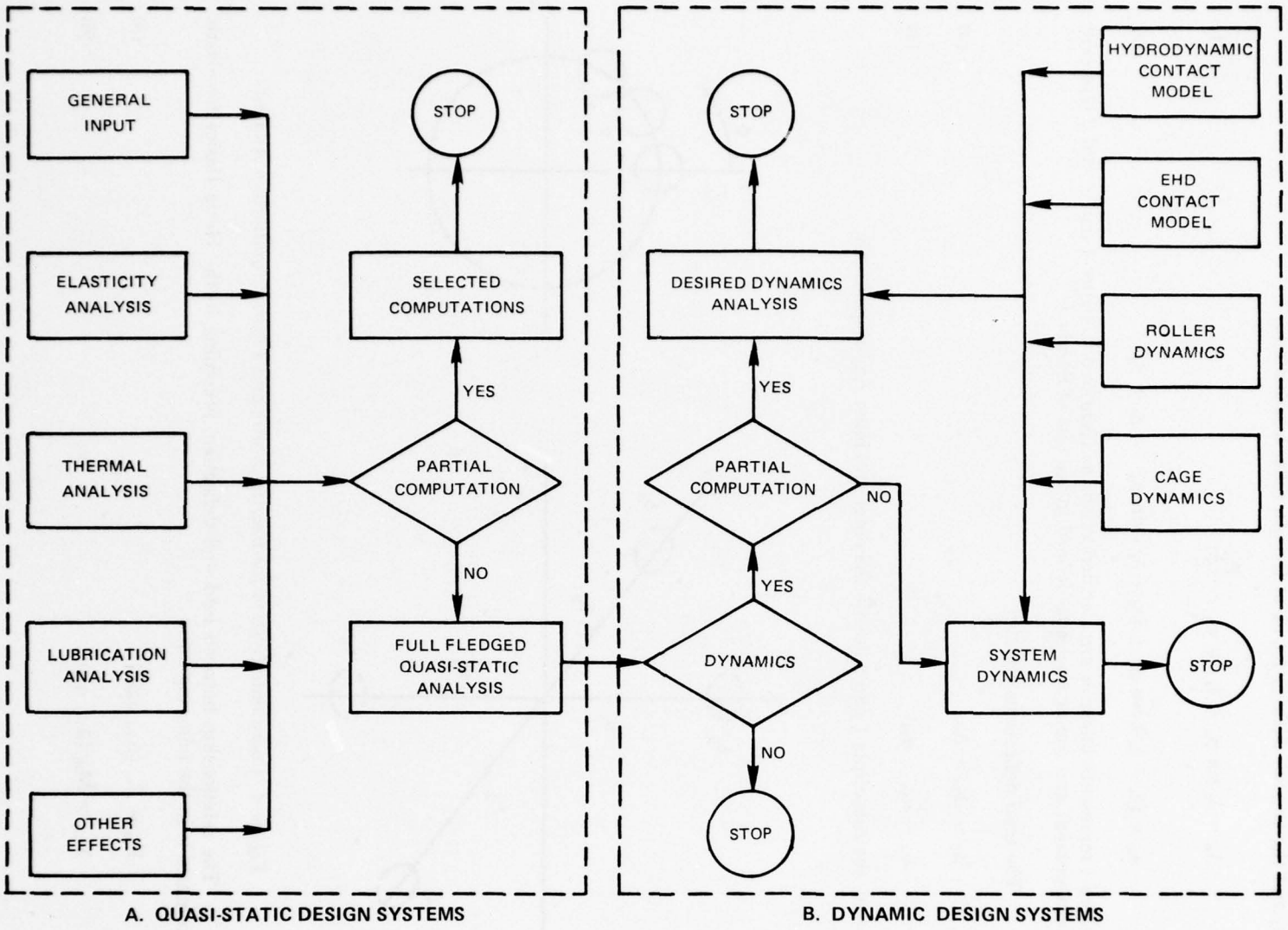

Figure 3. Roller Bearing Analytical Design and Simulation System

In the case of rigid rings with no out-of-roundness, for example, the total linear deflections, Δ_q and the angular deflections, α_q at the qth roller location are:

$$\Delta_q = \delta_2 \sin \phi_q + \delta_3 \cos \phi_q - \frac{P_D}{2} \tag{1}$$

$$\alpha_q = (\delta_4 + \delta_4'') \cos \phi_q + (\delta_5 + \delta_5'') \sin \phi_q + \beta_1 + \beta_2 \tag{2}$$

where δ represents linear or angular deflections as identified in figure 4 and δ'' and β represent misalignment and coning angles as defined in the List of Symbols.

The total deflections are also

$$\Delta_q = \Delta_{1q} + \Delta_{2q} \tag{3}$$

$$\alpha_q = \alpha_{1q} + \alpha_{2q} \tag{4}$$

where the subscripts 1 and 2 denote the outer and inner ring respectively.

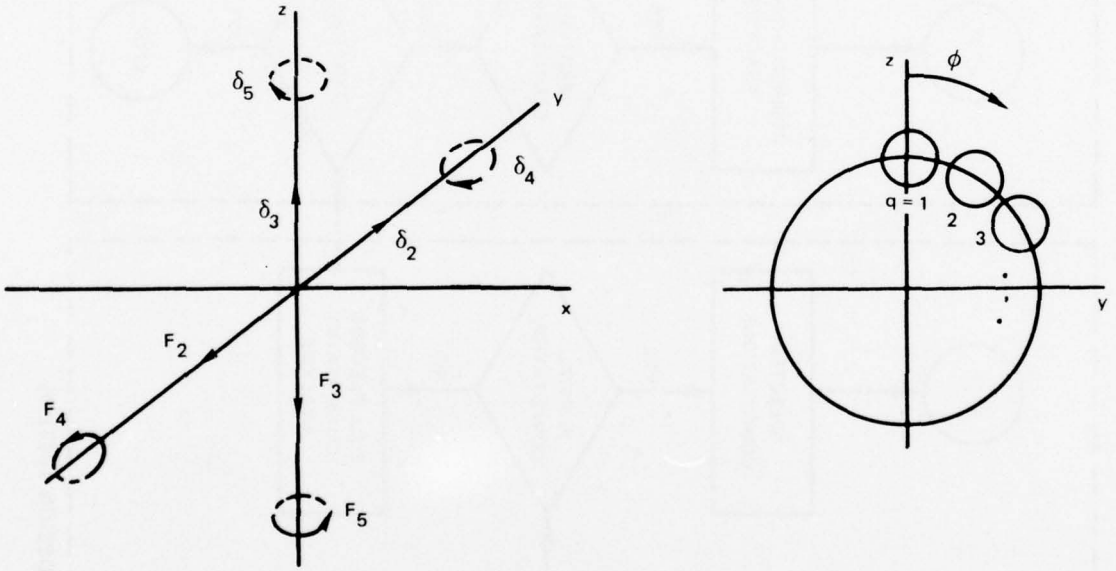

Figure 4. Coordinate System for Bearing Static and Elastic Equilibrium Analysis

The relationship between load and deflection, according to the Hertz theory for elastic contacts is in the following form:

$$P_{1q} = P_{1q} (\Delta_{1q}, \alpha_{1q}) \tag{5}$$

$$M_{1q} = M_{1q} (\Delta_{1q}, \alpha_{1q}) \tag{6}$$

Static equilibrium of the rollers requires that:

$$\sum_{i=1}^{2} P_{iq} + F_c = 0 \tag{7}$$

$$\sum_{i=1}^{2} M_{iq} = 0 \tag{8}$$

Furthermore, equilibrium of the entire bearing, i.e., rollers plus races, requires:

$$\sum_{q=1}^{n} P_{iq} \sin \phi_q + F_{1E} = 0 \tag{9}$$

$$\sum_{q=1}^{n} P_{iq} \cos \phi_q + F_{2E} = 0 \tag{10}$$

$$\sum_{q=1}^{n} M_{iq} \cos \phi_q + M_{1E} = 0 \tag{11}$$

$$\sum_{q=1}^{n} M_{iq} \sin \phi_q + M_{2E} = 0 \tag{12}$$

Determination of roller and race load distribution then requires simultaneous solution of Equations (1) through (12).

To account for the effects of roller crowning, misalignment, and moment loading and also to relate the deflections to the restoring moment, each roller element is divided into 18 laminae in the computation of deformation and stress field at the contact zone. The Hertzian contact theory is then applied to each individual lamina for computation of stress, deformation, moment, and load distribution. The results are then combined to characterize the elastic properties of a given roller.

b. Interference Fits

When the temperature field in the bearing has been determined, the relation of interface pressure to the interference fit is a function only of the geometry and material properties of the two contacting components. Exact determination of the contact pressure field may require the use of a quite sophisticated analysis such as the finite element method. However, it is very often found that the use of the load-deformation relationship for thickwall cylinders, as shown in Equation (13), is sufficient. This is the relation used in the existing roller bearing analysis:

$$P = \frac{\Delta/b}{\frac{1}{E_1}\left[\frac{(b/a)^2 + 1}{(b/a)^2 - 1} - \nu_1\right] + \frac{1}{E_2}\left[\frac{(c/b)^2 + 1}{(c/b)^2 - 1} + \nu_2\right]} \tag{13}$$

where

Δ = diametral interference between the two rings (in.)
a = smaller ring ID (in.)
b = smaller ring OD (in.)
c = larger ring OD (in.)
E = Young's Modulus (psi)
ν = Poisson's Ratio

In some engine bearing installations, a liner is used between the bearing ring and the housing structure. In such instances the interactive deformations of all three elements must be taken into account. This necessitates employment of iterative techniques to determine the fits between the contacting components.

2. Pseudodynamic Treatment

a. *Centrifugal Effect*

The effect of the centrifugal force of the rotating elements is considered throughout the static analysis as a static external force. The first section in which it appears is in the equilibrium calculation of the roller load distribution as described in Section IV.B.1.a. Thus, the force on the outer roller contact area must balance the sum of the forces acting at the inner contact combined with the individual roller centrifugal load.

The second area where the centrifugal effect of the rotating rollers and bearing inner ring is taken into account is for the determination of bearing operating fit and internal radial clearance. The related growth of the OD of the rotating bearing inner ring is estimated on the basis of the following equation[6].

$$\Delta D_{o/i} = \frac{\rho D_{o/i}^3 \, w}{16 E_2 g}\left[\left(\frac{D_{i/i}}{D_{o/i}}\right)^2 (3+\nu) + (1-\nu)\right] \tag{14}$$

The expansion of the ID of the outer ring due to the roller centrifugal loading is given by:

$$\Delta D_{i/o} = \frac{P D_{i/o}}{E_1}(\eta + \nu) \tag{15}$$

$$P = (4.5169 \times 10^{-6})\frac{w d_e N_e^2}{D_{i/o} L} \tag{16}$$

$$N_e = \frac{1}{2}\left[N_i\left(1 - \frac{d_o}{d_e}\right) + N_o\left(1 + \frac{d_o}{d_e}\right)\right] \tag{17}$$

$$w = 0.222268\, d_o^2\left[1 - \left(\frac{d_i}{d_o}\right)^2\right] n \ell_e \tag{18}$$

$$\eta = \frac{1 + \left(\frac{D_{i/o}}{D_{o/o}}\right)^2}{1 - \left(\frac{D_{i/o}}{D_{o/o}}\right)^2} \tag{19}$$

The change in bearing clearance due to speed is then composed of two terms as discussed above.

b. Skewing Moment

Within the static analysis, an approximation is made as to the magnitude of the individual roller skewing moment. The skewing moment S_{ij} is estimated to be:

$$S_{ij} = \mu_s M_{ij} \tag{20}$$

where

μ_s = coefficient of friction
M_{ij} = contact moment for jth roller at the ith surface

3. Thermal Analysis

The purposes of rendering a thermal analysis are to determine the bearing heat generation and associated operating temperatures, as well as temperature gradients from the inner ring to the outer ring of the bearing. Ideally, the temperatures to be determined are those of the inner ring and the hub or shaft upon which it is mounted, the outer ring and its support housing, the roller/cage assembly and the exit oil. These are all influenced by shaft speed, load, thermal environment of the bearing compartment, oil type, oil-in temperature, oil flowrate, bearing geometry, the method of cooling and the method of lubricating oil introduction. A determination of the bearing heat generation is necessary to the establishment of the engine design oil flow and for the purpose of sizing engine oil-system and heat exchanger requirements. Identifying the temperature levels in the bearing system is important to the design process for the purpose of determining the internal radial clearance of the bearing at operating conditions which influence bearing life which, in turn, impacts engine durability.

An analytical design system that would permit complete thermal analysis of the bearing system is inherently complicated. Detailed identification of heat sources, sinks and flowpaths is required and techniques such as finite difference, relaxation, or finite element methods must be employed. This approach has not been used for bearing systems because of this inherent complication. What has been developed is a system that is almost completely empirical and, as such, is applicable only to the specific size bearing of concern. The bearing is subjected to a combined rig and experimental engine test program and the resulting data used to establish a design system. This system is then utilized to optimize that specific design for the production version of that engine. Thus, no analytically based system currently exists that can be extrapolated to generate reliable design data for an application that is outside the immediate range of current experience. In other words the present system relies on experimental data as the source for design temperatures to optimize bearing fits and control internal radial clearance to an acceptable level. Thus, there is no analytically based thermal model relationship currently in use that could be construed as a reliable design system for applications that are outside the immediate range of current experience.

It should be noted here, however, that it is the intent of the new work being done under the subject contract to develop a heat generation and temperature prediction model that will be empirically based, employing the experimental data being generated in the test portion of the program. Generation of a comprehensive analytically based thermal model is considered beyond the scope of the present effort.

4. Support and Ring Flexibility

Along with the inclusion of ring flexibility in the analysis, a modification has been made to the equations for deflection at the roller inner and outer contacts, Equations (1) and (2). The new equations are:

$$\Delta_q = \delta_2 \sin \phi_q + \delta_3 \cos \phi_q - P_D/2 - \Delta_{q\ flex} \tag{21}$$

$$\alpha_q = (\delta_4 + \delta_4'') \cos \phi_q + (\delta_5 + \delta_5'') \sin \phi_q + \beta_1 + \beta_2 - \alpha_{q\ flex} \tag{22}$$

where

$$\Delta_{q\ flex} = \Delta_{1q\ flex} + \Delta_{2q\ flex} \tag{23}$$

$$= \sum_{j=1}^{n} [A_{qj} P_{1j} + B_{qj} M_{1j}] + \sum_{j=1}^{n} [A'_{qj} P_{2j} + B'_{qj} M_{2j}]$$

$$\alpha_{q\ flex} = \alpha_{1q\ flex} + \alpha_{2q\ flex} \tag{24}$$

$$= \sum [C_{qj} P_{1q} + D_{qj} M_{1j}] + \sum [C'_{qj} P_{2j} + D'_{qj} M_{2j}]$$

and

$$A_{qj},\ B_{qj},\ C_{qj},\ D_{qj},\quad A'_{qj},\quad B'_{qj},\quad C'_{qj},\quad D'_{qj}$$

are matrices representing the pertinent influence coefficients as shown in table 1. These influence coefficients define the magnitude of deflection at the qth roller location. Each matrix is of order n and is obtained through an elasticity analysis.

5. Preload/Outer Ring Out-of-Roundness

The purpose of using an outer ring with 2-point or 3-point out-of-roundness (OOR) is to minimize roller skidding. The additional load imposed on the bearing by the out-of-round condition is known as preload. The outer ring OOR is being optimized so that the preload requirements are met for each operating condition. In this portion of the computation, the preload/OOR is established on the basis of the equation for a cylinder pressed between two flat plates[4]. The equations used are:

$$L_p = \frac{P_{D\ min} - \dfrac{F_c}{K_1}}{\left[\dfrac{1}{K_{1s}} + \dfrac{1}{K_{2s}} + \dfrac{1}{K_2} + \dfrac{1}{K_1}\right]} \tag{25}$$

$$P_{D\ min} = P_D - \left[\frac{OOR}{2} + k\bar{f}\right]\left[1 - \frac{K_{1R}}{K_{1R} + K_H}\right] \tag{26}$$

$$OOR = OROD_{max} - OROD_{min} \tag{27}$$

$$K_{1s} = K_{1R} + K_H \tag{28}$$

$$K_{2s} = K_{2R} + K_s \tag{29}$$

$$K_{iR} = c\, E_{iR}\, W_i \left[\frac{OD_{iR} - ID_{iR\ Eq}}{OD_{iR} + ID_{iR\ Eq}} \right] \tag{30}$$

where

c = 4.4809 two-point OOR
= 21.0 three-point OOR
k = 0 tight OR fit
= 1 loose OR fit
i = 1 outer ring
= 2 inner ring

$$\frac{1}{K_i} = \frac{4(1-\nu_i^2)}{\pi E L} \left[\frac{1}{3} + \ln \frac{2D}{2.15} \sqrt{\frac{E}{L_p + F_c}} \right] \tag{31}$$

E = average Young's modulus of roller and ith ring

and $F_c = 0$ for inner ring.

TABLE 1. FORM OF INFLUENCE COEFFICIENT MATRICES A, B, C, D

	due to load (lb)	due to moment (lb)
deflection (in.)	A (n × n)	B (n × n)
slope (in./in.)	C (n × n)	D (n × n)

Example:

$$[A] = \begin{bmatrix} A_{11} & A_{12} & \cdots & A_{1n} \\ A_{21} & A_{22} & \cdots & \\ \vdots & \vdots & & \\ A_{n1} & & & A_{nn} \end{bmatrix} = \begin{bmatrix} \frac{\delta_1}{P_1} & \frac{\delta_1}{P_2} & \cdots & \frac{\delta_1}{P_n} \\ \frac{\delta_2}{P_1} & \frac{\delta_2}{P_2} & \cdots & \\ \vdots & \vdots & & \\ \frac{\delta_n}{P_1} & & & \frac{\delta_n}{P_n} \end{bmatrix}$$

or $(A_{qi}) = \left(\frac{\delta_q}{P_i} \right)$

Note that Equation (31) is for rollers with L/D ratio equal to 1 only. It should be emphasized here again that the analysis being discussed in this section represents the state-of-the-art as of 1975 and does not reflect improvements made since that time as a result of the new program effort. This work and the related results accomplished thus far will be discussed later in this report.

6. Roller/Flange Contact Point and Roller Skew Angle Determination

The magnitude of the skew angle through which a given roller can turn and the location of the contact point between the end of the roller and the guide flange surface is dictated primarily by such factors as axial end clearance, internal radial clearance of the bearing, and the flange layback angle. A properly designed roller is one for which this contact point is located away from the corners of the flange guiding surface so as to prevent the roller end from wearing due to excessive stress concentration.

The magnitude of the maximum skew angle and the location of the roller/flange contact point are dependent upon a number of parameters. The parameters considered in the existing analysis are as follows:

- End clearance between roller and guide flange, C_a
- Roller length, L
- Roller diameter, d
- Roller crown drop, ϵ
- Roller corner radius, r_c
- Guide flange layback angle, β
- Guide flange height, H

It is assumed that curvature of the inner ring is negligible, and contact occurs at point R on the roller and point F on the flange. This contact point does not necessarily occur in the x-y plane shown in figure 5a but can occur at some distance z_R from that plane, as seen in figure 5b.

Assuming that contact between the roller and the guide flange occurs at point R on the roller which lies somewhere on the endface circle defined by the intersection of the corner radius and the roller endface, then the y coordinate of R, shown in figure 5a is given by:

$$y_R = \frac{L}{2} \cos\theta + (s^2 - z_R^2)^{1/2} \sin\theta \tag{32}$$

where

$$s = \frac{d}{2} - \epsilon - r_c$$

On the other hand, the location of a point F on the flange guiding surface, shown in figure 5b, is

$$y_F = \left(\frac{d}{2} + z_F \right) \tan\beta + \frac{L}{2} + Ca \tag{33}$$

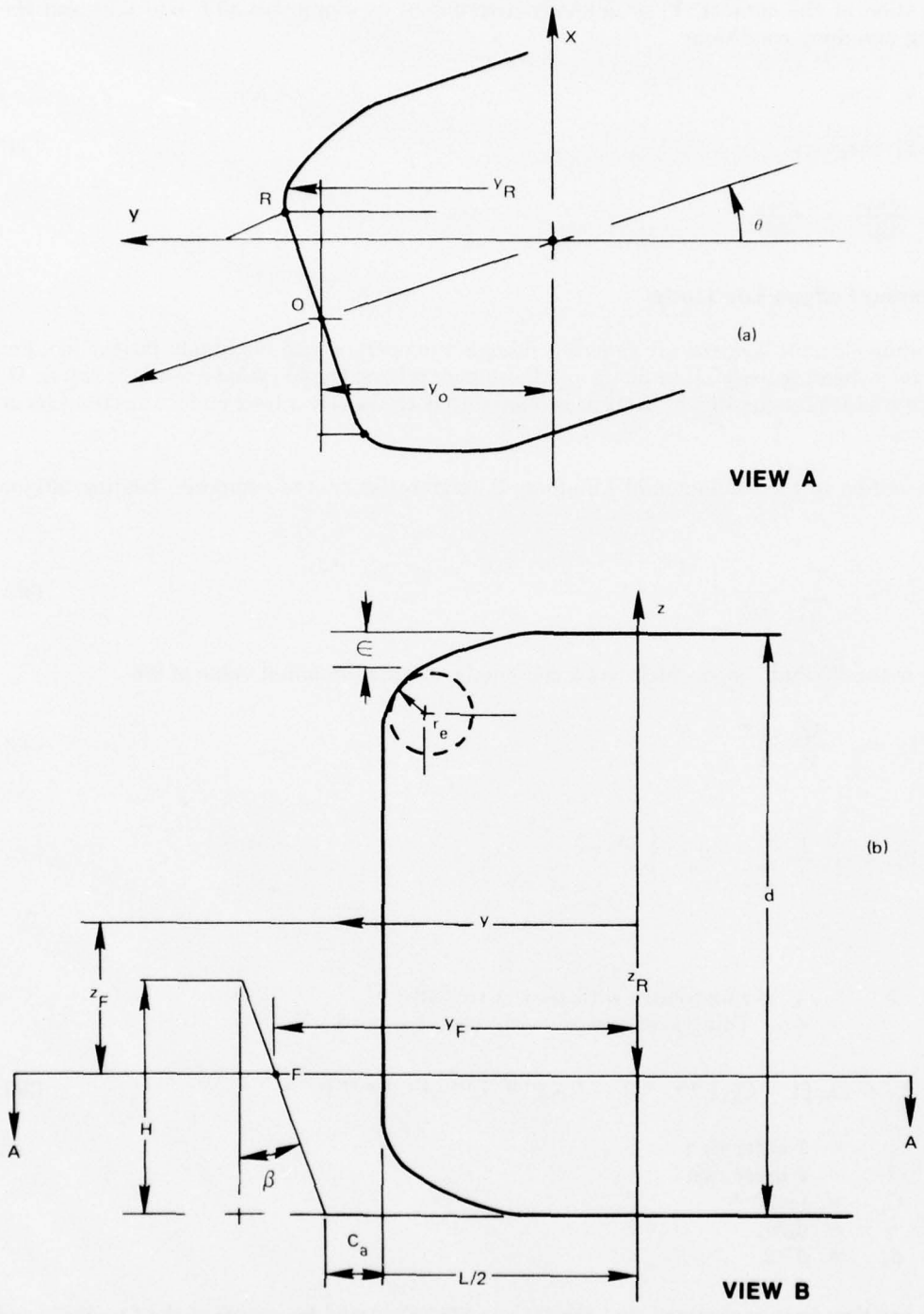

Figure 5. Parameters for Roller Contact Determination

The location of the contact, F, is uniquely determined by Equations (32) and (33) and the following matching conditions.

$$y_R = y_F$$

$$z_R = z_F = z \tag{34}$$

$$\frac{dy_R}{dz_R} = \frac{dy_F}{dz_F}$$

7. Bearing Fatigue Life Model

Rolling element bearings are generally designed to operate with maximum fatigue life. For a given roller bearing design, Lundberg and Palmgren[3] related the so-called basic load rating, Q_c to rolling contact fatigue which, in turn, is related to both the stress level and its distribution at the contact.

According to the fundamental Lundberg-Palmgren theory, the composite bearing fatigue life is:

$$L = \left[\sum_{i=1}^{2} \frac{1}{L_i^e} \right]^{-1/e} \tag{35}$$

where e is the Weibull slope which has a commonly accepted nominal value of 9/8

$$L_i = \left[\frac{Q_{ci}}{P_{ei}} \right]^4 \tag{36}$$

$$P_{ei} = \left[\frac{1}{n} \sum_{q=1}^{n} P_q^b \right]^{1/b} \tag{37}$$

where

b = 4 if ring rotates with respect to load
= 4.5 if ring is stationary with respect to load

$$Q_{ci} = f_i \lambda_i [1 - C_i\gamma]^{-1/4} \quad [1 + C_i\gamma]^{29/27} \ \ell_e^{7/9} \gamma^{2/9} d_x^{29/27} \Omega^{-1/4} \tag{38}$$

i = 1 outer ring
i = 2 inner ring
$C_i = (-1)^{i-1}$
$\gamma = d_x/d_e$
$d_x = d - 2_e$

It has long been recognized that the fatigue life calculated by means of the Lundberg and Palmgren model needs to be modified by a lubricant factor and a material factor in order to properly reflect experience with modern lubricants, surface textures and materials. These factors are input by the user in the existing design system.

8. Roller Bearing Optimization

The analyses identified in the previous sections 1 through 7 have been combined into an integrated "Roller Bearing Design Optimization System." The objective of the system, which assumes that the bearing rings are rigid, is to determine the optimum roller bearing geometry for maximum bearing fatigue life. The program calculates optimized values of internal radial clearance (IRC) and out-of-roundness with respect to input preload and race temperature criteria. Also, all bearing fits are optimized with regard to fit pressure requirements. After establishing the bearing internal geometry in this manner, the program then calculates values of roller flat length and crown radius for maximum bearing life at acceptable levels of roller edge stress.

In summary, the optimization system permits one to determine the best combination, for maximum fatigue life, of the following parameters at each operating condition:

- Preload
- OOR
- IRC
- Fit
- Roller flat length
- Roller crown radius.

The computer program lists these parameters in the output along with the following additional items:

- Distribution of radial load from roller to roller around the perimeter of the bearing
- Contact stress distribution along the length of the most heavily loaded roller
- Bearing life.

C. REFINEMENTS

The following paragraphs describe further improvements in the existing design system that have been generated as a result of this contractual effort. The entirely new analysis dealing with the dynamics of the roller and the cage and their interaction with each other and the raceways will be covered in the next major section of this report. The improvements made in the existing design systems are already proving useful in ongoing engine roller bearing design work.

1. Support and Ring Flexibility

The use of influence coefficients to represent the flexibility of bearing rings and other structural members in the system is well established as part of the existing roller bearing design system as described in Section IV.B. The effects of both the bearing support and ring flexibilities have, however, been calculated separately in a program outside of the existing optimization program. Provisions have been made to automate the computation of structural flexibility influence coefficients by permitting the user to tie in his own program for such computations with the improved static analysis computer program. A computer module is currently being developed to provide the user with an option for generating the influence coefficients internally within the program. These coefficients are to be generated on the basis of a simplified analysis which is adequate for use in the early stages of bearing design. Previously, the influence coefficients were determined separately and then supplied manually as input to the main program. This allows one

to obtain a more realistic estimate of the extent and shape of the roller/race load zone which results in better roller edge stress and life calculations. The user can always suppress these computations if the case of rigid ring/support is of interest.

2. Preload and Outer Ring Out-of-Roundness

Referring to Section IV.B.5, a roller L/D ratio equal to 1, which is a typical value for aircraft engine bearing design, has been assumed in deriving Equation (31). This assumption has been removed to allow for the selection of any desirable length-to-diameter ratio. Equation (31) now becomes

$$\frac{1}{K_{Ri}} = \frac{4(1-\nu_i^2)}{\pi EL}\left[\frac{1}{3} + l_n \frac{2}{2.15}\sqrt{\frac{dLE}{L_p + F_c}}\right] \tag{39}$$

A more rigorous treatment of the outer ring out-of-roundness has been introduced in the roller load distribution portion of the analysis. The distribution of outer ring OOR is taken into account by the use of radial raceway variations (RRV) calculated by using a simple relationship which is as follows:

$$\Delta_{q\ OOR} = -\frac{K_H}{K_{IR} + L_H}\left[\frac{OOR}{2}\right] \quad COS\ [n(\phi_q + \phi_p)] \tag{40}$$

where n = number of OOR points (2 or 3)

ϕ_p = angular location of the first pinch point

As a result, Equation (1) in Section IV.B.1 becomes:

$$\Delta_q = \delta_2 \sin\phi_q + \delta_3 \cos\phi_q - P_D/2 - \Delta_{q\,flex} - \Delta_{q\ OOR} \tag{41}$$

where $\Delta_{q\ flex}$, $\Delta_{q\ OOR}$ are the additional deflections due to structural flexibility and outer race out-of-round, respectively.

Incorporation of these improvements has resulted in not only a better prediction of the preload, but also of the bearing life.

3. Roller/Flange Contact Point and Roller Skew Angle Determination

The location of the roller/flange contact point and roller skew angle are also affected by several factors, in addition to those covered in Section IV.B.6., as defined in figure 6, namely:

- Pitch diameter, d_e
- Radial-undercut height above raceway surface, h_u
- Upper and lower crowned flange reference diameters, D_H, D_L
- Guide flange crown radius, R_f

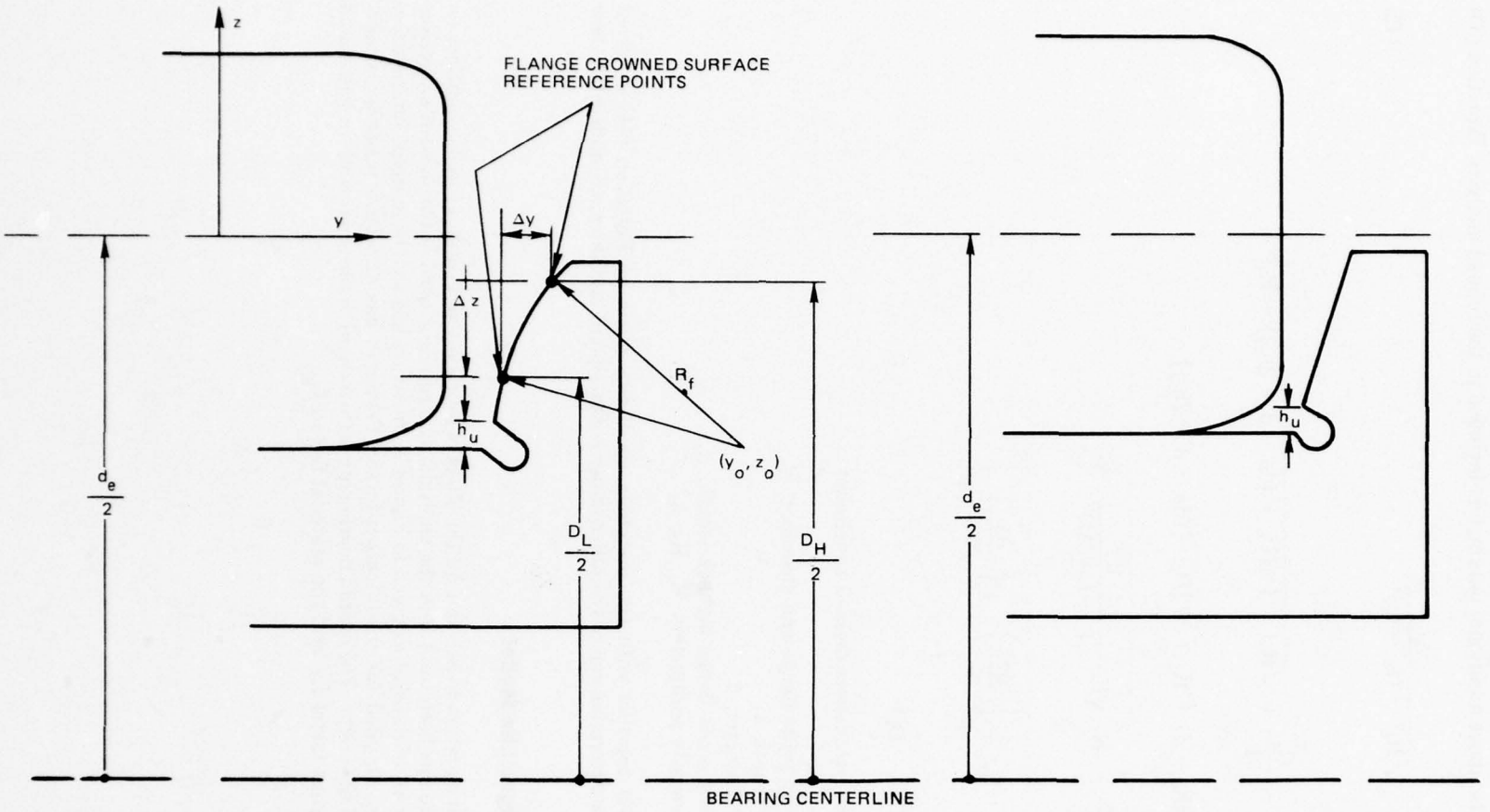

Figure 6. Additional Parameters for Inclusion in Roller/Flange Contact Determination

With all of the above additional parameters included in the refined analysis, Equation (33) now becomes:

$$y_F = y_o - \sqrt{R_F^2 - (z_F - z_o)^2} \tag{42}$$

where

$$y_o = \frac{L}{2} + \frac{C_a}{2} + \sqrt{R_F^2 - \{\tfrac{1}{2}[D_L - (de - d + 2h_u)] + K_1\}^2}$$

$$z_o = \tfrac{1}{2}(2h_u - d) + K_1 + \tfrac{1}{2}[D_L - (de - d + 2h_u)]$$

$$K_1 = \frac{\Delta z}{2} - K_2\sqrt{1 - \frac{1}{1 + (\Delta y/\Delta z)^2}}$$

$$K_2 = \sqrt{R_F^2 - \left[\left(\frac{\Delta z}{2}\right)^2 + \left(\frac{\Delta y}{2}\right)^2\right]}$$

$$\Delta z = \tfrac{1}{2}(D_H - D_L)$$

with the remaining parameters defined as follows:

- Roller to guide flange end clearance, C_a
- Roller length, L
- Roller diameter, d
- Crowned guide flange layback length, Δ_y
- Intermediate parameters, K_1, K_2, Δ_z

Equation (42) together with the matching conditions given by Equation (34) is solved simultaneously for determination of the roller/flange contact point and the maximum roller skew angle.

4. Bearing Fatigue Life Model

An empirical equation to account for the effect of lubricant and surface finish conditions on bearing fatigue life has been built into the analysis. The equation used in the present analysis is based upon the work of Skurka[5] as given in Figure 7. Provision has also been made for inclusion of a separate user-supplied life modification factor. Provision has also been made for a user-supplied material life factor. The overall bearing life is then equal to the product of the calculated L_{10} life, the lubricant factor L_F, and the material factor, L_M.

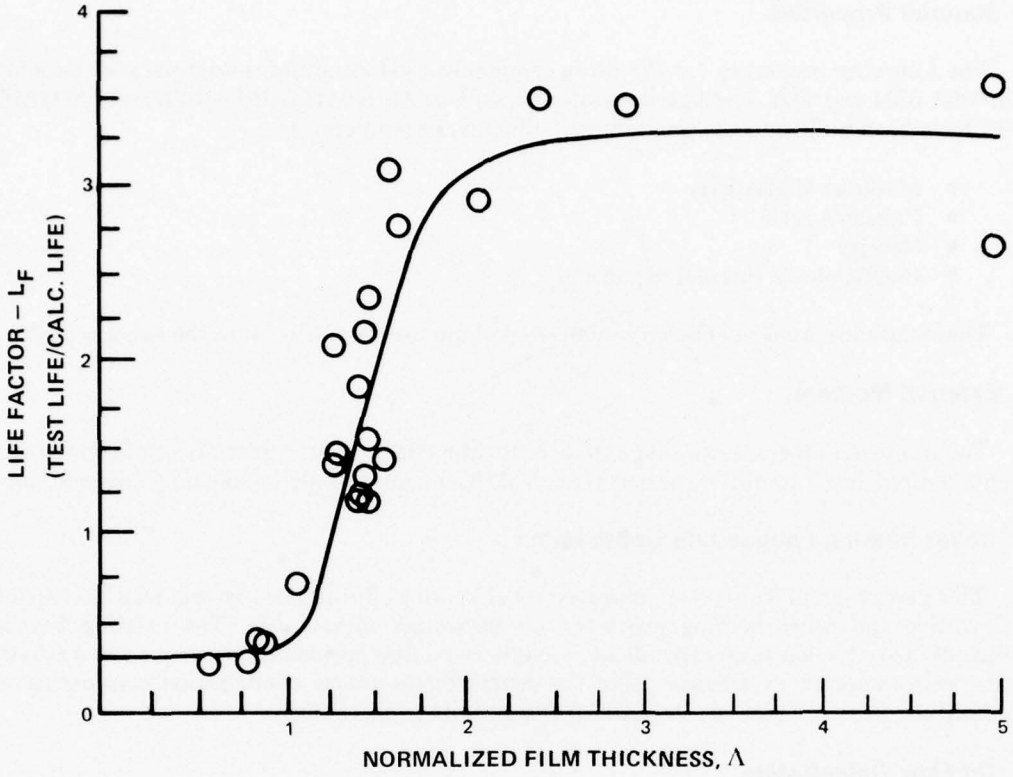

Figure 7. Lubricant Life Factor

5. Built-In Basic Lubricant and Material Properties

a. Lubricant Properties

The following properties for MIL-L-7808 and MIL-L-23699 oils have been built into the computer program as a function of temperature:

- Base viscosity
- Density
- Heat capacity
- Viscosity-pressure coefficient
- Viscosity-temperature coefficient
- Thermal conductivity.

These data are used in lubrication and heat transfer analyses and are input items in the existing program. Nevertheless, the user may also elect to override these data by inputting information for any type of oil that may be of interest.

b. Material Properties

The following properties for the most commonly used structural materials such as AMS 4928, 6260, 6304 and 6322, and bearing materials such as AMS 6444 (AISI 52100) and 6490 (AISI M-50) have been built into the program as a function of temperature:

- Modulus of elasticity
- Poisson's ratio
- Density
- Coefficient of thermal expansion.

These data are used in elasticity analyses and are user input items in the existing system.

6. External Moment

The improved program can take into account the effects of an externally applied moment, which is a direct input item. The parent version of this program could handle misalignment only.

7. Roller Bearing Fatigue Life Optimization

This new program features an improved roller bearing optimization system which is capable of providing the roller bearing geometry for maximum fatigue life. The existing bearing optimization system has been expanded to include an oil flow optimization scheme and a scheme for the determination of a single roller flat length/crown radius combination considering all operating conditions. These are detailed in the following subsections.

a. Oil Flow Optimization

The optimum oil flow is defined as the minimum amount of oil that must be supplied to the bearing so that neither the bearing ring temperatures nor the exit oil temperature ever exceed a predetermined level. Values of each of the following criteria are defined by the user:

- Maximum allowable change in oil temperature
- Maximum allowable temperature difference across bearing rings
- Maximum allowable ring temperature above oil-in temperature
- Maximum allowable ring temperature.

The optimization system is applicable to both regulated and nonregulated oil supply systems. The regulated oil supply system is one in which the oil flowrate rises as the high rotor speed increases, until it reaches a predetermined cutoff level and it is maintained at that level thereafter. For the nonregulated oil supply system, the flowrate is dependent upon the high rotor speed, and consequently the flowrate determination is more complicated than for the regulated system. Determination of the required oil flow for each operating condition (O/C) involves an iterative process. After the required oil flow for each of the anticipated operating conditions has been determined, the largest value of these flows is then taken and rounded-up to the next higher 0.25 ppm for proper selection of the oil pump. Ring temperatures for that iteration are then calculated for each operating condition and subsequently used as input into other routines of the overall optimization program.

b. Roller Flat Length/Crown Radius Optimization

The optimum roller geometry defined within this analysis is one which allows the bearing to achieve a maximum theoretical B_{10} fatigue life without violating any design criteria. The two roller parameters which are varied in order to achieve the optimum life are the roller flat length

and the roller crown radius. The two design criteria, either of which must not be violated, are a maximum allowable normal stress level at the intersection of the crown and corner radius and a maximum blend angle at the intersection of the flat length and crown radius.

The use of these two design criteria is illustrated in figure 8. For a specific set of operating conditions and roller diameter, the largest roller flat length will yield the highest fatigue life. However, as the total load on the roller due to the combination of external and centrifugal loads increases, the contact area between the roller and raceway surfaces extends into the intersection of the crown and corner radius. Contact at this location is undesirable since the presence of a stress riser at this point is possible. The addition of misalignment accentuates this problem. In a similar manner, a blend-angle criterion relating acceptable flat length/crown radius combinations avoids building another stress riser into the roller contour at their intersection. Since contact at the crown/corner radius intersection might occur only during a small fraction of the entire flight cycle, the program allows edge stress levels there up to a user-supplied limit for each operating condition. The loading conditions for each O/C, along with its particular edge stress limit, will then determine the best flat length/crown radius combination for longest life.

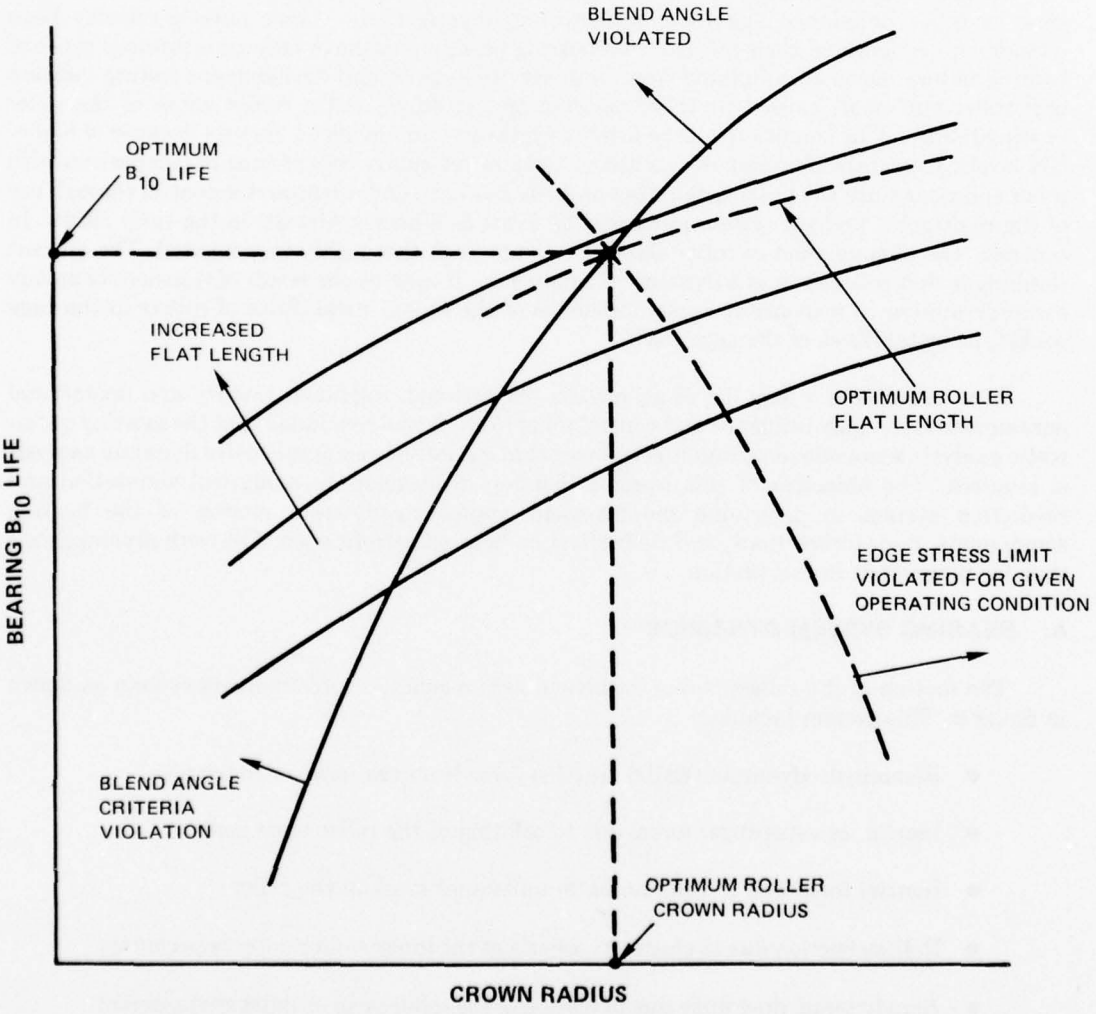

Figure 8. Roller Flat Length/Crown Radius Optimization

SECTION V
DEVELOPMENT OF THE DYNAMIC SIMULATION AND PREDICTION SYSTEM

Previously established design systems used for aircraft mainshaft engine roller bearings have been primarily based on the analysis and a corresponding computerized analytical design system developed by A. B. Jones.[2] The program was based on a quasi-static treatment of the elasticity problem; that is, the dynamic load due to orbiting of the rollers was added to other static loads in the determination of the distribution of the stress field and deformation at the contacts between the rollers and the raceways. The results are then used to determine bearing life in accordance with the fatigue life model correlated by Lundberg and Palmgren.[3] This approach has proven to be adequate for designing bearings for operation in low to moderate DN ranges where the basic failure mode has been identified as that due to rolling contact fatigue. Bearing life, according to this model, is relatively insensitive to detailed variations in roller and raceway geometry.

As gas turbine engine speeds and shaft sizes increase, some of the "secondary" factors — such as roller unbalance due to manufacturing imperfection — that have previously been considered negligible in their influence on bearing performance have become a primary cause of bearing failure. Data accumulated from both service engines and development testing indicate that roller end wear, caused by roller skewing and skidding, is the major cause of the roller bearing failure. This condition will be further aggravated in advanced engines because of higher DN levels. Currently, skidding is considered to be of secondary importance in comparison with roller end wear since the bearing skidding problem has been under reasonable control through use of the multipoint preload system pioneered by Pratt & Whitney Aircraft in the early 1950's. In contrast, the phenomenon of roller skewing has not been thoroughly investigated. The current thinking is that roller skew is a dynamic phenomenon. It may be the result of transient or steady dynamic motion in response to mass unbalance of the roller, instabilities of rollers in the cage pocket, or instabilities of the cage itself.

After examining a long list of geometric, dimensional, tolerance, quality and operational parameters which may influence and control roller skew, it was concluded that the existing quasi-static analysis is not adequate and it is believed that a relatively comprehensive dynamic analysis is required. The objective of this work is therefore to develop an analytical simulation and prediction system to determine the transient and/or steady-state motion of the bearing components, their interactions, and their effect on bearing performance. The work accomplished thus far is reported in this section.

A. BEARING SYSTEM DYNAMICS

The motion of the rollers is due to the action of a complex force/moment system as shown in figure 9. This system includes:

- Elastohydrodynamic (EHD) traction force from the inner or outer race
- Inertia, or centrifugal force, due to orbiting of the roller mass center
- Inertial force due to rotation of an unbalance mass in the roller
- Rolling friction due to elastic hysteresis at the inner and/or outer race contact
- Aerodynamic drag force due to motion of the roller in an oil-mist environment
- External loading transmitted through the roller/race contact

- Gravity force due to roller's own weight
- Reaction forces from the walls of the cage pocket
- Reaction forces from the roller guide flange
- Fluid shear drag.

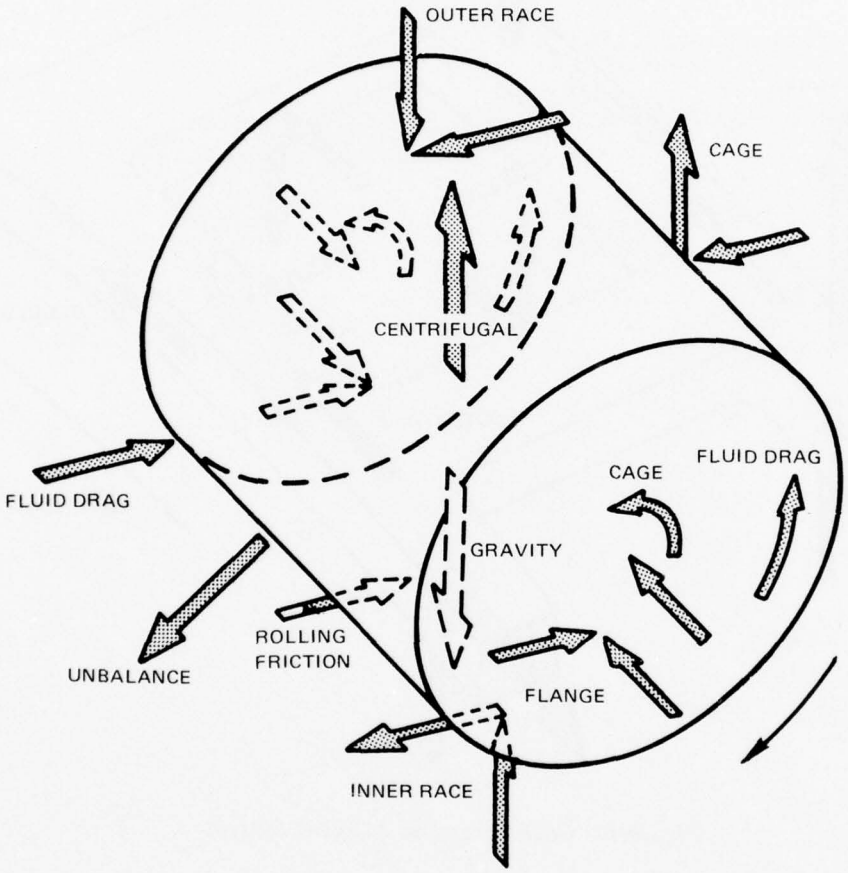

Figure 9. Roller Force and Moment System

Similarly, a bearing cage is also subjected to the combined effect of a force/moment system, as shown in figure 10, which consists of:

- Hydrodynamic force from land riding surface of the raceway guide flange
- Inertia force due to whirling of the cage
- Inertia force due to the rotation of an unbalance mass in the cage
- Aerodynamic drag due to motion of the cage in an oil-mist environment
- Reaction forces from the rollers
- Fluid shear drag.

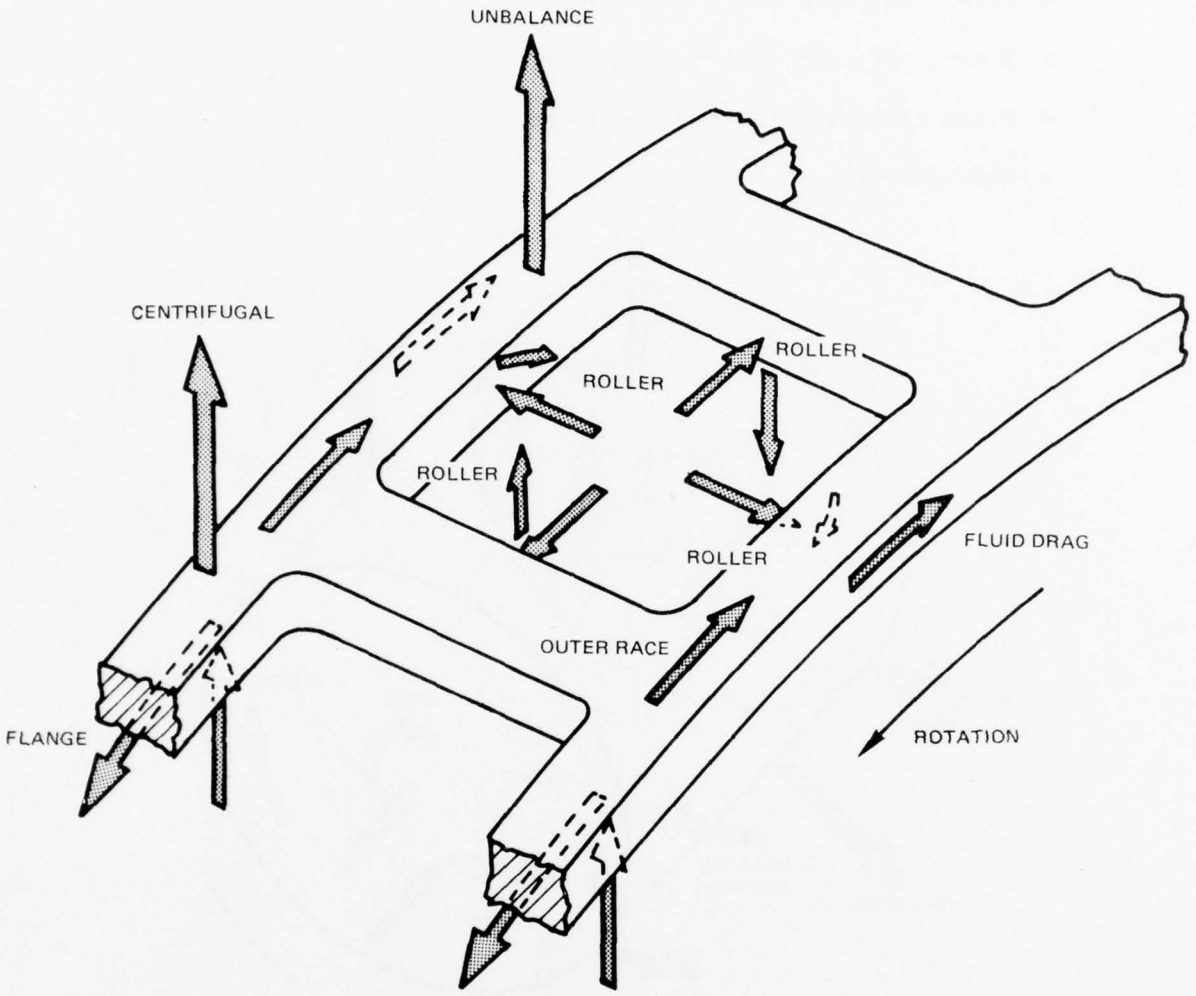

Figure 10. Cage Force and Moment System

It is apparent that the motion of each of the rollers is affected by that of the cage and vice versa as a result of forces and moments transmitted through various interfaces. In a loaded bearing, an individual rolling element and the cage may take turns driving each other. This motion may result in intermittent contact between the moving elements. Intuitively, the contacting process may involve one or a combination of the modes listed below and shown in figure 11.

Hydrodynamic contact occurs when the rollers are far enough away from the wall of the cage pocket so that a hydrodynamic oil film is maintained at the interface.

Elastohydrodynamic contact always exists when the contacting surfaces are extremely close and the pressure generated in the interposed lubricant film is sufficient to cause simultaneous elastic deformation of the surfaces.

Elastic contact is the contact mode when the approach velocity is such that contact occurs before the lubrication film has sufficient time to develop or when the roller forces are large enough to break through an existing oil film.

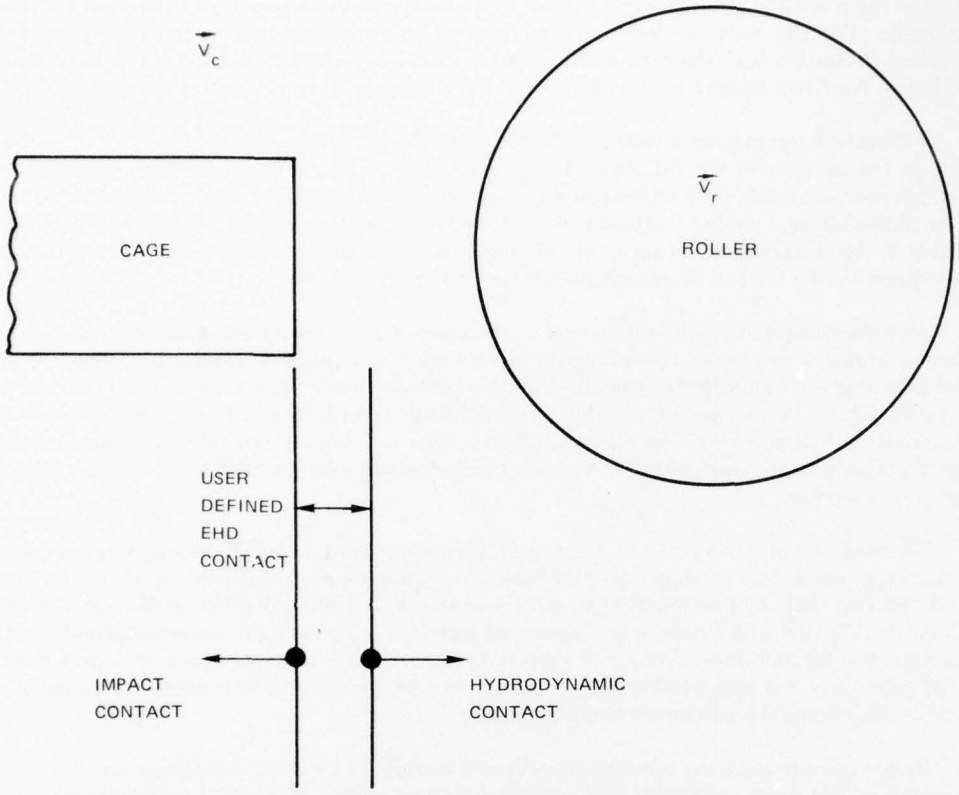

Figure 11. Roller/Cage Contact Criteria

Furthermore, the motion of the rollers and the cage also interacts with the ambient fluids. Determination of the roller and cage motion thus requires simultaneous solution of their respective equations of motion.

B. GENERAL APPROACH

The approach used to account for the various interactions between the cage, rollers and the shaft are summarized below.

The interaction between the cage and the inner ring is mainly at the interface between the cage and the guide flange land riding surface. The analysis given in Section V.C.1 is used to determine the force acting at this interface.

The rollers interact with the races at three locations in the following manner:

- EHD contact at the inner raceway surface
- EHD contact at the outer raceway surface
- A more complex contact mode between the roller end and the face of the inner ring shoulder.

For the inner and outer raceway surface contacts, the analysis presented in Section V.C.4 is applicable. For the roller end/guide-flange contact, a finite element hydrodynamic model described in Section V.C.3 and an elastic contact model described in Section V.C.5 have been developed. An EHD contact model for this interface remains to be developed.

When the roller motion is restricted by the guide flange, various modes of contact can occur between the rollers and the sidewalls of the cage pocket. The forces involved are assumed to originate predominantly from either hydrodynamic contact, analyzed in a manner similar to that of the finite element model discussed in Section V.C.3, or pure elastic contact as treated in Section V.C.5. Interaction between the roller and the cage in the circumferential direction is determined by the models developed in Sections V.C.2 and V.C.5.

As mentioned earlier, determination of the contact forces is normally accomplished in a reference frame where the computational processes are the simplest. Consequently, these forces need to be transformed into the reference frames where the respective equations of motion are to be solved. This process is further complicated by the fact that, for a given roller, computation of the contact forces is highly dependent upon the relative positions and velocities between the contacting surfaces. These velocities and positions must then be transformed into the working frames of reference.

There are about 30 rollers in a typical aircraft engine mainshaft roller bearing. The complete dynamics problem is, therefore, described by 180 second-order differential equations for the roller, together with another 6 similar equations for the cage. These 186 differential equations are reduced to 372 first-order nonlinear differential equations of time-dependent coefficients and, naturally, forcing functions. This set of coupled nonlinear differential equations with prescribed initial conditions is solved simultaneously at each instant in time in this program by means of a modified Hamming's predictor-corrector method.[7]

Before one can solve the relevant equations of motion for both the rollers and the cage, it is necessary at this point to develop the various analytical models to be used in determining the force/moment system acting on these components. Development of the basic models is given in the next two subsections.

C. DEVELOPMENT CONTACT MODELS

In order to fully describe the motion of the cage and rollers, it is necessary to develop analytical models that account for the forces and moments generated at the interfaces between elastic or fluid film contact surfaces. The fluid film contact models considered thus far in the present analysis are illustrated in figure 12. These models are:

- Hydrodynamic contact at the cage/flange
- Hydrodynamic contact at the roller/cage pocket interfaces
- Hydrodynamic contact at the roller end/guide flange interfaces
- EHD contact at the roller raceway interfaces.

Further, it is intended in the future to develop EHD and/or boundary lubrication models to accompany the hydrodynamic model for the roller end/guide-flange interface. This subsection will discuss the various analyses used to establish these models and outline the methods by which the differential equations have been derived and solved.

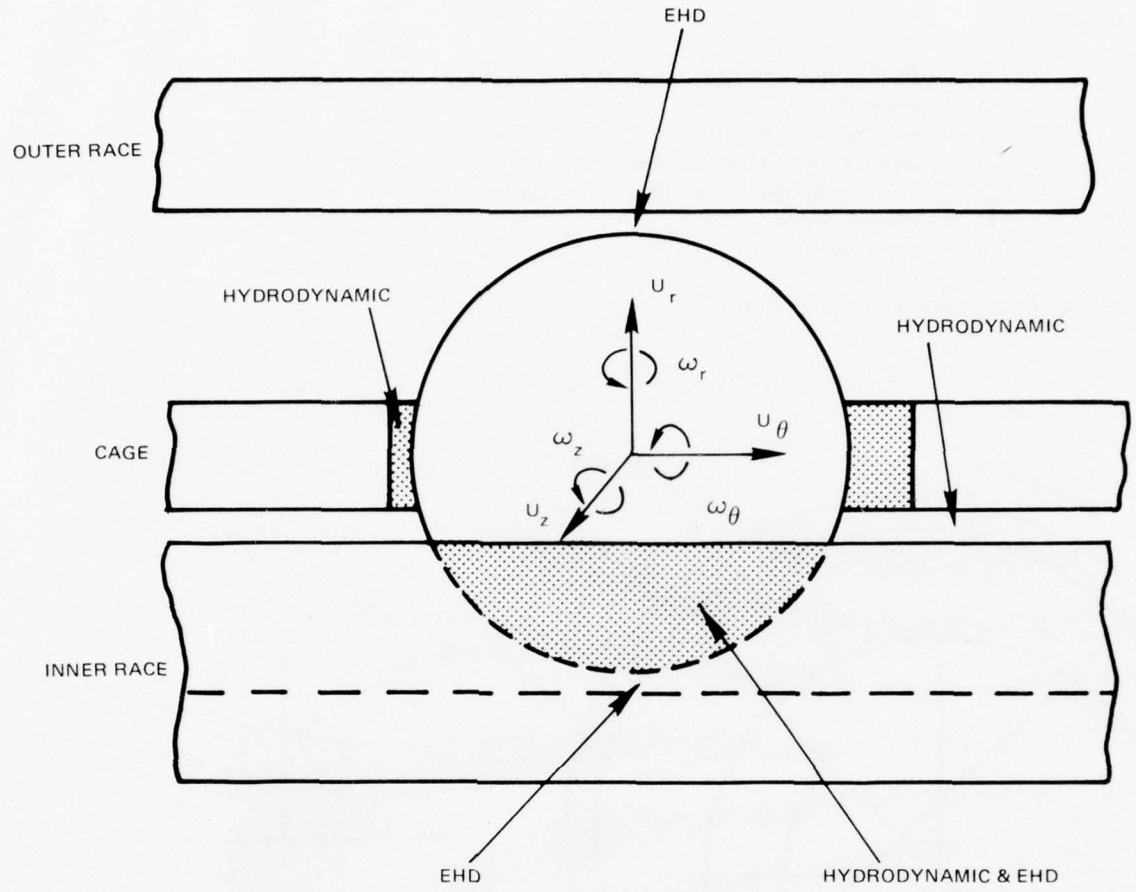

Figure 12. Fluid Film and EHD Contacts

1. Cage/Flange Hydrodynamic Contact Model

Contact between the inner surface of the cage and the outer surface of the inner ring, i.e., the film riding surface, is generally hydrodynamic in nature. The cage/flange load system shown in figure 13 is a two-dimensional illustration of the problem. The hydrodynamic problem can be analyzed most readily by assuming that the technique developed for solving the short journal bearing problem applies. In this case, the journal (inner ring) and sleeve (cage) are both free to rotate and translate linearly, whereas the shaft has its motion prescribed. The short journal bearing assumption is valid due to the very small ratio of cage land width to inner ring land diameter. For example, this ratio is less than 0.03 for the 124.4 mm test bearings to be evaluated under this contract. Referring to figure 13 again, the general governing equation for the lubricant film was first derived in the local reference frame x′ y′ z′. Using standard notation:

$$\frac{\partial}{\partial x'}\left(\frac{h^3}{12\mu}\frac{\partial p}{\partial x'}\right) + \frac{\partial}{\partial z'}\left(\frac{h^3}{12\mu}\frac{\partial p}{\partial z'}\right) = \frac{1}{2}\frac{\partial}{\partial x'}(U_c + U_{IR})\,h + \frac{\partial h}{\partial t} \qquad (43)$$

where

h = fluid film thickness = $C(1 + \epsilon \cos \theta)$, in.
p = pressure, psi
μ = viscosity, lb$_f$-sec/in.^{2}
U_c = surface velocity at the cage bore, in./sec
U_{IR} = velocity at the flange film riding surface, in./sec
C = clearance, in.
ϵ = eccentricity ratio

and with boundary conditions that

$$\text{at} \quad z' = \pm \frac{\ell}{2} \qquad p = p_a \tag{44}$$

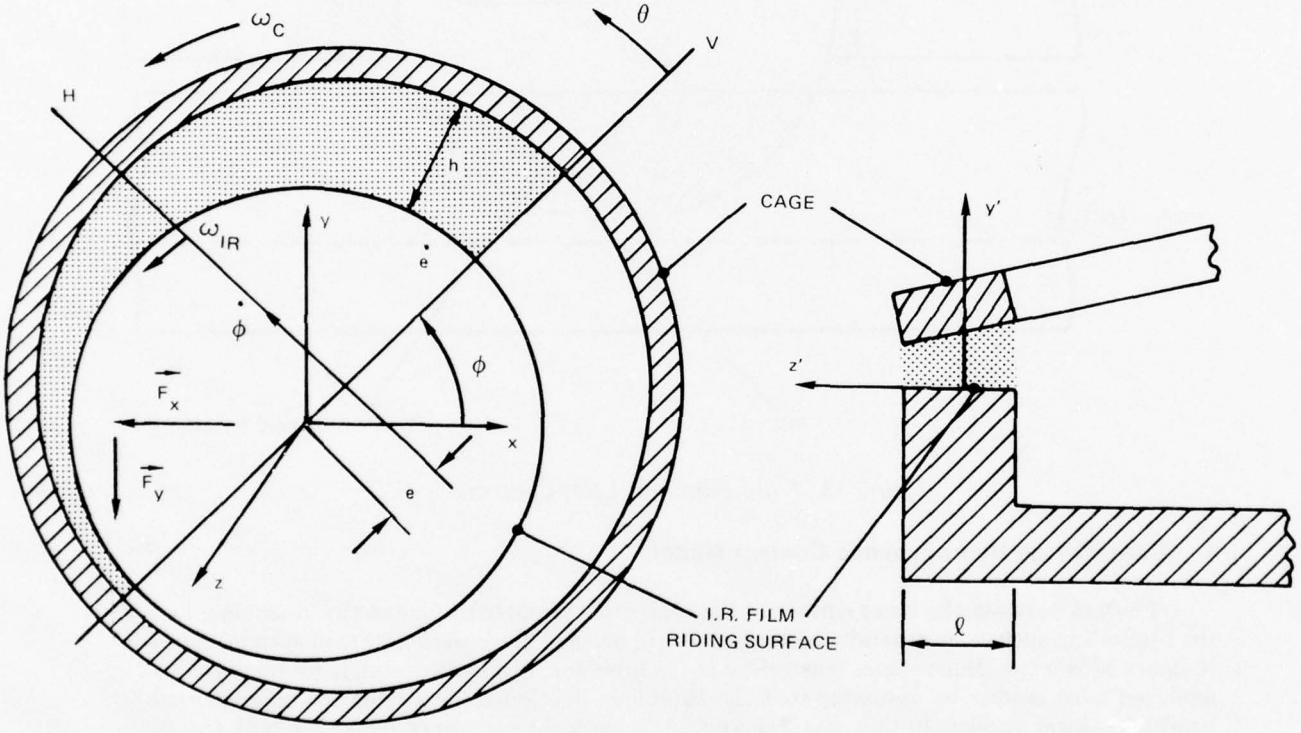

Figure 13. Coordinate System for Cage/Land Hydrodynamic Contact Model

For the present system:

$$\frac{\partial}{\partial z'} \gg \frac{\partial}{\partial x'} \tag{45}$$

In polar coordinates, which are more convenient for analyzing the present problem, Equation (43) reduces to:

$$\frac{\partial}{\partial z'}\left(\frac{h^3}{\mu}\frac{\partial p}{\partial z'}\right) = \frac{6}{R}\frac{\partial}{\partial \theta}(U_c + U_{IR})\,h + 12\,\frac{\partial h}{\partial t} \tag{46}$$

At this stage of the development, we further assume that:

- The fluid film is isothermal
- The film thickness is independent of z′.

It should be pointed out that any deviation from the above assumptions would require a considerably more sophisticated analysis which is beyond the scope of the present work.

Equation (46) can be integrated and, together with the boundary condition, Equation (44), yields:

$$p - p_a = \frac{3\mu\,(X\cos\theta - Y\sin\theta)}{h^3\,(R/C^2)}\left(z'^2 - \frac{\ell^2}{4}\right) \tag{47}$$

where

$$X = -(1 + \epsilon\cos\theta)\frac{d\epsilon}{dt} + \epsilon^2\frac{d\phi}{dt}\sin\theta - 2\frac{R}{C}\frac{d\epsilon}{dt} \tag{48}$$

$$Y = -\epsilon(1 + \epsilon\cos\theta)\frac{d\phi}{dt} - \epsilon\frac{d\epsilon}{dt}\sin\theta + \epsilon\frac{R}{C}(\omega_c + \omega_{IR}) \tag{49}$$

The pressure profile given by Equation (47) has a subambient region in the circumferential direction. The exact location and the extent of the subambient pressure region depends on the relative velocities of the moving components. The common practice, which is adopted here, is to ignore the negative pressure region. This is consistent with the general observation that the tensile strength of lubricating oil is negligibly small and cavitation will occur before significant subambient pressure can be generated.

Let θ_1 and θ_2 represent respectively the angular locations of the beginning and the end of the noncavitated region. The force components resulting from hydrodynamic pressure can be obtained by integrating Equation (47) over the positive pressure region, namely.

$$\begin{Bmatrix} F_{p_h} \\ F_{p_v} \end{Bmatrix} = \frac{\mu\ell^3}{2C}\int_{\theta_1}^{\theta_2}\frac{X\cos\theta - Y\sin\theta}{(1 + \epsilon\cos\theta)^3}\begin{Bmatrix} \sin\theta \\ \cos\theta \end{Bmatrix} d\theta \tag{50}$$

The shearing stress at the cage bore is

$$\tau_\theta = \mu\frac{U_{IR} - U_c}{h} - \frac{h}{2}\frac{1}{R}\frac{\partial p}{\partial\theta} \tag{51}$$

and the resulting force components are computed from

$$\begin{Bmatrix} F_{\tau H} \\ F_{\tau v} \end{Bmatrix} = \int_{-\ell/2}^{\ell/2}\int_{\theta_1}^{\theta_2}\left[\frac{\mu\,(\omega_{IR} - \omega_c)\,R^2}{h} - \frac{h}{2}\frac{\partial p}{\partial\theta}\right]\begin{Bmatrix} \cos\theta \\ -\sin\theta \end{Bmatrix} d\theta dz \tag{52}$$

The torque induced by fluid friction is given by

$$T_z = \int_{-\ell/2}^{\ell/2}\int_{\theta_1}^{\theta_2}\left[\frac{\mu\,(\omega_{IR} - \omega_c)}{h}R^2 - \frac{h}{2}\frac{\partial p}{\partial\theta}\right] R d\theta dz \tag{53}$$

2. Roller/Cage Hydrodynamic Contact Model

The rollers interact with the cage at four places — at the two fore and aft cross-bar surfaces and at the two side pocket walls. Contact between the roller ends and the sidewalls of the cage pocket will be handled by the finite element model formulated in Section V.C.3. As for the other contacts, one may adopt the infinitely long bearing assumption to simplify the generalized Reynolds equation. This approximation is acceptable for the present problem since the roller length is substantially larger than the circumferential extent of the hydrodynamic film at the roller/cross-bar interface. This reduces the problem to that of determining the pressure and shear distribution between a cylinder and a plane. For the case at hand it is desirable to take into account the tangential and the normal relative velocities between the cage and the roller. However, the solution for this particular problem is not available from the literature and is developed herein to satisfy the needs of this program.

Referring to figure 14, the simplified Reynolds equation in the local coordinate system is:

$$\frac{\partial}{\partial x'}\left[\frac{h^3}{\mu}\frac{\partial p}{\partial x'} - (U_r + U_c)\,h\right] = 12\,(V_r - V_c) \tag{54}$$

where

U_r, U_c = velocity components of the roller and the cage pocket wall, respectively, in the x' direction

V_r, V_c = velocity components of the roller and the cage pocket wall in the y' direction

h = $h\,(x', z', t)$ = film thickness

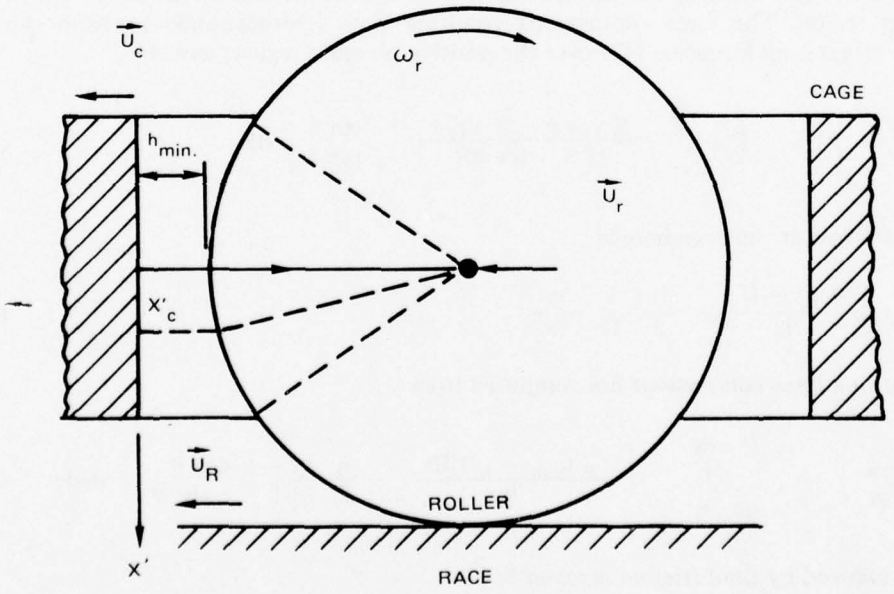

Figure 14. Coordinate System for Roller/Cage Hydrodynamic Contact Model

The boundary conditions are:

$$\begin{aligned} &\text{at } x' = x'_c \text{ (film rupture)} \qquad \frac{\partial p}{\partial x'} = 0 \\ &\qquad\qquad\qquad\qquad\qquad\quad p = p_a \\ &x' = 0 \text{ (entrance)} \qquad\quad p = p_a \end{aligned} \tag{55}$$

Solution of Equations (54) and (55) is, in dimensionless form

$$P = \frac{6\delta}{(1+\delta)^2} \left\{ \int_{\eta_0}^{\eta} \frac{2\bar{U} + \sqrt{1-\eta^2}}{\left[1 - \frac{(1-\eta^2)^{1/2}}{1+\delta}\right]^2} d\eta + \frac{1}{1+\delta} \int_{\eta_0}^{\eta} \frac{\eta(2\bar{V}+\eta) - (1+\delta)C}{\left[1 - \frac{(1-\eta^2)^{1/2}}{1+\delta}\right]^2} d\eta \right\} \tag{56}$$

where the integration constant, C, is determined by the boundary Equation (55). The dimensionless variables are defined as follows:

$$P = \frac{(p - p_a)\, h_{min}}{\mu\, \omega_r\, R_r}$$

$$\eta = \frac{x'}{R_r}$$

$$\delta = \frac{h_{min}}{R_r}$$

$$\bar{U} = \frac{1/2\,(U_r + U_c)}{\omega_r\, R_r}$$

$$\bar{V} = \frac{(V_r - V_c)}{\omega_r\, R_r}$$

The net force components acting on the cage are obtained from the following relationship:

$$F_N = \frac{\mu\, \omega_r\, R_r\, L}{\delta} \int_{\eta_0}^{\eta_c} P\, d\eta \tag{57}$$

The corresponding tangential force due to shear can be evaluated approximately from

$$F_\tau = \frac{\mu\, \omega_r\, R_r\, L}{1+\delta} \int_{\eta_0}^{\eta_c} \left[\frac{U_c + \sqrt{1-\eta^2}}{1 - \frac{(1-\eta^2)^{1/2}}{1+\delta}} - \frac{(1+\delta)^2}{2\delta} \left(1 - \frac{\sqrt{1-\eta^2}}{1+\delta}\right) \frac{dP}{d\eta} \right] d\eta \tag{58}$$

In general, the pressure-induced term in Equation (58) is negligible as to the pure shear term. Thus, considering the shear term only simplifies this equation as follows:

$$F_\tau \cong \frac{\mu\, \omega_r\, R_r\, L}{1+\delta} \int_{\eta_0}^{\eta_c} \frac{U_c + \sqrt{1-\eta^2}}{1 - \frac{\sqrt{1-\eta^2}}{1+\delta}} d\eta \tag{59}$$

When the roller skews in the cage pocket, as shown in figure 15a, the film thickness along the roller face is no longer constant in the local axial direction. A nonparallel condition would result in a restoring moment being applied to the roller, in addition to the force system, due to a shift of the center of pressure in the oil film. This situation can be treated approximately by dividing the roller into a number of axial laminae, each with an equivalent film thickness, as shown in figure 15b and applying the long bearing solution to each of these laminae. The total skewing moment is then

$$M_r = \sum_{i=1}^{M} F_{Ni}\, r_i \tag{60}$$

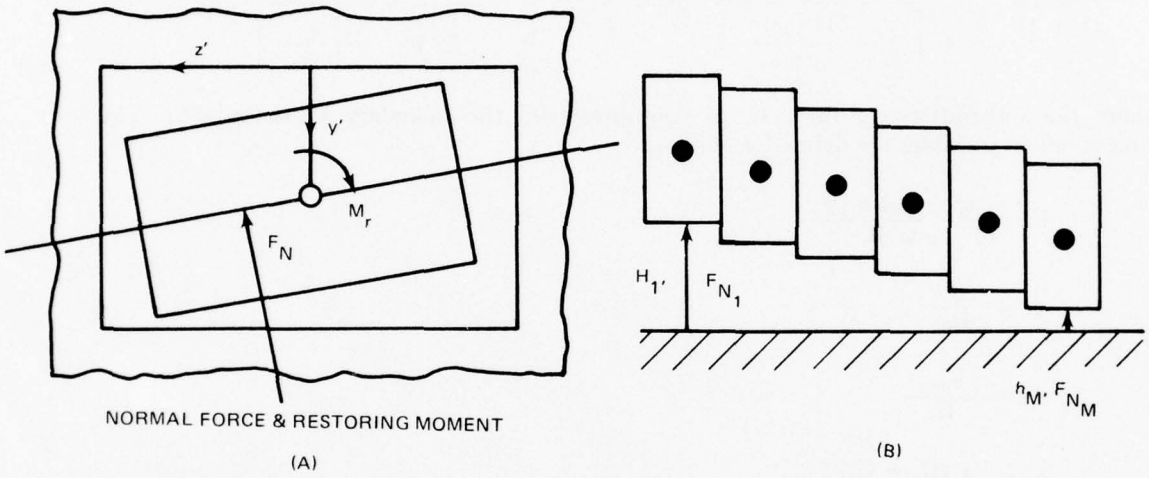

Figure 15. Treatment of Skewed Roller

The total force is found by summing the force contribution of each lamina, i.e.,

$$\begin{Bmatrix} F_N \\ F_r \end{Bmatrix} = \sum_{i=1}^{M} \begin{Bmatrix} F_{N_i} \\ F_{r_i} \end{Bmatrix} \tag{61}$$

3. Roller/Flange Hydrodynamic Contact Model

Roller tracking control is critical for high speed applications. The roller guide flanges must limit roller centerline skewing without causing excessive contact forces on the roller end surfaces. Experimental studies conducted at Pratt & Whitney Aircraft have identified eccentric roller end wear as one of the primary failure modes of roller bearings operating at high DN levels. Experimental and analytical results recently obtained suggest that this type of failure is most probably a result of dynamic interaction among the contacting bearing components. The studies also show that mass unbalance in the roller, due to manufacturing imperfection, can promote roller skewing, while a properly designed guide flange may generate sufficient fluid film stiffness and damping to limit the amplitude of the roller skewing motion. This supports the belief that a better understanding of the characteristics of the oil film at this interface is required.

Intuitively, it seems possible that the mode of contact at the roller/guide-flange interface, illustrated in figure 16, could be either hydrodynamic, elastohydrodynamic, or purely elastic in nature. However, an analysis for either of these problems is not currently available and development of a representative, yet tractable, analytical model is a major undertaking because of the extreme complexity of the associated geometry and surface motion. A finite element model has been developed to represent the hydrodynamic contact problem as a first step towards the goal of acquiring some understanding of the lubrication mechanism at this interface. This type of analysis is ideal for the present situation because it can be developed in such a manner as to include the effect of surface motion in three dimensions, as well as providing the capability for handling the complex geometry and fluid film distribution caused by the guide flange layback angle, the compound or higher order surface, and roller skew.

Neglecting the effect of body forces, and assuming no surface diffusion since the subject bearing is not permeable, the generalized Reynolds equation can be reduced to the following vector form:

$$\vec{\nabla} \cdot \left(\frac{h^3}{12\mu} \vec{\nabla} P \right) = \vec{\nabla} \cdot (h\vec{U}) + \frac{\partial h}{\partial t} \tag{62}$$

where

$$\vec{U} = \frac{U_{xr} + U_{xf}}{2} \vec{i} + \frac{V_{xr} + V_{xf}}{2} \vec{j} = U_x \vec{i} + U_y \vec{j} \tag{63}$$

and $\vec{i}$, $\vec{j}$ are unit vectors in the local coordinate system. The general boundary conditions are

$$p = p_a \quad \text{on } S_p \tag{64}$$

$$Q = h \left(\vec{U} - \frac{h^2}{12\mu} \vec{\nabla} p \right) \cdot \vec{n} \quad \text{on } S_q \tag{65}$$

in which S_p and S_q represent, respectively, where the pressure or, the flow boundary condition applies and $\vec{n}$ is the unit normal vector of the boundary surface.

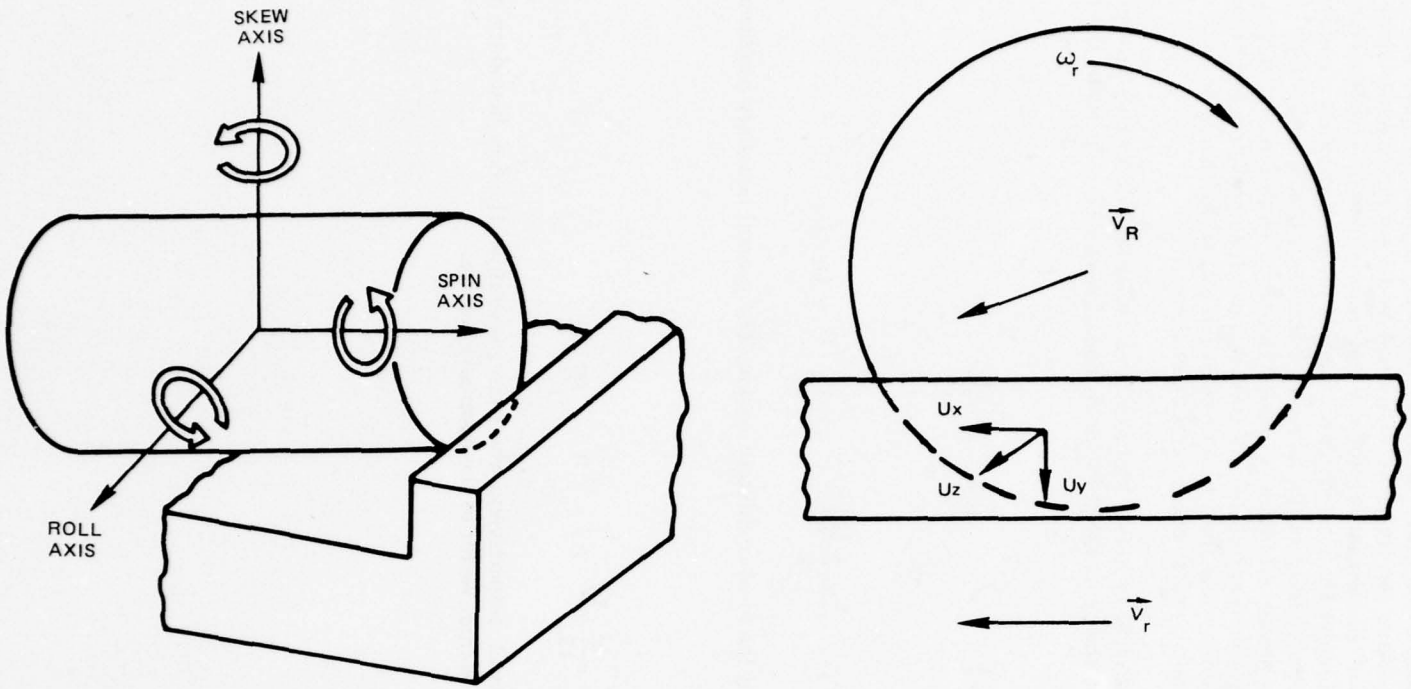

Figure 16. Roller/Guide Flange Hydrodynamic Contact Model

According to the variational principle, the solution of Equations (62) through (65) is the function p that satisfies the pressure boundary condition and minimizes the functional:

$$I(p) = \int_a \left[\left(\frac{h^3}{24\mu} \vec{\nabla} p - h\vec{U} \right) \cdot \vec{\nabla} P + \frac{\partial h}{\partial t} P \right] da + \int_{sq} QP ds \tag{66}$$

where "a" defines the domain of the system or the element as the case may be. Equation (66) can be discretized by introducing finite elements of polygonal shape in the solution domain. In the present analysis, a most elementary three-node triangular element, as shown in figure 17, has been selected. The discretization process involves the development of expressions within each element for the pressure and other forcing functions in Equation (66) in terms of the interpolation function:

$$N_i = \frac{a_i + b_i x + c_i y}{2\Delta} \qquad i = 1, 2, 3 \tag{67}$$

where the coefficients a_i, b_i and c_i are functions of the nodal position and Δ is the area of the triangle. One may now formulate the variables such as p in Equation (66), in standard finite element method notation, as:

$$p = [N] \{p\} = \sum_{i=1}^{3} N_i p_i \tag{68}$$

Substituting Equation (67) into Equation (68), and similar expressions for other variables in Equation (66), and minimizing the functional for one element, one obtains, after rearranging the terms, a set of element equations of the form:

$$[K_p] \{p\} = \{q\} - [K_{u_x}] \{U_x\} - [K_{u_y}] \{U_y\} - [K_h^{\cdot}] \{\dot{h}\} \tag{69}$$

The K's in Equation (69) are 3×3 matrices and the variables are 3×1 column matrices. Furthermore, the coefficients in Equation (69) are often quite complex, e.g.:

$$K_{P_{ij}} = - \int_a \frac{h^3}{12\mu} \left(\frac{\partial N_i}{\partial x} \frac{\partial N_j}{\partial x} + \frac{\partial N_i}{\partial y} \frac{\partial N_j}{\partial y} \right) da \tag{70}$$

$$q_i = \int_{sq} QN_i \, ds \tag{71}$$

$$K_{u_{xij}} = \int_a h \frac{\partial N_i}{\partial x} N_j \, da \tag{72}$$

$$K_{uy_{ij}} = - \int_a h \frac{\partial N_i}{\partial y} N_j \, da \tag{73}$$

$$K_{h_{ij}} = - \int_a N_i N_j \, da \tag{74}$$

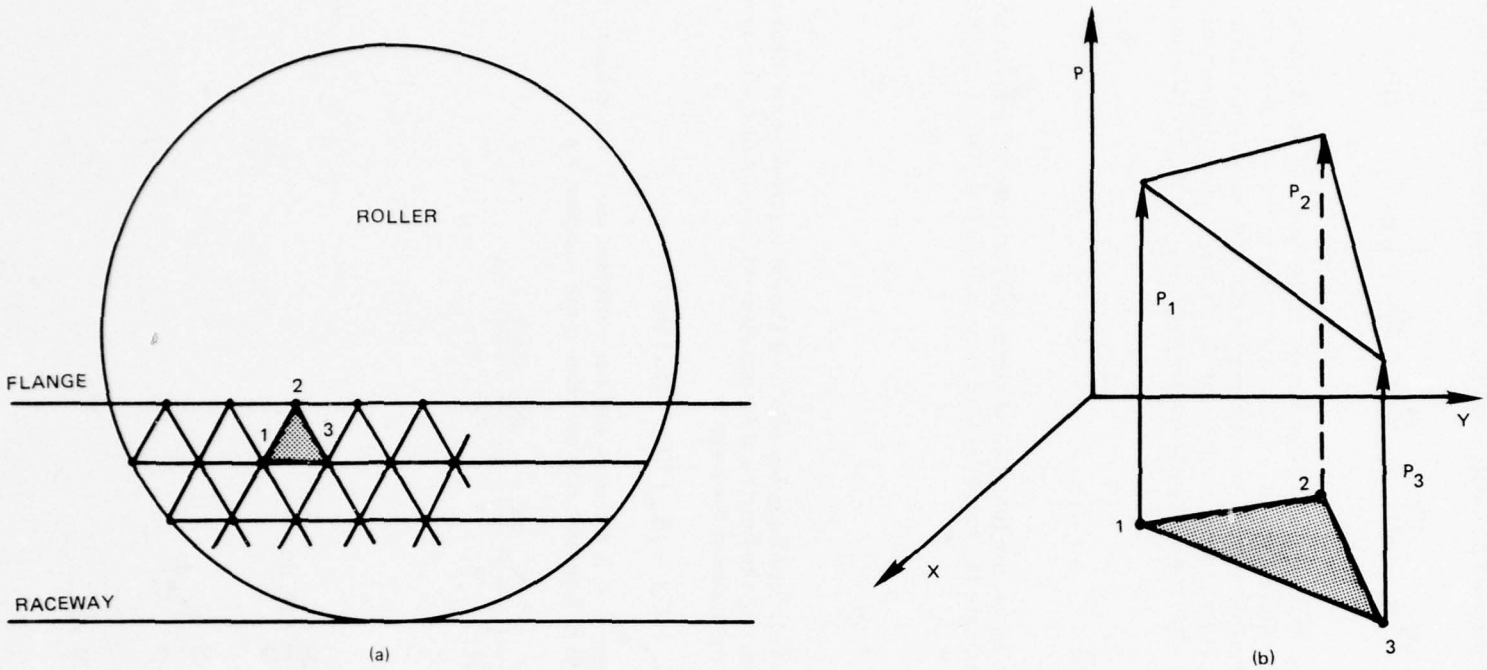

Figure 17. Roller/Guide Flange Finite Element Model

The finite element model developed for the entire fluid film region then requires one to assemble the preceding equations for a discrete element into a system equation. This, together with appropriate boundary conditions, fully defines the pressure at each nodal point. The normal or tangential forces and the location of the center of pressure are symbolically given by:

$$F_N = \int_A p(x, y)\, dA \tag{75}$$

$$F_\tau = \int_A \mu \left[\frac{\partial}{\partial Z} (u\,\vec{i} + v\,\vec{j}) \right]_0^h dA \tag{76}$$

and

$$\begin{Bmatrix} \bar{x} \\ \bar{y} \end{Bmatrix} = \frac{\int_A \begin{Bmatrix} x \\ y \end{Bmatrix} p\,(x, y)\, dA}{F_N} \tag{77}$$

where A indicates the domain of the system.

Equations (75), (76) and (77) fully define the force and moment system acting on the end of the roller and, locally, on the flange.

4. Roller/Race Elastohydrodynamic Contact Model

Contact between the roller and the race is elastohydrodynamic (EHD) in nature, as reported by numerous authors, such as Dowson and Higginson[8], on this subject. In order to select a suitable model to account for this effect, Pratt & Whitney Aircraft Group has enlisted the expertise of Battelle Columbus Laboratories (BCL).

a. EHD Film Thickness Model

Battelle Columbus Laboratories reviewed the EHD film thickness models available from the literature and recommended the use of a model, correlated by Loewenthal, Parker and Zaretsky[1] as follows:

$$\bar{H} = K_1\, \bar{U}^{0.62}\, \bar{P}_H{}^{-0.22}\, \phi_s \tag{78}$$

where

$\bar{H}$ = normalized minimum film thickness = h_{min}/R'

R' = equivalent radius = $\left(\frac{1}{R_r} + \frac{1}{R_R} \right)^{-1}$, in.

$\bar{P}_H$ = normalized maximum Hertz stress, P_H/E'

E' = reduced modulus of elasticity = $\left(\frac{1 - \gamma_1{}^2}{\pi E_1} + \frac{1 - \gamma_2{}^2}{\pi E_2} \right)^{-1}$, psi

$\bar{U}$ = normalized speed = $\mu_o\, U/E'\, R'$

U = mean surface speed, in./sec

K_J = empirical lubricant constant

ϕ_s = stress factor = $\bar{P}_H (150 - 2750 \bar{P}_H) + 0.806$

Equation (78) was developed from experimental data obtained for several fluids. For Type II ester, the constant, K_J, in the above equation has a value of 18.2 according to Loewenthal, et. al.[1] For Type I lubricant, the value of K_J is not available from the open literature and therefore is a user-supplied item. In the event that the user does not have any information on the value of K_J for Type I oil, then the value of 10.9 is recommended. Cheng[9] and Wilson [10] have developed an additional factor, defined as ϕ_T, to account for large inlet heating effects; however, it was found that results computed from Equation (78) agree reasonably well with test data if, and only if, the thermal reduction factor was not included in the computation. As a result it was decided at this juncture to exclude this factor from the present model.

b. EHD Traction Model

An indepth review of existing EHD traction models, as summarized by McGrew, et. al.[11], was made by P&WA and BCL. It was observed that although the models proposed by various authors seemed to yield reasonable agreement with experimental data, the agreement is usually limited to a narrow operating range or to a specific bearing design or to a specific lubricant type. Furthermore, the models are generally complex and require numerical integration across the contact region. Such a numerical integration scheme would undoubtedly increase the required computational time because of the large numbers of EHD contacts in a roller bearing. For reasons of computational efficiency a closed-form solution was sought. Battelle Columbus Laboratories suggested that the following model developed by Kannel and Walowit[12] is probably the simplest available that still provides an acceptable solution:

$$\tau = \frac{\mu_o \; e^{\alpha \bar{P}} | \Delta u |}{\wedge \; h_{min}} \quad \frac{\sinh^{-1} \wedge}{\sqrt{1 + \wedge^2}} \tag{79}$$

where

μ_o = reference viscosity at ambient pressure, lb_f-sec/in.^{2}

α = pressure-viscosity coefficient, (psi)$^{-1}$

Δu = relative surface velocity, in./sec

$$\wedge = \left(\frac{\mu_o \; \delta \; e^{\alpha \bar{P}}}{8K} \right)^{1/2} \Delta u$$

δ = temperature-viscosity coefficient, (F)$^{-1}$

K = lubricant thermal conductivity, Btu/sec-in.-F

$\bar{P}$ = mean Hertzian pressure, psi

The traction force per unit contact length is represented by

$$F_T = \int_0^{2a} \tau dx \tag{80}$$

where a = Hertzian half-width

Further examination of Equations (79) and (80) and comparison of calculated results from these equations with previous P&WA in-house experimental data indicates that this model is applicable to the low-slip region only.

It was concluded, therefore, that a practical and more reliable means for obtaining EHD traction forces over a wider range of bearing design and operating conditions would be a system that would permit direct interpolation/extrapolation of the available experimental data. Since the EHD traction force, as presented in various articles [11-13], is basically a function of four variables (rotational speed, slip velocity, contact pressure, and temperature), a four-dimensional interpolation scheme was therefore developed. A linear interpolation method has been adopted for use with the BCL/P&WA data as the basic input. The computer program is flexible enough to permit the inclusion of any additional user-supplied data as desired.

5. Elastic Impact Model

It is assumed that impacts between the roller and the cage, as well as between the cage and the inner ring, are purely elastic in nature with no corresponding loss in energy.

The force-deflection relationship is then of the following form:

$$P = c\delta^n$$

The classical impact theory gives the maximum deflection δ_m and the duration of impact t_i as,

$$\delta m = \left[\frac{n+1}{C} \left(\frac{v_o^2}{2} \right) \frac{m_1 m_2}{m_1 + m_2} \right]^{\frac{1}{n+1}} \tag{81}$$

$$t_i = \frac{2\delta_m}{v_o} \int_0^1 \frac{dz}{(1 - z^{n+1})^{1/2}} \tag{82}$$

Equations (81) and (82) are used to adjust the time step of integration when any one or a number of rollers are in contact with the cage.

D. DEVELOPMENT OF DYNAMIC MODELS

1. Cage Dynamics Model

As noted earlier, the motion of a bearing cage is subjected to the influence of a very complex force system.

The forces considered in the present analysis are illustrated in figure 18. These consist of:

- Fluid pressure and shear forces generated at the cage/flange interface
- Fluid and/or elastic forces at the cage/roller interface
- Gravitational force
- Unbalance force
- Inertia force.

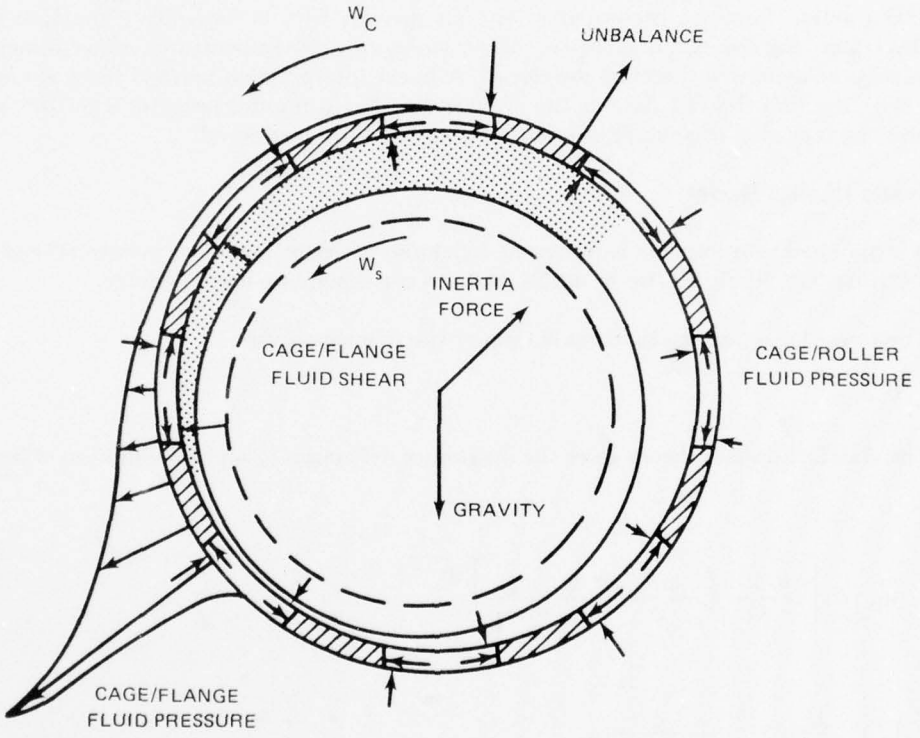

Figure 18. Force System for Cage Dynamics Model

With these forces supplied by various models developed in the preceding sections, one may proceed to derive the equation of motion for the center of mass of the cage.

a. Coordinate Systems and Transformations

In the analysis of problems related to dynamic systems, it is important to select a coordinate system in which the physical problem considered can be formulated mathematically with the least degree of computational complication. Quite often this depends upon the relative complexity, in terms of the number of computations, between the inertial acceleration terms and the forcing functions in the evaluation of the pertinent equations of motion.

For the cage problem, the coordinate systems selected are shown in figure 19 in which the XYZ coordinate system is the absolute inertial frame of reference, the X′Y′Z′ coordinate represents a translatory frame of reference with its origin fixed at the center of mass of the cage, O_c, and its axes are always parallel to the inertial frame. The $X_cY_cZ_c$ frame, however, is a body frame of reference with its origin fixed at O_c. This coordinate system is chosen such that the axes X_c, Y_c, Z_c are also the principal axes of the cage and are rotating together with the cage at an angular velocity, ω_c, with respect to the inertial frame. Vectors $\vec{i}, \vec{j}, \vec{k}$ and $\vec{I}, \vec{J}, \vec{K}$ are the unit vectors in the $X_cY_cZ_c$ and XYZ/X′Y′Z′ frames respectively.

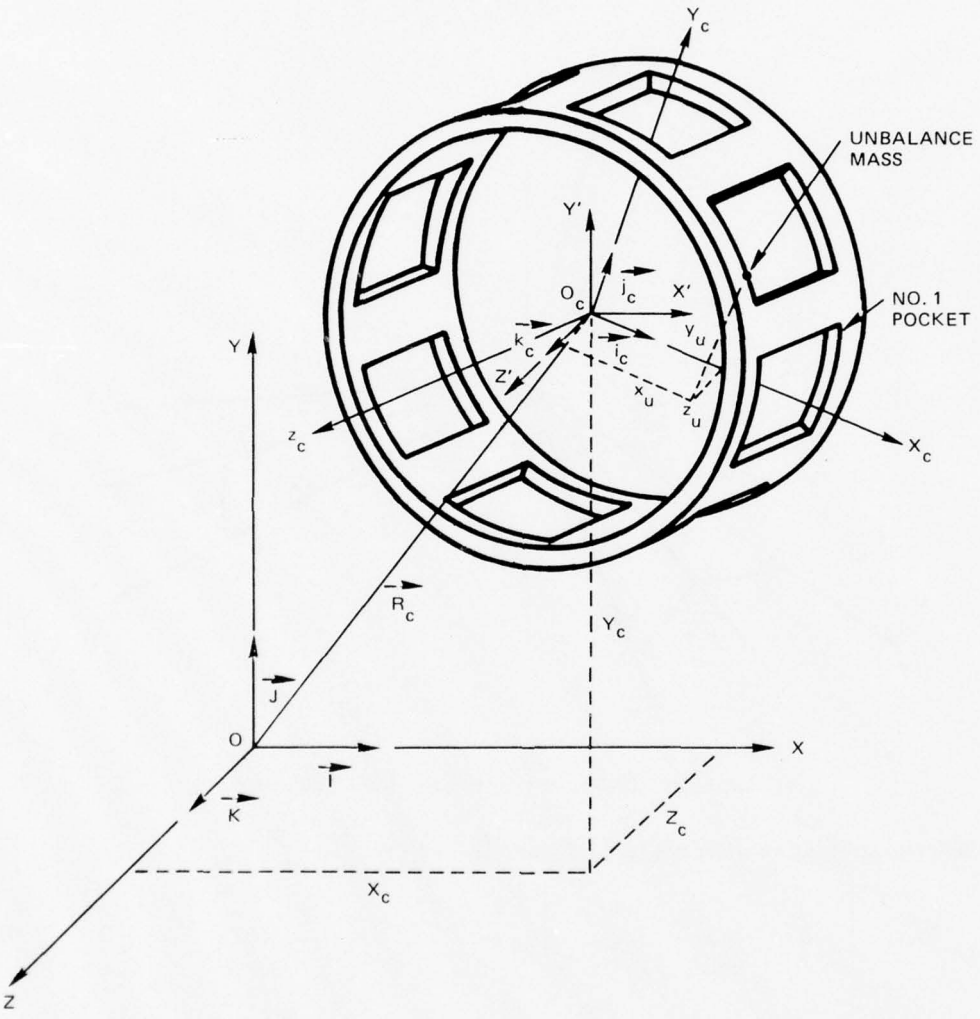

Figure 19. Coordinate System for Cage Dynamics Model

The transformation from the body frame $X_cY_cZ_c$ to the inertial frame XYZ is defined by the Euler angles ψ, θ, ϕ as shown in figure 20.

In mathematical form, one has

$$\{X_c\} = [\phi_c]\,[\theta_c]\,[\psi_c]\,\{X'\} \tag{83}$$

where the column vectors $\{X'\}$ and $\{X_c\}$ represent, respectively, the coordinates of a point in the $X'Y'Z'$ and $Z_cY_cZ_c$ system, i.e.

$$\{X'\} = \begin{Bmatrix} X' \\ Y' \\ Z' \end{Bmatrix} \text{ and } \{x_c\} = \begin{Bmatrix} x_c \\ y_c \\ z_c \end{Bmatrix} \tag{84}$$

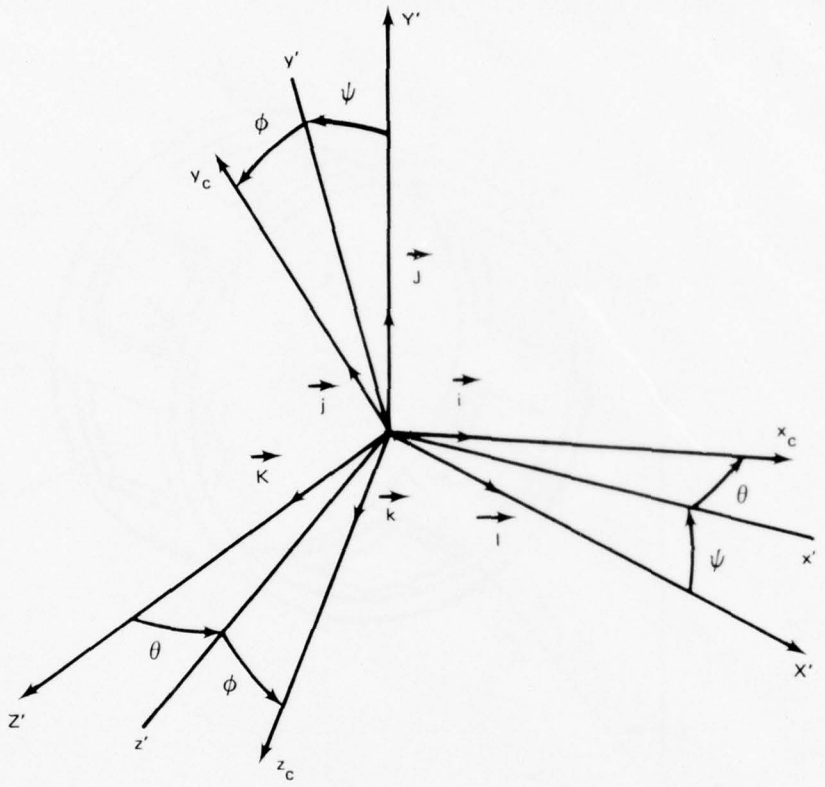

Figure 20. Eulerian Coordinate Transformations

The transformation matrices $[\phi_c]$, $[\theta_c]$ and $[\psi]$ are given by

$$[\phi_c] = \begin{bmatrix} 1 & 0 & 0 \\ 0 & \cos\phi_c & \sin\phi_c \\ 0 & -\sin\phi_c & \cos\phi_c \end{bmatrix} \tag{85}$$

$$[\theta_c] = \begin{bmatrix} \cos\theta_c & 0 & -\sin\theta_c \\ 0 & 1 & 0 \\ \sin\theta_c & 0 & \cos\theta_c \end{bmatrix} \tag{86}$$

$$[\psi_c] = \begin{bmatrix} \cos\psi & \sin\psi_c & 0 \\ -\sin\psi_c & \cos\psi_c & 0 \\ 0 & 0 & 1 \end{bmatrix} \tag{87}$$

The relationship between the angular velocities of the rotating frame $X_cY_cZ_c$, and hence the cage, and the stationary frame XYZ or the translatory frame X'Y'Z' is

$$\begin{Bmatrix} \omega_x \\ \omega_y \\ \omega_z \end{Bmatrix} = [T_c] \begin{Bmatrix} \dot{\phi}_c \\ \dot{\theta}_c \\ \dot{\psi}_c \end{Bmatrix} \tag{88}$$

The transformation matrix $[T_c]$ is

$$[T_c] = \begin{bmatrix} 1 & 0 & -\sin\theta_c \\ 0 & \cos\phi_c & \cos\theta_c \sin\phi_c \\ 0 & -\sin\phi_c & \cos\theta_c \cos\phi_c \end{bmatrix} \tag{89}$$

and the inverse relationship is

$$\begin{Bmatrix} \dot{\phi}_c \\ \dot{\theta}_c \\ \dot{\psi}_c \end{Bmatrix} = [T_c]^{-1} \begin{Bmatrix} \omega_{xc} \\ \omega_{yc} \\ \omega_{zc} \end{Bmatrix} \tag{90}$$

b. Equations of Motion

The motion of the cage center of mass is governed by the following equation

$$M_c \frac{d^2\vec{R}_c}{dt^2} = \vec{F}_c \tag{91}$$

where R_c is the position vector and the forcing function $\vec{F}_c$ is given by

$$\vec{F}_c = \vec{F}_{c\ flange} + \vec{F}_{c\ unbalance} + \vec{F}_{c\ roller} + \vec{F}_{c\ gravity} + \vec{F}_{c\ others} \tag{92}$$

In the above equation, $\vec{F}_{c\ flange}$ represents the hydrodynamic normal and shearing forces generated at the cage/flange interface as indicated in figure 18. This force is evaluated in an intermediate rotating frame with one of its axes passing through the center of mass of both the cage and the shaft section in the following sequence, e. g.

$$\vec{F}_{c\ flange} = F_v\ \vec{i}' + F_H\ \vec{j}' + F_A\ \vec{k}' \tag{93}$$

Local Coordinate System

$$\vec{F}_{c\ flange} = F_{F11}\ \vec{i}_c + F_{F12}\ \vec{j}_c + F_{F13}\ \vec{k}_c \tag{94}$$

Cage Coordinate System

$$\vec{F}_{c\ flange} = F_{F01}\ \vec{I} + F_{F02}\ \vec{J} + F_{F03}\ \vec{K} \tag{95}$$

Inertial Coordinate System

The force $F_{c\ unbalance}$ due to a concentrated unbalance mass is given by

$$F_{c\ unbalance} = \sum_{i}^{n} F_i = \sum_{i}^{n} m_i \frac{d^2 R_{oi}}{d t^2} \tag{96}$$

where subscript "i" denotes quantities associated with the i^{th} unbalance mass. Since the position vector r_i, of the unbalance mass, m_i, in the cage coordinate system is constant, the acceleration term can be expressed as follows:

$$\frac{d^2\vec{R}_{ui}}{dt^2} = \frac{d^2\vec{R}_c}{dt^2} + \frac{d\vec{\Omega}_c}{dt} \times \vec{r}_i + \vec{\omega}_c \times (\vec{\omega}_c \times \vec{r}_i) \tag{97}$$

Furthermore, both $\vec{\Omega}_c$ and $\vec{r}_i$, which are normally expressed in terms of unit vectors in the local cage coordinate systems, need to be transformed into the inertial coordinate system before separating Equation (97) into component form.

The roller force $\vec{F}_{roller}$ is to be determined simultaneously with the roller dynamic analysis and the associated contact models, while the generalized force field $\vec{F}_{c\ other}$ is reserved for future development to account for other forces not included in the present analysis. The gravity force $F_{c\ gravity}$ is simply

$$\vec{F}_{c\ gravity} = -M_c\, g\ \vec{J} \tag{98}$$

This force is very small as compared to other forces except when the cage is under initial transient operation.

The equations of motion for angular motion are desired in the cage fixed frame, $X_cY_cZ_c$, which is also the principal axes system of the cage. The equations are therefore

$$\left(\frac{d\vec{h}_{oc}}{dt}\right)_{x_c,\ y_c,\ z_c} + \vec{\omega}_c \times \vec{h}_{oc} = \vec{M}_{oc} \tag{99}$$

where the subscript $_{oc}$ denotes quantities defined in the cage frame and

$\vec{h}_{oc}$ = angular momentum of the cage

$\vec{M}_{oc}$ = net moment acting on the cage

$$= \vec{M}_{c\ flange} + \vec{M}_{c\ unbalance} + \vec{M}_{c\ roller} + \vec{M}_{c\ other} \tag{100}$$

In component form, Equation (99) reads

$$\begin{aligned}
I_{cx}\ \frac{d\omega_{cx}}{dt} &= M_{cx} + (I_{cy} - I_{cz})\ \omega_{cy}\ \omega_{cz} \\
I_{cy}\ \frac{d\omega_{cy}}{dt} &= M_{cy} + (I_{cz} - I_{cx})\ \omega_{cz}\ \omega_{cx} \\
I_{cz}\ \frac{d\omega_{cz}}{dt} &= M_{cz} + (I_{cx} - I_{cy})\ \omega_{cx}\ \omega_{cy}
\end{aligned} \tag{101}$$

Equations (91), (99) and the extremely complicated forcing functions are solved simultaneously with the application of the modified Hammings predictor-corrector method. Note that the numerical procedures and final presentation of the data also involve frequent multiple transformations of the variables and coefficients from one coordinate system to another.

Development of a computer program, CADYN, based on this analysis is basically complete. The program was developed for analyzing the six-degree-of-freedom cage motion. The in-plane motion portion of the program has been fully debugged and is completely functional. Debugging of the six-degree-of-freedom version has yet to be completed.

CADYN, as it stands now, can nevertheless be used to establish

- Basic cage geometry
- Lubricant requirements
- Allowable cage unbalance
- Required rating of the lubrication system oil filter based on the oil film thickness.

CADYN can be used to predict the transient dynamics and steady-state motion of the cage so that stable operation can be maintained at the cage/land interface, and the minimum oil film thickness can be ascertained for compatibility with the rating of the oil filter selected for minimum wear. Thus the development of CADYN represents a significant achievement, since traditionally bearing cages have been designed without any consideration of cage dynamic performance.

2. Roller Dynamics Model

The force system acting on a roller is even more complex than that acting on a cage, as clearly indicated in figure 21. The forces considered in the work completed thus far are

- Hydrodynamic fluid pressure and shear generated at the roller/cage interface
- Hydrodynamic fluid and/or elastic forces at the roller/flange interface
- EHD forces at the roller/inner race and/or roller/outer race interface
- Gravitational force
- Unbalance force
- Inertia force.

Components of this primary force system are computed from various models established in the other sections of this report.

a. Coordinate Systems and Transformations

The coordinate systems selected for analyzing the roller dynamics problem are shown in figure 22. Similar to the cage coordinate system, the local coordinate xyz is a roller body frame of reference with its origin, O_r, fixed at the center of mass of the roller. Angular motion of the roller is to be analyzed in this reference frame. However, the translatory motion of O_r is to be determined with a cylindrical coordinate system, $R_r\theta_r Z_r$, which is rotating with an angular velocity $\dot{\theta}\vec{K}$ in the inertial reference frame. The position vector for O_r is

$$\vec{R}_r = R_r \vec{I}_r + Z_r \vec{K} \tag{102}$$

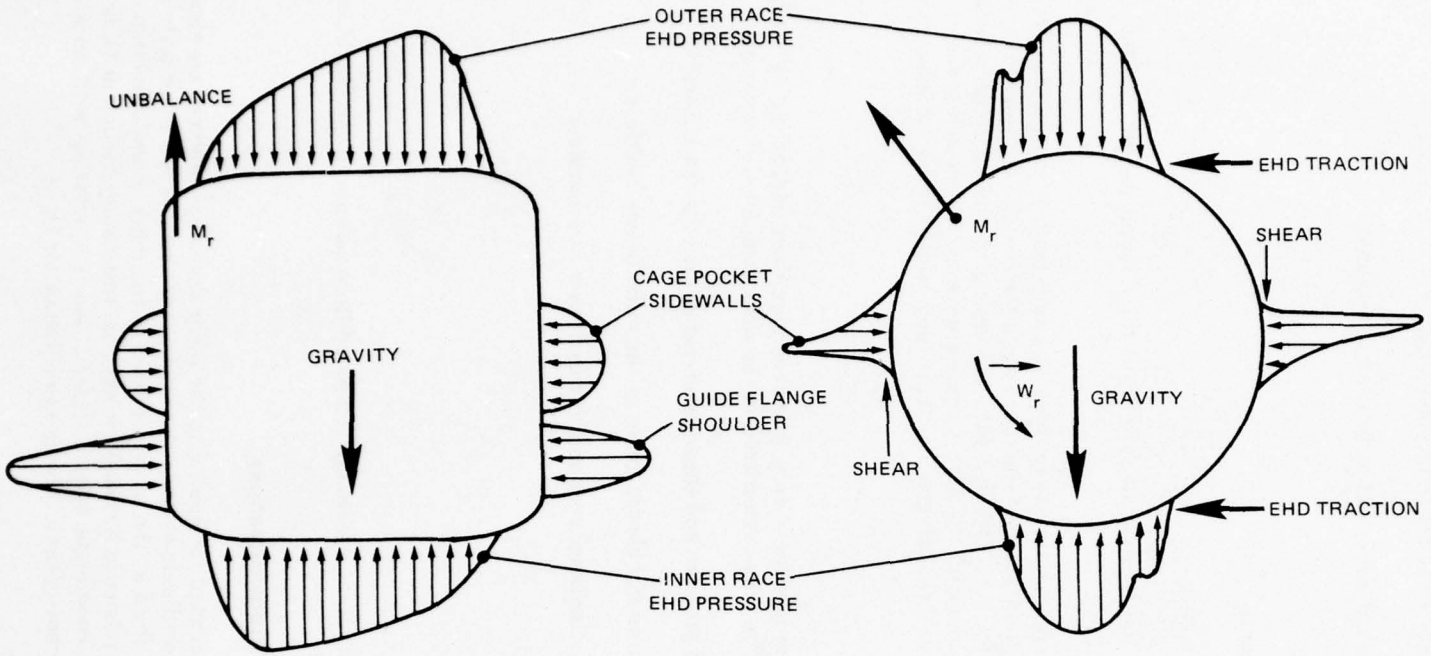

Figure 21. Primary Force System Acting on a Roller

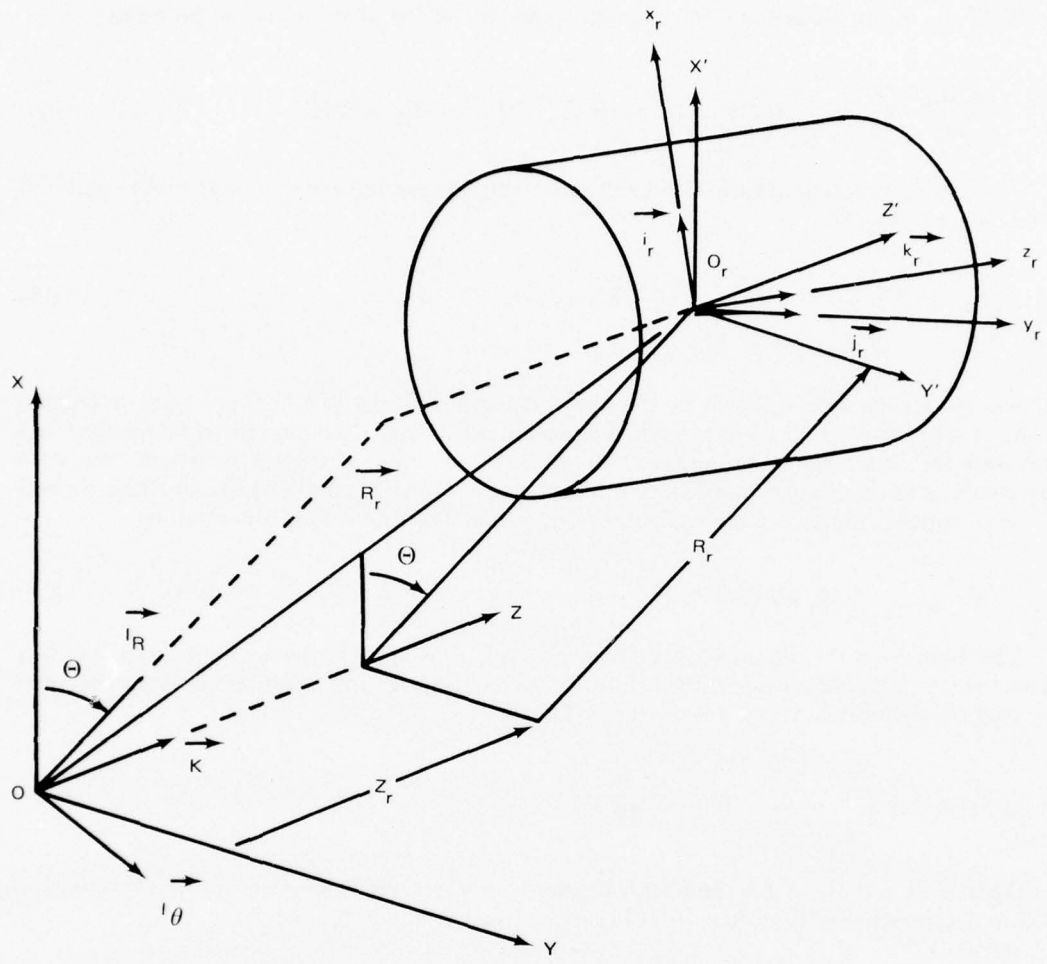

Figure 22. Roller Coordinate System

The Eulerian transformations of the $X_rY_rZ_r$ frame into the XYZ, and the X'Y'Z' frames are similar to those given in Equations (85) through (87). The relationship between the time derivative of the Eulerian angles and the angular velocities of the roller, and therefore the $X_rY_rZ_r$ frame of reference, expressed in terms of the local coordinate system, is similar to that given by Equation (90). Expressions for these functional relationships are therefore omitted here for conciseness.

b. Equations of Motion

Referring to figure 22, the translatory motion of the center of mass of the roller, O_r, is

$$M_{rk} \frac{d^2 \vec{R}_{rk}}{dt^2} = \vec{F}_{rk} \tag{103}$$

With the aid of Equation (102), the left-hand side of the above equation becomes

$$\frac{d\,\vec{R}_{rk}}{dt^2} = (\ddot{R}_{rk} - R_{rk}\,\dot{\theta}^2)\;\vec{I}_{rk} + (R_{rk}\ddot{\theta} + 2\dot{R}_{rk}\,\dot{\theta})\;\vec{I}_{\theta k} + \ddot{Z}\,\vec{K} \tag{104}$$

The forcing function in Equation (103) represents the net force acting on the roller and is of the following form:

$$\vec{F}_{rk} = \vec{F}_{rk\ cage} + \vec{F}_{rk\ flange} + \vec{F}_{rk\ inner\ race} + \vec{F}_{rk\ outer\ race} + \vec{F}_{rk\ gravity} + \vec{F}_{rk\ unbalance} + \vec{F}_{rk\ other} \tag{105}$$

Almost all the forces shown in the above equation are derived in some local coordinate system. It is necessary to transform each of these forces, such as those presented by the first four terms and the last term in Equation (105), from the coordinate system in which they were computed into the rotating cylindrical coordinate system $R\theta Z$. This may require, at times, several successive transformations of the variables in question. The gravity force is given by

$$F_{rk\ gravity} = M_k\,g\,(-\cos\theta_k\;\vec{I}_{rk} + \sin\theta_k\;\vec{I}_{\theta k}) \tag{105}$$

The expression for the unbalance force, $\vec{F}_{rk\ unbalance}$ is slightly more complicated. Let M_{rk} denote the jth unbalance mass in the kth roller and $\vec{r}_{rjk}$ and $\vec{R}_{rjk}$, its position vector in the roller body and the cylindrical frame respectively. Then

$$\vec{F}_{rk\ unbalance} = \sum_{j=1}^{m} m_{jk}\,\frac{d^2\,\vec{R}_{rjk}}{dt^2} \tag{107}$$

Since $\vec{R}_{rjk} = \vec{R}_{rk} + \vec{r}_{rjk}$ and both $\vec{R}_r$ and r_{rj} are in their respective rotating frames, the absolute acceleration in Equation (107) becomes rather complicated, i.e.

$$\frac{d^2\,R_{rjk}}{dt^2} = \frac{d^2\,\vec{R}_{rk}}{dt^2} + \vec{\alpha}_{rk} \times \vec{r}_{rjk} + \vec{\omega}_{rk} \times (\vec{\omega}_{rk} \times \vec{r}_{rjk}) \tag{108}$$

The differential equations governing the angular motion of the rollers are derived in the roller frame and are similar to Equation (101), namely:

$$\begin{aligned}
I_{rkx}\ \frac{d\,\omega_{rkx}}{dt} &= M_{rkx} + (I_{rky} - I_{rkz})\,\omega_{rky}\,\omega_{rkz} \\
I_{rky}\ \frac{d\,\omega_{rky}}{dt} &= M_{rky} + (I_{rkz} - I_{rkx})\,\omega_{rkz}\,\omega_{rkx} \\
I_{rkz}\ \frac{d\,\omega_{rkz}}{dt} &= M_{rkz} + (I_{rkx} - I_{rky})\,\omega_{rkx}\,\omega_{rky}
\end{aligned} \tag{109}$$

The moment components M_{rkx}, M_{rky}, and M_{rkz} represent the net contribution from the following:

- EHD film at the inner or outer race due to misalighment
- EHD or hydrodynamic films or dry contact reaction from the foller/flange shoulder interface
- EHD and/or hydrodynamic film, similar to those above, from the foller/cage pocket interface
- Mass unbalance
- Others.

Note that, again, these moments are computed in the local frame of reference and that they have to be transformed into the roller body frame before one may proceed to integrate these equations. The details of these transformations are not presented here due to their unusual length.

SECTION VI

COMPUTER PROGRAM DEVELOPMENT — TASK I

A. GENERAL DESCRIPTION

Development of the overall roller bearing design and simulation system is progressing smoothly. Updating or development of the following computer programs is practically complete:

- Quasi-static analysis computer programs
- Fluid-film contact simulation computer programs
- Transient and steady-state cage dynamics prediction computer programs

These programs can now be used independently in bearing design.

The roller dynamics program, RODYN, and the systems dynamics program, SYSDYN, have been developed in their basic forms and are currently being refined. The general philosophy adopted in the development of the programs is that user convenience is considered to be of the utmost importance. Emphasis is being placed on a number of user convenience-related factors as described in the following paragraphs.

1. Modularized Program Structure

Motion of the rolling elements and the cage is dictated by a complex force/moment system. Accurate prediction of these forces and moments requires an in-depth understanding of *interdisciplinary engineering subjects such as elasticity*, dynamics, heat transfer, thermodynamics, fluid mechanics and tribology. Many of the subjects involved could demand the work of one's lifetime as the technologies are not available at the present time.

Under these circumstances, P&WA conceived and elected to develop the required computer progams based upon a "modular" or "building block" concept. The basic thinking employed is to break up the entire program into a number of interacting computer "modules." Each module is to provide information obtained from one of the analytical models which, in turn, is developed according to the latest state-of-the-art in the related disciplines. In some instances it was found necessary to develop an entirely new and original analysis not available elsewhere. The advantage of employing this type of modular concept is apparent. Above all, this will permit one to update the individual modules, as needed, to reflect technological advances and developments in a specific area without having to change and sometimes disturb the entire system.

The entire program, hereafter referred to as *TRIBO I*, consists of various levels of computer modules as illustrated symbolically in figure 3. The main program, TRIBO I, is a command module which controls the flow of the entire program and the general input/output. There are two major first-level management programs, STATIC and SYSDYN, controlling input/output and computation related to the static and the dynamic analyses respectively. Each of these programs is supported by a certain number of second-level management programs such as RODYN and CADYN which are simulating, respectively, the roller and cage dynamics. These programs are further fed by a cluster of lower-level management or working programs, and so on.

2. Partial Computation

During the course of the investigation, it became apparent that because of the complexity of the system, the computer time required to run the entire program in its final form may be as high as several hours per case. It was decided, therefore, to structure TRIBO I in such a way as

to allow partial computation. This was done in recognition of the fact that substantial cost savings could be realized if some of the individual modules could be used independently to provide preliminary design of the bearing components. The larger main computer program could then be used to zero in on the final detailed design configuration of the bearing system.

The cage dynamics computer program, CADYN, for example, is one of the modules that can be used to establish the basic cage geometry, lubricant requirements, allowable cage unbalance and required rating of the oil filter.

3. Interaction with User-Supplied Systems or Data

Provisions have been made in the computer program to allow the user to supply certain items. For example, the structural and/or thermal analysis of a bearing may require the use of complex, large-scale computer programs such as those developed on the basis of finite-element methods. The subject computer analysis allows interaction with such programs. The user may also elect to supply externally generated data for inclusion in the program.

4. Internally Supplied Optional Programs

Because of the concern over the computer time required to run such a large scale program, it has been the intent of this effort to develop subprograms based upon simplified or approximate solutions for certain purposes such as the estimation of structural flexibility. The user may elect to use either this option, or supply direct input of externally generated data, or connect this program to another external program. The simplified analyses are found to be quite adequate for most applications, especially during the early design stage of bearing development.

5. Computational Efficiency

It is anticipated that use of the entire computer program will be relatively time-consuming as a result of the complexity of the physical problem. One of the objectives is, therefore, to seek acceptable approximate closed-form solutions to reduce computational time. This quite often demands a compromise, as a balance is sought between accuracy and computational time.

6. Automatic Time-Step Adjustment and Cutoff

An algorithm is built into the program to select the best estimate of time steps to realize fast convergence when integrating the dynamic equations of motion for the system or the components.

7. User-Oriented Output

The user can also select presentation of the output in either printed or plotted form. Also, the printed output can be obtained in a condensed summary form or in its entirety at the discretion of the user.

B. PROBLEM SOLVING CAPABILITY

As mentioned previously, several of the subsections within TRIBO I are operational and already can be used individually in the bearing design process.

1. Static Program

STATIC is the overall quasi-static roller bearing optimization program. The program capability has been discussed in the analysis section and is summarized here for completeness. The program in its existing form contains the following features:

- Basic elasticity analysis
- Preload/out-of-roundness calculation
- Ring and structural flexibility
- Misalignment and-moment load
- Built-in material properties
- Built-in Type I and II oil properties
- Static skew analysis
- Roller optimization
- Oil flow optimization.

As a result of this effort, STATIC has become the most advanced and powerful roller bearing design tool available to date. STATIC was employed to design the geometry of the basic bearing used in the experimental test portion of this program.

2. CADYN Program

The transient dynamic and steady-state motion of the bearing cage is predicted by CADYN. The in-plane motion portion of this program is fully operational. During the course of its development, the uncoupled cage motion was checked against results available from the literature as shown in figure 23. The agreement is extremely good. The six-degree-of-freedom portion of the program is still under development. Nevertheless, CADYN, as it stands now, can be used to establish:

- Basic cage geometry
- Lubricant requirements
- Allowable cage unbalance
- Required micron rating of the oil filter.

The objective is to ensure stable operation of the cage and maintain an adequate oil film at the cage/land interface for minimum wear. Until recently, the bearing cages have been designed by bearing manufacturers without any consideration of their dynamic performance.

Two examples are given here to illustrate the usefulness of CADYN. The basic bearing assumed is a 124 mm bore cylindrical roller bearing. The baseline conditions assumed for these cases are:

Ratio of Roller Diameter to Inner Race Diameter	=	1/9
Cage Bore Diameter	=	5.678 in.
Radial Clearance	=	0.009 in.
Cage Land Width	=	0.140 in.
Initial Displacement in the X-direction	=	0.000 in.
Initial Displacement in the Y-direction	=	−0.799 in.
Initial Velocity in the X-direction	=	0.000 in./sec
Initial Velocity in the Y-direction	=	0.000 in./sec
Cage Mass	=	0.4153 lb_m
Lubricant Viscosity	=	4.6×10^{-7} lb-sec/in.^{2}

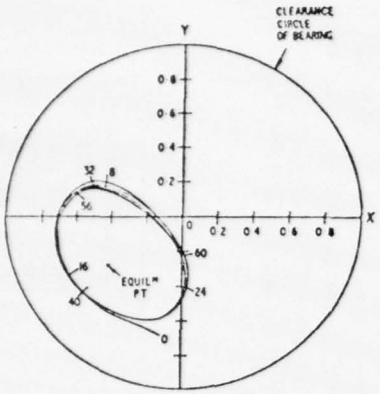

REPRODUCED FROM ASME TRANSACTION (REF. 14)

AKERS, MICHAELSON & CAMERON

- FINITE BEARING

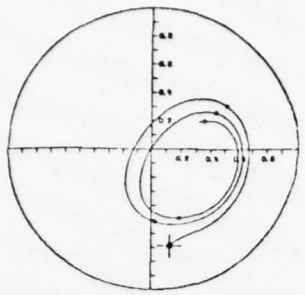

REPRODUCED FROM ASME TRANSACTION (REF. 15)

GUNTER & KIRK

- SHORT BEARING

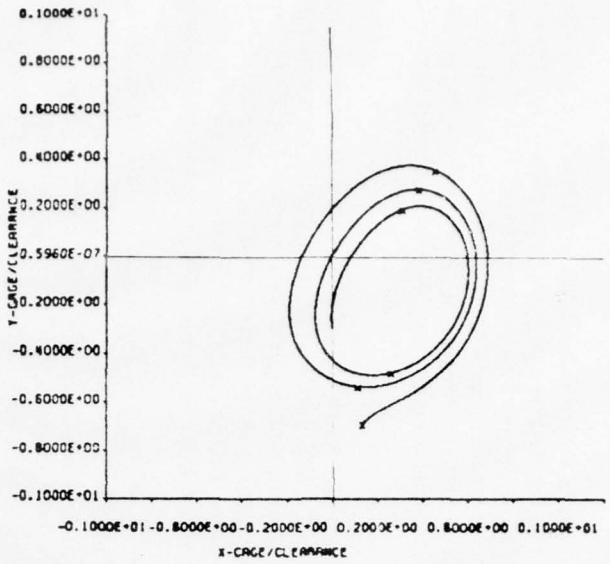

P&WA

- SHORT BEARING

Figure 23. Comparison of Cage Transient Motion

a. *Example 1: Effect of Cage Speed*

For these examples, the shaft speed is varied from 3,000 to 24,000 rpm and the cage is perfectly balanced. The results corresponding to this case have been plotted in figure 24 which shows that the cage analyzed will operate with a good sized minimum oil film of several mils up to approximately 13,500 rpm. A further increase in shaft speed causes the minimum oil film to drop abruptly indicating the onset of hydrodynamic instability. Experience from rotor dynamics technology suggests that one should avoid operating rotating components under such potentially hazardous conditions.

The results show that the minimum oil film thickness drops down to approximately 0.1 to 0.15 mil in the speed range of 16,500 to 24,000 rpm. This should prompt an assessment of the adequacy of the system oil filter. The procedure to be used is to compare the minimum oil film thickness in this range with the absolute rating of the proposed oil filter. Examination of figure 24 makes it apparent that a 2 μm absolute filter is probably needed to ensure that dirt or wear debris contained in the oil could pass through the oil film freely without causing cage wear.

There is some uncertainty about the validity of the theory in these extremely thin film regions, e.g. whether or not the finite whirl orbit is indeed a limit cycle, or just a mathematical solution which is not necessarily valid in reality. It is advisable therefore to redesign the cage under these circumstances in order to minimize the risk. If it is not possible to redesign the cage or prevent it from operating in this region, then an oil filter with the finest particle size rating available should be used. Furthermore, operation of this bearing should be monitored very closely.

b. *Example 2: Effect of Cage Clearance and Unbalance*

The effects of both cage clearance and unbalance were also studied to provide the design engineer with information needed for selecting the proper cage clearance and establishing the allowable unbalance level for stable operation of the cage so as to avoid undue wear damage. The results plotted in figure 25 show that in general the cage minimum oil film thickness decreases with increasing radial clearance. It is interesting to note that the rate of reduction for the 10-gm-cm unbalanced cage is less than that for a perfectly balanced cage. Again, the data indicate that a "super" filter is needed to exclude dirt and wear debris that could bridge the oil film, causing surface damage.

3. RODYN Program

Development of the roller transient dynamic and steady-state motion simulation system is essentially complete. The program has been checked out for the case of an uncoupled single roller moving within concentric raceways. The geometry used for the test case was taken from a typical 124 mm cylindrical roller bearing. The roller was assumed to move momentarily from a set of arbitrary initial conditions under the influence of EHD traction forces at the contact points. It was anticipated that the motion of the roller would reach a steady state corresponding to the no-slip condition regardless of its initial conditions. Without going into excessive detail, the results are tabulated here for comparison.

	Spin Velocity (rpm)		*Orbital Velocity (rpm)*	
Case	*Initial*	*Final*	*Initial*	*Final*
1	100,000	126,500	8,000	10,950
2	150,000	126,500	8,000	10,950
3	100,000	126,500	14,000	10,950
4	150,000	126,400	14,000	10,960
No-slip	—	126,600	—	10,960

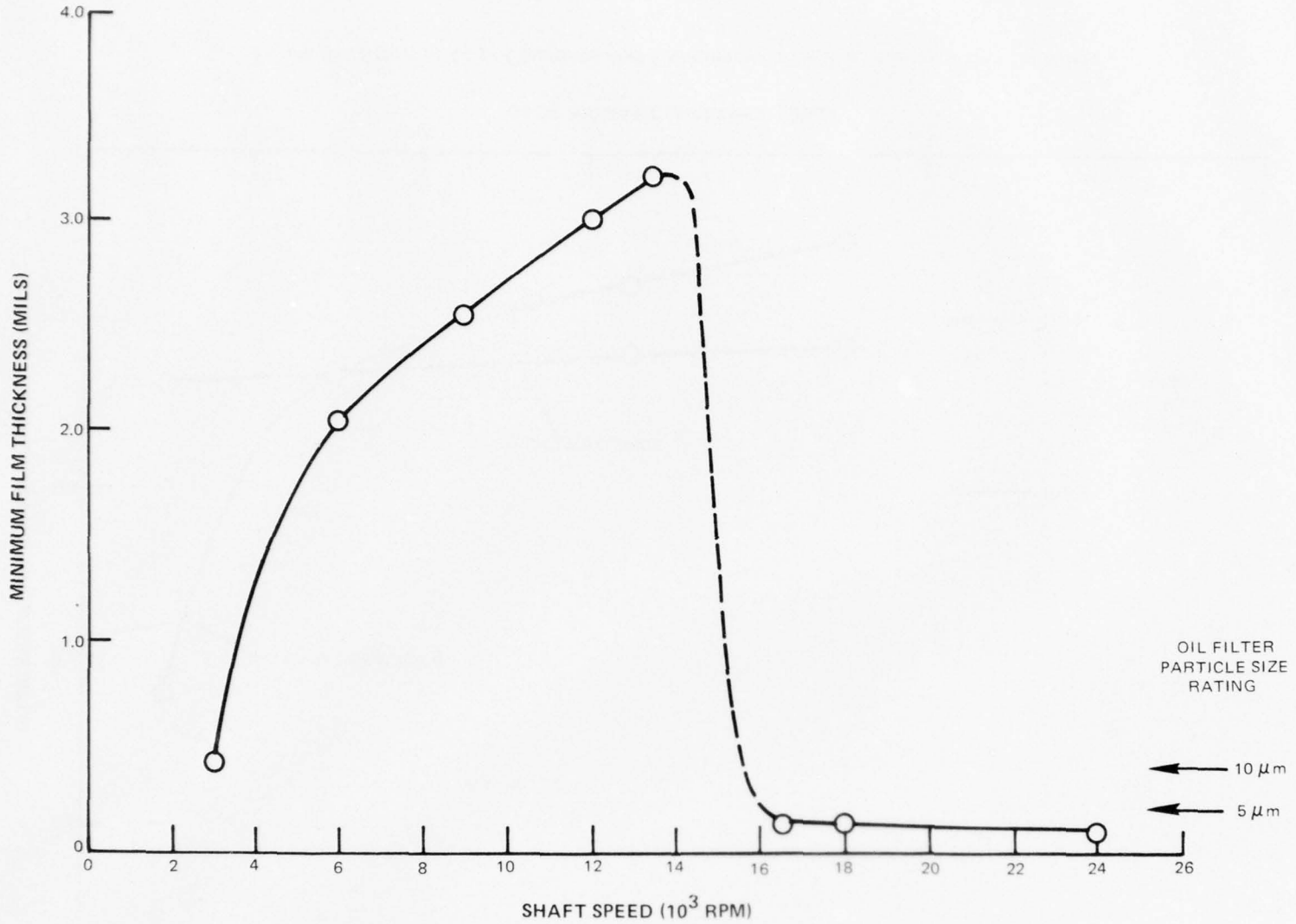

Figure 24. Effect of Shaft Speed on Cage Minimum Film Thickness

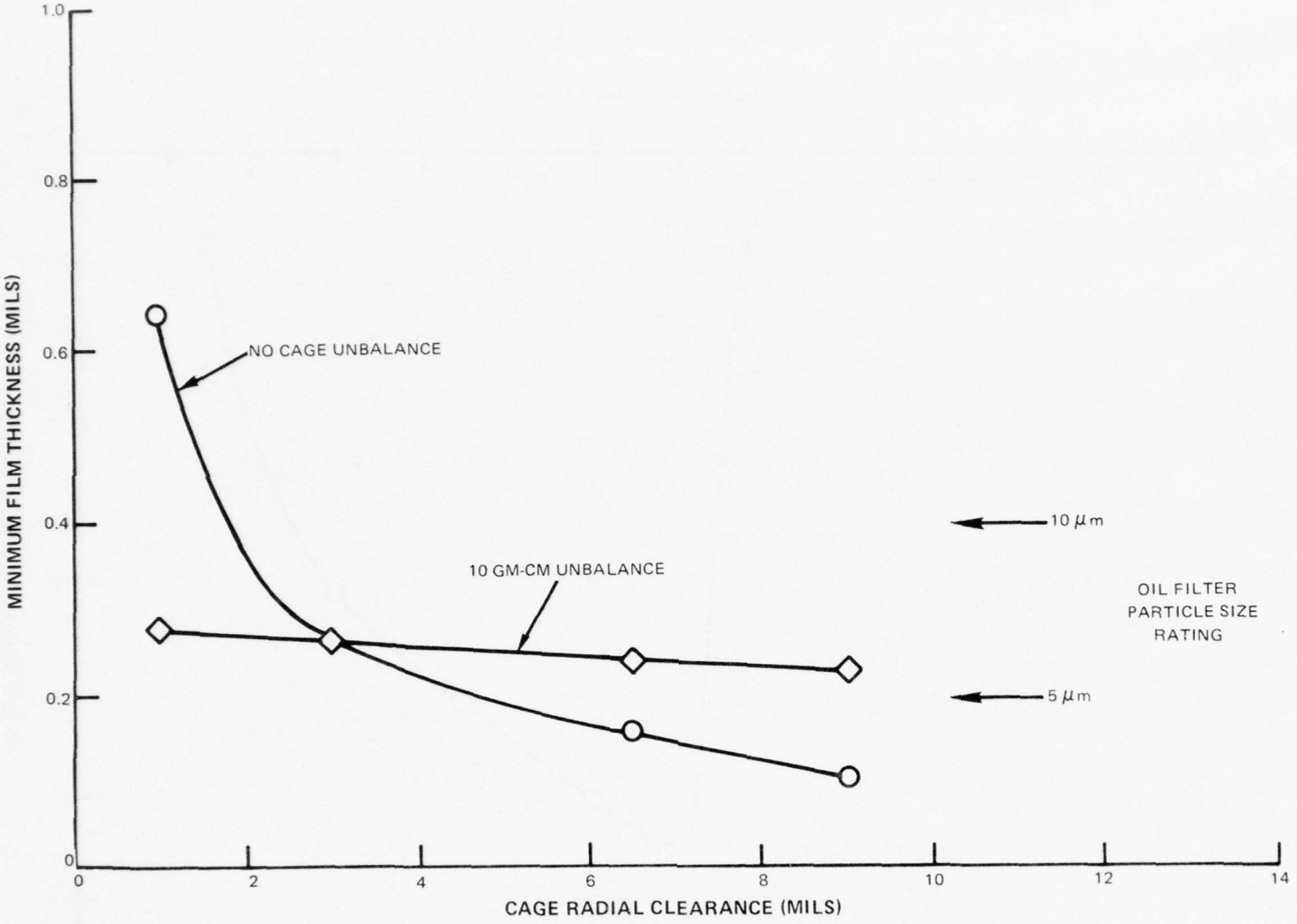

Figure 25. Effect of Cage Clearance and Unbalance on Cage Minimum Film Thickness

It is obvious that the results are consistent with what one expects from such a physical situation. Further refinement of the computational system is currently underway.

4. SYSDYN Program

This program integrates the CADYN and RODYN computer modules and permits full interaction among the relevant bearing components. The program is operational for the following combined modes of operation:

Shaft	• Center fixed in space • Constant rotational speed
Cage	• Spinning Motion • Whirling Motion
Rollers	• Spinning motion • Orbital motion • Skewing motion

The results for a simple model test case, consisting of the raceways, cage, and four hypothetical rollers, show that the program is working properly. Work on further refinement to the program is progressing as planned.

SECTION VII
PARAMETRIC AND VERIFICATION TESTING — TASK II

A. PARAMETER SELECTION

The main obstacle to advancing high speed roller bearing technology is related to roller element skewing and skidding and the resultant wear and surface damage. Those bearing variables that are considered as having an influence on roller skew and skid have been identified in this study. Quantification of the influence of these variables is the objective of the experimental portion of this program. A total of 30 separate variables were identified and are shown in table 2. Operational variables, such as bearing speed, externally applied load, or lubricant temperature, were not counted in this total. The basic categories considered were design geometries, including internal lubrication arrangements, manufacturing tolerances, and quality control variables.

It was apparent that any experimental program of reasonable scope could not address a thorough evaluation of all 30 variables. Therefore, some judgement had to be made as to the relative importance of these variables in order to reduce the list to manageable proportions. Applying certain criteria, the list of 30 variables was divided into three categories, which are also identified in the table. Category I includes 14 variables that are considered to have the greatest direct influence on the roller bearing wear phenomena normally identified as skidding damage and roller end wear of either the uniform and concentric type or of the uneven and eccentric type. Category II is composed of eight variables considered to have less direct impact on wear, and Category III is composed of eight variables judged to have the least direct effect. The criteria employed in making these assessments, although somewhat subjective, were based, in a large measure, on experience available from experimental test results and from field service reports, in addition to analytical studies, manufacturing surveys and an understanding of the physical phenomena affecting fundamental bearing behavior.

Two groups of bearings were selected for evaluation in a statistically designed experiment. Each group incorporated parameters from table 2 which could be varied in a sensible manner. By varying the parameters in a planned manner, it is possible with statistical experiments to isolate and rank the effect produced by any one parameter on surface damage due to roller skidding and skewing.

A statistically designed test program incorporating the fractional factorial method was selected. Table 3 shows the number of main effects and the number of interactions that can be determined with programs consisting of 5, 6, 8 and 10 bearing designs with variations in the number of bearing parameters to be studied. For each parameter the level of variation was maintained at two. The combination of eight test bearing designs was chosen for Group-N which is to be evaluated under Task II of the Contract. This choice was dictated largely by cost considerations. Seven was the number of parameters chosen for investigation so that the maximum number of main effects could be evaluated. The seven parameters to be studied with the Group-N bearings were all selected from Category I of table 2. These variables are the following:

- Bearing preload
- Coupled roller end radius runout
- Roller end circular runout to roller outer diameter
- Inner race taper
- Roller flat centrality
- Raceway angular misalignment
- Lubrication flow

TABLE 2. RELATIVE RANKING OF ROLLER BEARING VARIABLES

Roller Bearing Variable	*Possible Effect of Variation*	*Rationale*
CATEGORY I:		
Roller Length/Diameter Ratio	Uneven roller end wear	Alters roller element gyroscopic action stability achieved by L/D ratio of 0.87.
Roller Unbalance (Nonhomogeneous material, roller end run out, crown radius run out)	Uneven roller end wear	Alters skewing forces as rollers impact guide flanges.
Preload	Controls skidding and can reduce damage on roller surfaces and raceway surfaces.	Roller element skids or slips "out of gear" due to insufficient loading.
Cage Unbalance	Local cage bore wear for inner land guided cage, end wear adjacent roller(s) and skidding damage.	Rub causes local overheating and decreases effectiveness of oil film.
Roller Flat Centrality	Uneven roller end wear	Alters tractive force profile of roller as well as stability about transverse axis due to unsymmetrical roller mass distribution.
Roller End Squareness	Uneven roller end wear	Affects roller stability about transverse axis and modifies roller end face contact stress.
Roller End Shape	Uneven and concentric roller end wear.	Alters lubrication film and roller end contact stresses.
Raceway Taper	Concentric roller end wear	Alters distribution of roller tractive forces.
Roller End Clearance	Uneven roller end wear	Alters maximum roller skewing angle thus changing end face contact forces.
Roller Diameter Variation	Uneven roller end wear/ roller skid damage	Alters maximum roller skewing angle/ alters roller tractive forces.
Lubrication	Uneven and concentric roller end wear, roller skid damage, cage wear.	Alters effective oil film thickness.
Flange Height	Uneven and concentric roller end wear	Alters roller skewing angle and roller end contact stress and location.
Raceway Angular Misalignment	Concentric roller end wear/ reduced fatigue life	Alters roller tractive forces and distribution/alters roller load profile.
Percent Flat Length of Roller	Fatigue life and uniform end wear	Alters roller load profile, tractive forces and skewing moment.
CATEGORY II:		
Roller Clamping Load	Concentric roller end wear	Reduction in roller end clearance due to guide flange deflection alters oil film thickness and roller end contact profile.

TABLE 2. RELATIVE RANKING OF ROLLER BEARING VARIABLES (CONTINUED)

Roller Bearing Variable	*Possible Effect of Variation*	*Rationale*
Flange Face Run Out	Uneven roller end wear	Alters maximum roller skewing angle and dynamic end face loads.
Roller Crown Radius	Fatigue life and concentric roller end wear	Alters roller load profile, modifies tractive forces and skewing moments.
Extended Roller Flat Length	Fatigue life and uniform end wear	Alters roller load profile, tractive forces and skewing moment.
Flange Face Waviness	Uneven roller end wear	Alters maximum roller skewing angle and dynamic end face loads.
Flange Layback Angle	Uneven roller end wear/ concentric roller end wear	Alters maximum roller skewing angle oil film thickness and location of end face contact area.
Roller-Cage Pocket Clearance	Uneven roller end wear	Affects transmission of any cage instability altering roller-to-guide flange contact loads and tractive forces.
Flange Contour	Uneven roller end wear/ concentric roller end wear	Alters maximum roller skewing angle oil film thickness, and roller end contact area and location.
CATEGORY III:		
Roller Length Variation	Uneven roller end wear	Alters maximum roller skewing angle
Cage Pocket Offset	Not apparent unless extreme, causing uneven roller end wear	Alters resultant skewing force of roller element.
Roller End Surface Finish	Uneven and concentric roller end wear	Alters oil film thickness requirements at roller ends.
Flange Surface Finish	Uneven and concentric roller end wear	Alters oil film thickness requirements at roller ends.
Raceway Surface Finish	Skid damage	Alters roller tractive forces and oil film thickness requirements at roller raceway contacts.
Cage Pocket Squareness	Concentric roller end wear	Alters resultant skewing force acting on roller element.
Raceway Waviness	Skid damage	Imposes dynamic loads on roller affecting variations in tractive forces and oil film thickness requirements at contacts.
Roller Taper	Uneven roller end wear	Alters tractive force profile of rollers as well as roller stability about transverse axis due to unsymmetrical mass distribution.

The second group of bearings, which will be evaluated under Task VI, were designated as Group-AF. The scope of this portion of the program limited the size of this group to five individual bearing designs. Four is the maximum number of parameters for which the main

effects can be investigated employing five bearing designs. These four parameters, selected from Category II, are: inner ring guide flange layback, inner ring guide flange contour, inner ring guide flange run out, and extended roller flat length.

TABLE 3. PARAMETRIC STUDY POSSIBILITIES

No. of Test Assemblies	*No. of Parameters of 2 Levels To Be Investigated*	*Remarks*
10	9	Main Effects Can Be Determined
	8	Main Effects and One Interaction Can Be Determined
	7	Main Effects and Two Interactions Can Be Determined
	6	Main Effects and Three Interactions Can Be Determined
8	7	Main Effects Can Be Determined
	6	Main Effects and One Interaction Can Be Determined
	5	Main Effects and Two Interactions Can Be Determined
6	5	Main Effects Can Be Determined
	4	Main Effects and One Interaction Can Be Determined
5	4	Main Effects Can Be Determined

B. DESIGN OF PARAMETRIC BEARINGS

The basic roller bearing selected for the design of the parametric bearings is shown in figure 26. This bearing is used in the No. 5 mainshaft position of the TF30 model production engine and has accumulated many thousands of hours of successful rig and engine operation. In addition, this design includes geometric and tolerance control features directed at minimizing roller skewing and skidding.

Using the partial factorial statistically designed experiment approach, the eight bearing designs that are necessary to incorporate the seven study parameters with two levels of variation each were prepared. The combinations of the variables for these eight Group-N bearings were established by the matrix shown in table 4. Here the two levels of parameter variation are represented by the symbols H and L, for high and low. Initially this matrix was prepared with one bearing design distributed in each of the eight vertical columns in such a manner that the main effects of each variable could be determined. However, limitations in manufacturing and inspection capabilities made it necessary to alter the arrangement of the test variables which resulted in the matrix as shown in table 4. It is anticipated that it will be possible to determine the main effects of five or six of the Group-N variables, and with an additional test combination, the main effects of all the variables may be determined. The actual levels of the parameter variation for each of the Group-N designs, as well as the basic or baseline bearing, are presented in tabular form in figure 27. These levels were established on the basis of experimental, analytical, manufacturing, and production experience. The parameters of the Group-N bearings which were not being studied were maintained at the level used in the basic bearing. Figure 27 also classifies the variable parameters as either design or tolerance controlled. The design parameters are those whose levels of variation are established by the design process, whereas the variation levels for the tolerance parameters are established by roller bearing manufacturing capabilities.

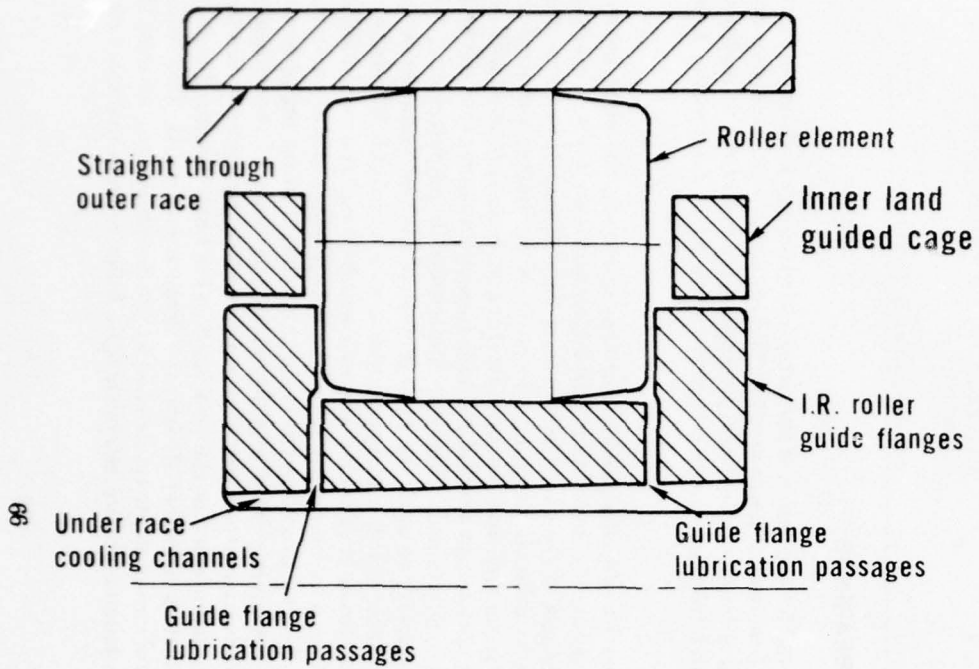

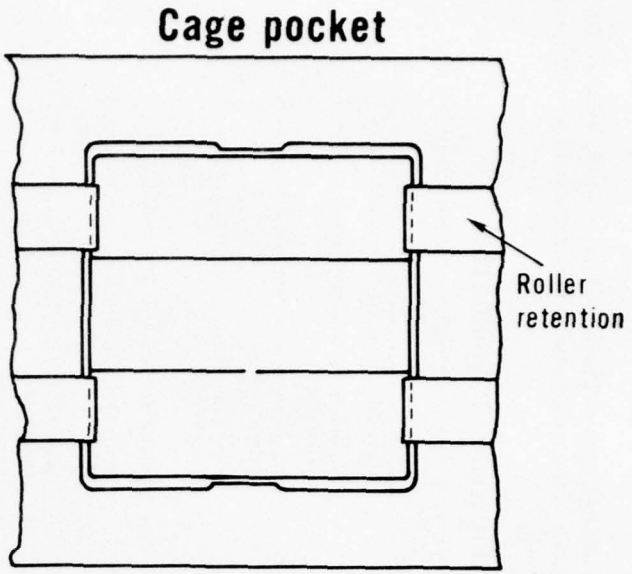

Inner race bore dia.	: 124.3mm
Basic roller size, L/D	: 13mm X 13mm
No. of rollers	: 28
No. of radial lube holes	: 3 per side
Bearing material	: VIM-VAR M-50

Cage material : AMS-6414
Cage plating : Silver per AMS-2412

Figure 26. Basic Bearing for Parametric and Verification Testing

TABLE 4. TEST MATRIX — GROUP-N PARAMETRIC BEARINGS

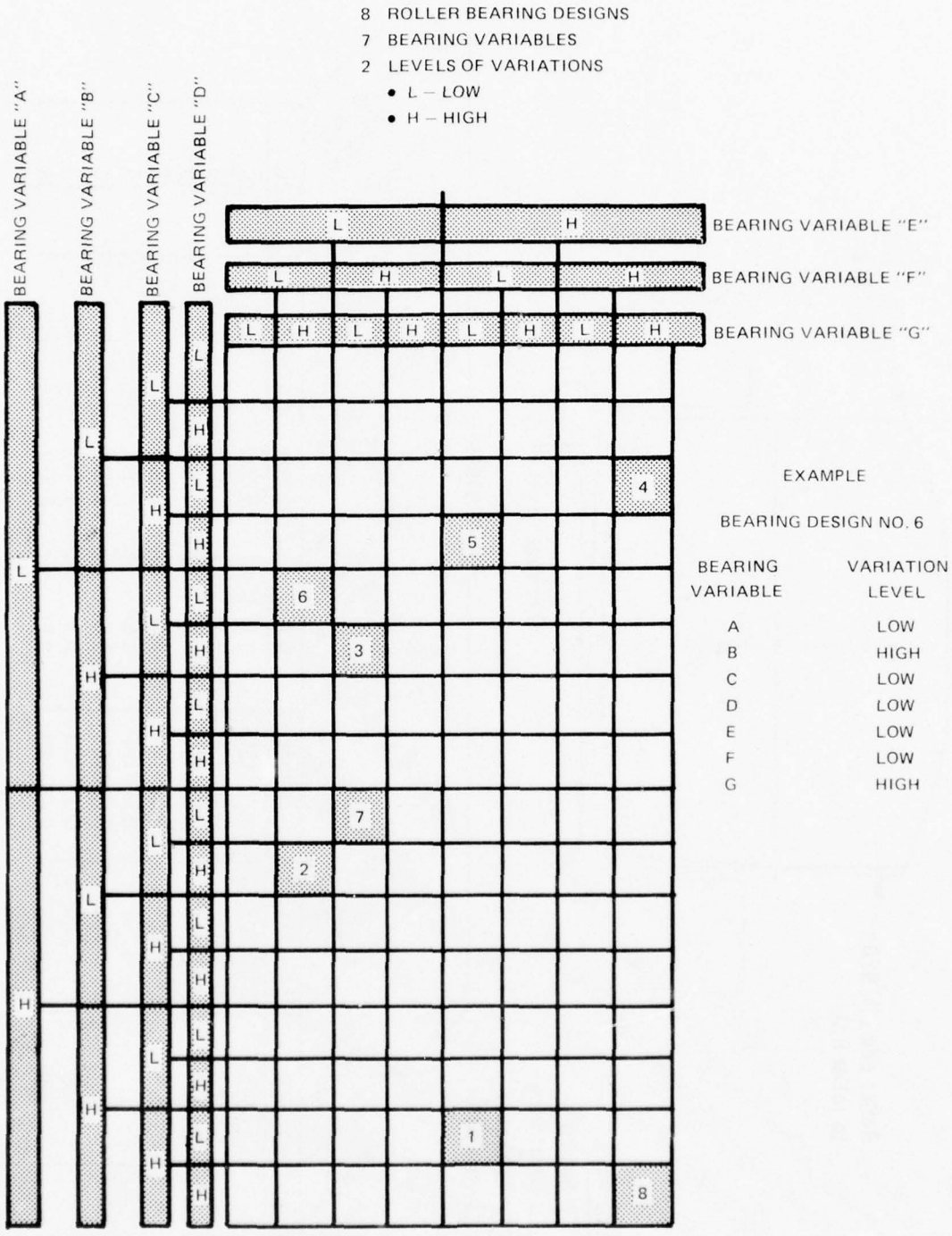

NOTE: NUMBERS IN MATRIX INDICATE BEARING IDENTIFICATION NUMBERS

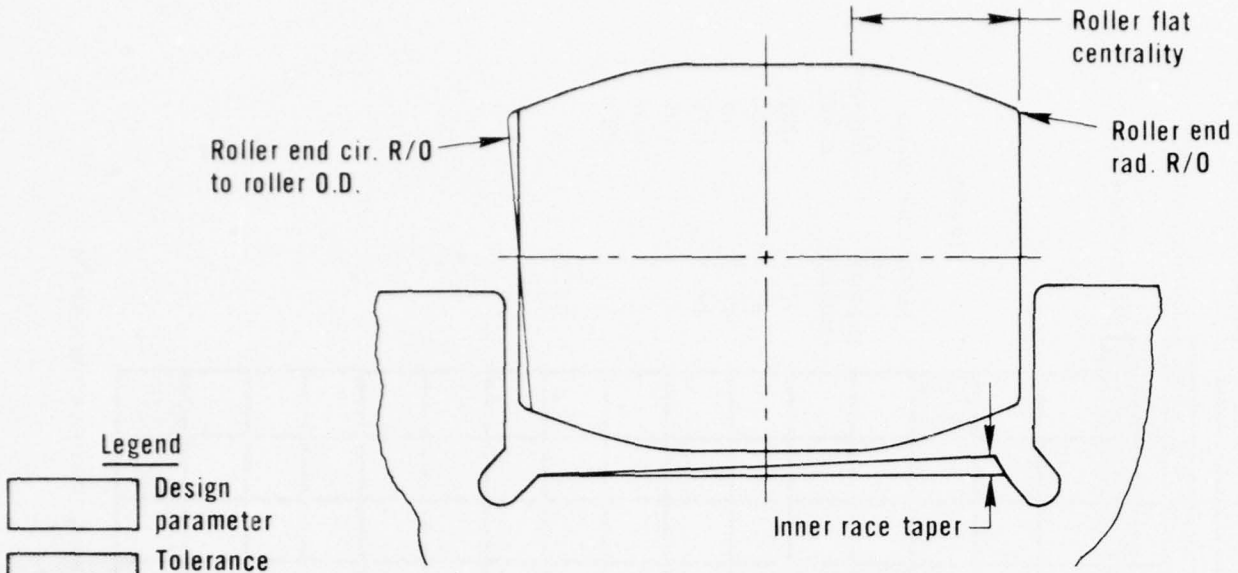

Parameters

Bearing serial no.	Bearing preload, lbs.	1. Max. coupled roller end radius R/O inch	2 Roller end cir. R/O to roller O.D., inch	3 Inner race taper minutes	4 Roller flat centrality, inch	5 Raceway angular misalignment degree	6 Lubrication flow, lb/min.	7
Baseline	500	0.001	0.000120	0.8	0.010	0	20	
1	500	0.005	0.000180	0.8	0.050	0	10	
2	500	0.001	0.000050	3.58	0.010	0	30	
3	0	0.005	0.000050	3.58	0.010	0.5	10	
4	0	0.001	0.000180	0.8	0.050	0.5	30	
5	0	0.001	0.000180	3.58	0.050	0	10	
6	0	0.005	0.000050	0.8	0.010	0	30	
7	500	0.001	0.000050	0.8	0.010	0.5	10	
8	500	0.005	0.000180	3.58	0.050	0.5	30	
9	Same as No. 7							
10	Same as No. 8							

Figure 27. Group-N Parametric Bearing Designs

Employing a procedure similar to that conducted for establishing the Group-N bearing designs, the Group-AF bearing designs were next prepared following the matrix shown in table 5. This matrix will permit the main effects of each of the four parameters to be studied. Figure 28 shows the actual levels of parameter variations for each of the Group-AF designs as well as for the basic or baseline bearing. Again, as in the case of the Group-N bearing design, the parameters not being studied were maintained at the same level used in the basic or baseline bearing.

C. PROCUREMENT OF BEARING HARDWARE

The bearing manufacturer selected to fabricate the two groups of parametric bearings was the Split Ballbearing Co. (SBB), Division of MPB Corporation. SBB is a producer of the basic No. 5 mainshaft position roller bearing used in production TF30 engines. In addition, SBB has supplied experimental hardware of the basic 124.3 mm bearing which has been evaluated in baseline tests to speeds of 3.0 MDN.

A total of 10 Group-N parametric bearings were manufactured for testing by SBB. One each of the eight designs shown in figure 27 and two duplicate bearings for repeat testing were procured. The bearings selected for repeat testing were those identified as No.'s 7 and 8 in figure 27.

Split Ballbearing Co. manufactured a total of six Group-AF bearings for test. One each of the five designs shown in figure 28 was produced and a duplicate of bearing No. 22 was manufactured for repeat testing.

For each of the Group-N and Group-AF bearings, detailed dimensional measurements of the bearing components were made and recorded by SBB. This was done to ensure the tight quality control required as dictated by the demands of any statistically planned program and to assist in the post-test analysis of the experimental results. Some of the specific measurements that were provided were:

- Dimensions on each roller (all rollers being serialized to facilitate identification) — length, diameter, corner radius runout, crown radius, length of central cylindrical section, flatness of central cylindrical section, off-set of central cylindrical section, roller end circular runout, and crown drop
- Diameters of the inner and outer rings
- Inner and outer raceway eccentricity and taper
- Roller guide shoulder parallelism
- Cage-pocket squareness and parallelism
- Roller guide flange angle
- Unmounted internal radial clearance
- Cage land clearance
- Surface finish of rollers, raceway and guide shoulders
- Cage unbalance
- Roller-to-guide flange clearance.

The inspection data which accompanied each of the Group-N and Group-AF bearings were reviewed and no significant deviations were uncovered. Since up to 94 pages of inspection results were provided for each bearing, the inclusion of a complete compilation of this data in this report would be unrealistic. However, a summary of these inspection results has been provided in tables 6 and 7 with average measurements shown where possible.

TABLE 5. TEST MATRIX — GROUP-AF PARAMETRIC BEARINGS

5 ROLLER BEARING DESIGNS
4 BEARING VARIABLES
2 LEVELS OF VARIATION
- L – LOW
- H – HIGH

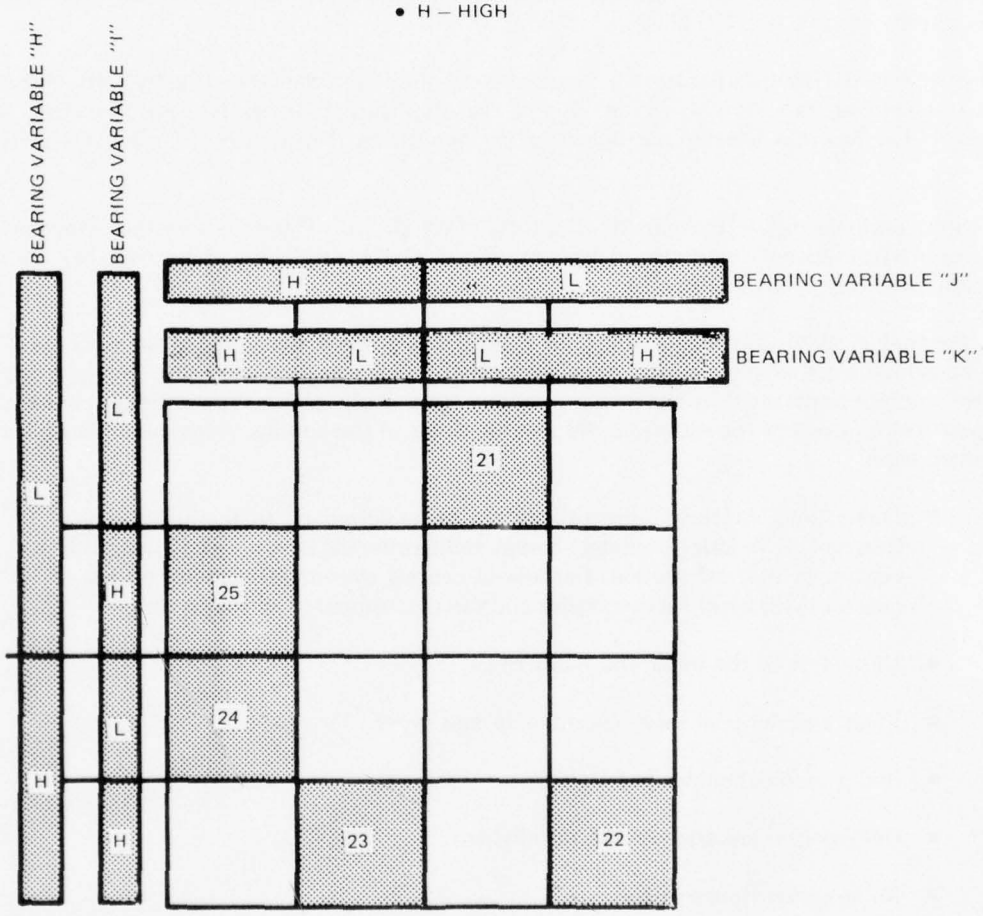

NOTE: NUMBERS IN MATRIX INDICATE BEARING IDENTIFICATION NUMBERS

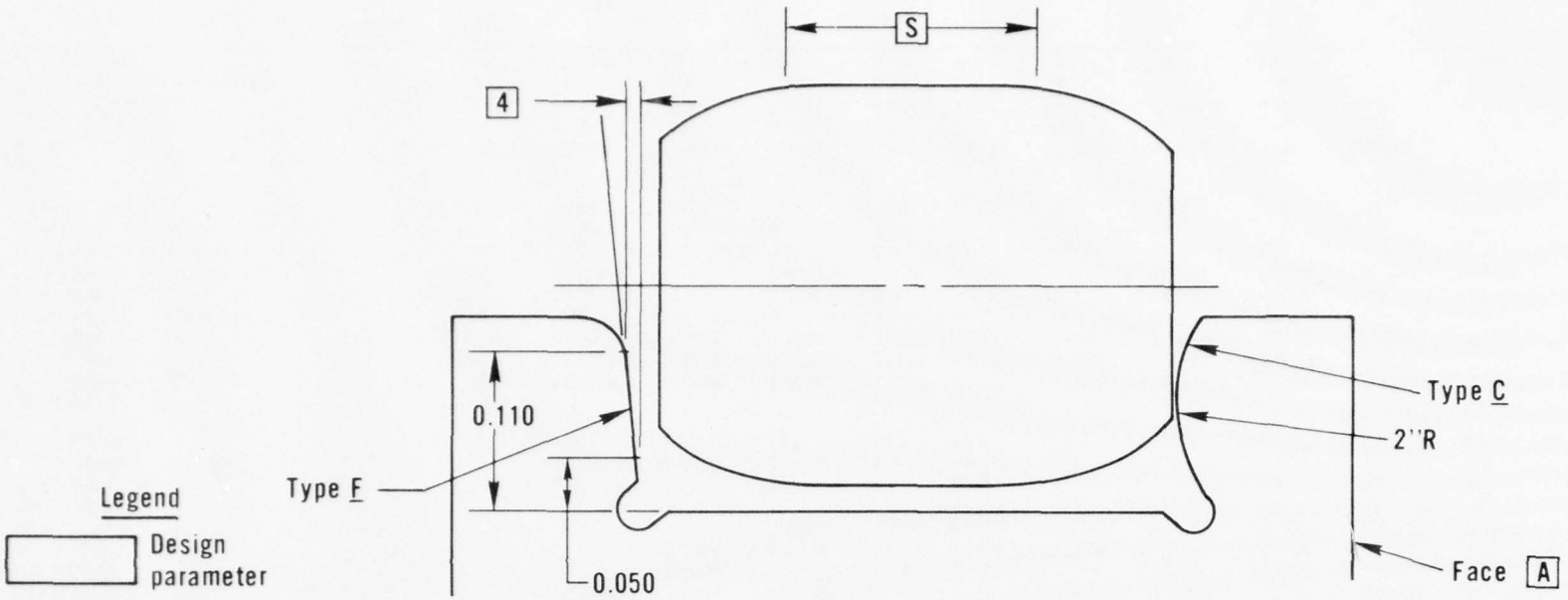

Bearing no.	Extended roller flat, % of roller length, S	IR guide flange layback, inch 4	IR guide flange contour	IR guide flange runout to face A, inch, max.
	Parameters			
Baseline	40	0.00025 max.	Type F	0.0004
21	48	0.00025 max.	Type F	0.0004
22	67	0.0009-0.0011	Type F	0.0020
23	67	0.0009-0.0011	Type C	0.0004
24	67	0.00025 max.	Type C	0.0020
25	48	0.0009-0.0011	Type C	0.0020
26	Same as No. 22			

Figure 28. Group-AF Parametric Bearing Designs

TABLE 6. SUMMARY OF MANUFACTURING INSPECTION DATA — GROUP-N BEARINGS

	Bearing Number										
	B/L	*1*	*2*	*3*	*4*	*5*	*6*	*7*	*8*	*9*	*10*
Bearing Assembly											
Cage Clearance, in.	0.0176	0.0177	0.0193	0.0172	0.0175	0.0170	0.0182	0.0179	0.0190	0.0170	0.0182
Roller End Clearance,in.	0.0012	0.0012	0.0010	0.0013	0.0009	0.0010	0.0012	0.0011	0.0011	0.0014	0.0011
Internal Radial Clearance (Unmounted), in.	0.0040	0.0045	0.0044	0.0043	0.0042	0.0044	0.0042	0.0039	0.0046	0.0042	0.0052
Rollers											
Length, in.	0.51175	0.51188	0.51162	0.51168	0.51160	0.51160	0.51190	0.51176	0.51150	0.51169	0.51181
Diameter, in.	0.51166	0.51194	0.51168	0.51170	0.51137	0.51139	0.51140	0.51173	0.51194	0.51174	0.51134
Surface Finish (AA), μin.	—	3.5	2.5	1.5	6.0	5.25	1.0	2.5	6.7	2.25	5.0
Corner Radius R.O., in.	0.001	0.00370	0.00023	0.00335	0.00017	0.00020	0.00335	0.00024	0.00370	0.00005	0.00350
Crown Radius, in.	24	30	30	30	30	30	30	30	30	30	30
Cylinder Length, in.	0.209	0.203	0.247	0.250	0.191	0.210	0.231	0.244	0.186	0.238	0.172
Cylinder Flatness, μin.	—	12	24	21	14	14	19	12	13	24	15
Cylinder Off-Set, in.	0.010	0.050	0.005	0.006	0.051	0.044	0.008	0.004	0.049	0.005	0.060
Crown Profile R.O., μin.	—	160	—	—	95	75	—	—	150	—	145
End Squareness, μin.	120	245	45	50	170	155	50	45	185	40	190
Crown Drop, in.	0.00085	0.00060	0.00060	0.00065	0.00060	0.00048	0.00053	0.00060	0.00053	0.00058	0.00063
Hardness (R_c)	60 min	62.0	63.0	62.5	62.0	62.0	61.0	62.5	—	63	62
Outer Ring											
OD Max, in.	6.7561	6.7559	6.7554	—	—	—	—	6.7562	6.7558	6.7563	6.7559
OD Min, in.	6.7350	6.7351	6.7358	—	—	—	—	6.7351	6.7351	6.7352	6.7352
OD Avg, in.	6.7456	6.7455	6.7456	6.7459	6.7458	6.7458	6.7459	6.7457	6.7455	6.7458	6.7456
ID, in.	6.4246	6.4247	6.4247	6.4244	6.4244	6.4249	6.4242	6.4249	6.4243	6.4247	6.4245
Eccentricity, μin.	25	18	38	13	8	15	18	19	18	18	38
ID Flatness, μin.	15	12	27	15	18	12	12	12	22	27	24
Surface Finish (AA), μin.	4.0	4.5	2.5	2.5	1.5	2.0	2.0	4.0	4.0	4.5	5.0
Hardness (R_c)	62.0	63.5	62.5	62.5	62.5	63.0	63.5	63.0	63.5	63.0	62.5
Inner Ring											
Bore Diameter, in.	4.8936	4.8938	4.8936	4.8936	4.8938	4.8937	4.8936	4.8938	4.8936	4.8936	4.8937
OD Overall, in.	5.6773	5.6771	5.6770	5.6772	5.6768	5.6771	5.6772	5.6772	5.6773	5.6771	5.6770
OD Roller Path, in.	5.3966	5.3966	5.3965	5.3968	5.3970	5.3970	5.3964	5.3969	5.3955	5.3966	5.3961
Roller Path Eccentricity, μin.	18	20	18	20	8	10	20	19	18	18	18
Roller Path Taper, deg-min	0-0	0-0	0-3 42	0-3.58	0-0	0-3.25	0-0	0-0	0-3.00	0-0	0-3.58
Guide Flange Angle, deg-min	0-6	0-3.7	0-3.4	0-6.4	0-5.16	0-5.59	0-6.45	0-4.30	0-3.23	0-4.09	0-2.69
Guide Flange Finish (AA), μin.	4.9	2.5	3.5	5.0	3.0	3.0	5.0	5.0	3.0	4.0	2.5
Roller Path Finish (AA), μin.	3.0	2.5	4.5	3.0	3.0	3.0	2.5	4.0	3.0	3.5	3.0
Hardness (R_c)	63.0	63.0	63.0	62.5	62.5	62.5	62.0	62.5	63.0	63.0	63.0
Cage											
ID, in.	5.6977	5.6973	5.6971	5.6974	5.6973	5.6974	5.6968	5.6975	5.6950	5.6973	5.6970
Pocket Squareness, μin.	450	150	440	130	190	240	350	460	440	120	470
Pocket Parallelism, in.	0.0011	0.0021	0.0012	0.0015	0.0016	0.0013	0.0013	0.0015	0.0011	0.0013	0.0013
Unbalance, gram-centimeter	1.32	1.21	1.44	1.40	1.13	2.03	2.73	1.17	1.40	2.14	1.91
Hardness (R_c)	33.0	33.5	32.5	33.5	33.0	33.0	33.0	33.0	32.5	33.0	33.5

TABLE 7. SUMMARY OF MANUFACTURING INSPECTION DATA — GROUP-AF BEARINGS

	Bearing Number						
	B/L	21	22	23	24	25	26
Bearing Assembly							
Cage Clearance, in.	0.0176	0.0172	0.0172	0.0170	0.0182	0.0173	0.0167
Roller End Clearance, in.	0.0012	0.0010	0.0095	0.00105	0.00105	0.0012	0.00115
Internal Radial Clearance (Unmounted), in.	0.0040	0.0041	0.0045	0.0046	0.0041	0.0044	0.0042
Rollers							
Length, in.	0.51175	0.51068	0.51194	0.51187	0.51194	0.51067	0.51196
Diameter, in.	0.51166	0.51089	0.51182	0.51183	0.51187	0.51085	0.51181
Surface Finish (AA), μin.	—	2.75	2.25	2.25	2.25	3.0	2.25
Corner Radius R.O., in.	0.001	0.000175	0.0002	0.000175	0.000190	0.000175	0.0002
Crown Radius, in.	24	30	30	30	30	30	30
Cylinder Length, in.	0.029	0.2665	0.335	0.3355	0.327	0.276	0.326
Cylinder Flatness, μin.	—	24	22	24	18	27	22
Cylinder Off-Set, in.	0.010	0.004	0.008	0.007	0.0055	0.010	0.0045
Crown Profile R.O., μin.	—	—	—	—	—	—	—
End Squareness, μin.	120	70	75	70	75	80	75
Crown Drop, in.	0.00085	0.00057	0.00018	0.00020	0.00015	0.0005	0.00020
Hardness (R_c)	60 Min	61.5	63.0	63.5	63.5	61.5	62.5
Outer Ring							
OD Max, in.	6.7561	6.7558	6.7558	6.7558	6.7562	6.7566	6.7562
OD Min, in.	6.7350	5.7353	6.7353	6.7349	6.7353	6.7354	6.7353
OD Avg, in.	6.7456	6.7456	6.7456	6.7454	6.7458	6.7460	6.7458
ID, in.	6.4246	6.4245	6.4249	6.4247	6.4247	6.4247	6.4248
Eccentricity, μin.	25	25	38	10	18	25	18
ID Flatness, μin.	15	19.5	24	12	25	6	30
Surface Finish (AA), μin.	4.0	3.5	4.0	4.0	4.0	3.0	4.8
Hardness (R_c)	62.0	63.5	63.0	63.0	63.0	63.0	63.0
Inner Ring							
Bore Diameter, in.	4.8936	4.8937	4.8937	4.8937	4.8937	4.8936	4.8937
OD Overall, in.	5.6773	5.6769	5.6773	5.6772	5.6773	5.6773	5.6773
OD Roller Path, in.	5.3966	5.3981	5.3960	5.3957	5.3962	5.3980	5.3963
Roller Path Eccentricity, μin.	18	18	18	20	20	18	18
Roller Path Taper, deg-min	0-0	0-0	0-0	0-0	0-0	0-0	0-0
Guide Flange Angle, deg-min	0-6	0-7.16	0-50.4	0-55.6	0-0.01	0-52.3	0-49.2
Guide Flange Finish (AA), μin.	4.9	3.5	6.5	7.0	7.0	8.9	6.5
Roller Path Finish (AA), μin.	3.0	3.5	2.5	3.5	3.0	3.5	3.5
Hardness (R_c)	63.0	64.0	62.0	62.0	62.5	63.0	63.0
Cage							
ID, in.	5.6977	5.6976	5.6974	5.6966	5.6985	5.6976	5.6971
Pocket Squareness, μin.	450	380	110	330	150	510	410
Pocket Parallelism, in.	0.0011	0.001	0.0019	0.0013	0.0013	0.0013	0.0021
Unbalance, gram-centimeter	1.32	2.29	1.28	1.20	1.35	2.40	1.20
Hardness (R_c)	33.0	33.0	33.0	33.0	34.0	33.0	33.0

D. PRE-TEST PREPARATION AND INSPECTION OF TEST BEARINGS

Preparation of all the Group-N bearings for test was completed. Each bearing outer ring was instrumented with a strain gage to permit measurement of roller pass frequency during test. Thus, for each of the program test combinations imposed it could then be determined whether or not the roller elements are skidding. Also, the end faces of every other roller element were copper-flashed for the purpose of highlighting end wear that may occur during testing. This procedure was incorporated since a dynamic measurement system to determine the amount of roller skew or the amount of pressure generated by the roller ends on the inner ring guide flanges in a bearing has not been successfully developed. Pre-test preparation also included the weighing of each roller. Repeating this weighing process after test will permit determination of the amount of roller mass loss attributable to wear. For this measurement, a laboratory Christian Becker TORBAL Scale, Model EA-1, was used. Also each of the rollers was measured for static skew angle of turn

allowed by the inner raceway guide flanges. The pretest roller weight and static skew angle measurements obtained for the Group-N bearings are found in table 8. Also shown are the pretest average roller weights for the baseline bearing. Similar measurements are now being made on the Group-AF bearings.

TABLE 8. PRE-TEST WEAR RELATED MEASUREMENTS — GROUP-N BEARINGS

Bearing No.	*Avg Roller Weight (Grams)*		*Avg Skew Angle (Minutes)*	
	Unflashed	*Flashed*	*Unflashed*	*Flashed*
Baseline	—	13.3875	—	—
1	13.2457	13.2474	14.94	15.29
2	13.2918	13.2924	11.95	11.79
3	13.2417	13.2377	14.19	14.19
4	13.2755	13.2736	13.71	13.62
5	13.2768	13.2788	13.43	13.76
6	13.2411	13.2421	14.98	14.22
7	13.2866	13.2853	10.87	10.87
8	13.2446	13.2486	14.47	14.59
9	13.2999	13.2938	13.96	13.85
10	13.3340	13.3317	15.10	14.78

In addition to the bearing manufacturer's pretest inspection data, in-house inspection measurements were made and recorded during installation of the bearings into the test rig. These measurements included the fits of the inner ring on the shaft and the outer ring in the support housing, the installed internal radial clearance of the test bearing and the axial misalignment of the installed outer ring. The actual measurements recorded for the Group-N bearings that have been tested to date as well as for the baseline bearing tested are shown in table 9. It is planned to make similar pretest measurements on the remainder of the Group-N bearings as well as on the Group-AF bearings.

TABLE 9. PRE-TEST RIG RELATED INSPECTION MEASUREMENTS — GROUP-N BEARINGS

	Bearing Numbers				
	B/L	*2*	*6*	*7*	*9*
Inner Ring Fit on Shaft, in.	0.0022T	0.0014T	0.0019T	0.0021T	0.0020T
Internal Radial Clearance Installed, in.	0.0025	0.0043	0.0036	0.0016	0.0025
Outer Ring Fit in Housing, in.	0.0008L	0.0008L	0.0005L	0.0008L	0.0007L
Outer Ring Misalignment, deg	0	0	0	0.4	0.4

Note: T = Tight Fit, L = Loose Fit

E. ROLLER BEARING TEST RIG AND INSTRUMENTATION

The test rig shown in figure 29 is that which is being used for the experimental evaluation of the parametric bearings. It was originally designed and fabricated specifically for development testing of 115 and 124.3 mm bore diameter cylindrical roller bearings. Relatively trouble-free operation has been experienced with this rig in the more than 5000 hours of testing accumulated to date, of which over 250 hours were at speeds of 3.0 MDN.

The test rig consists of a cylindrical housing, with a hydraulic load cylinder located centrally on top of the housing to apply a radial load to the test bearing. Three bearings are located on a common shaft assembly in the rig. The two bearings nearest the ends of the shaft assembly are rigidly mounted to the housing. The center or test bearing is mounted in a carrier attached to the load cylinder piston and is radially guided by tracks in the housing.

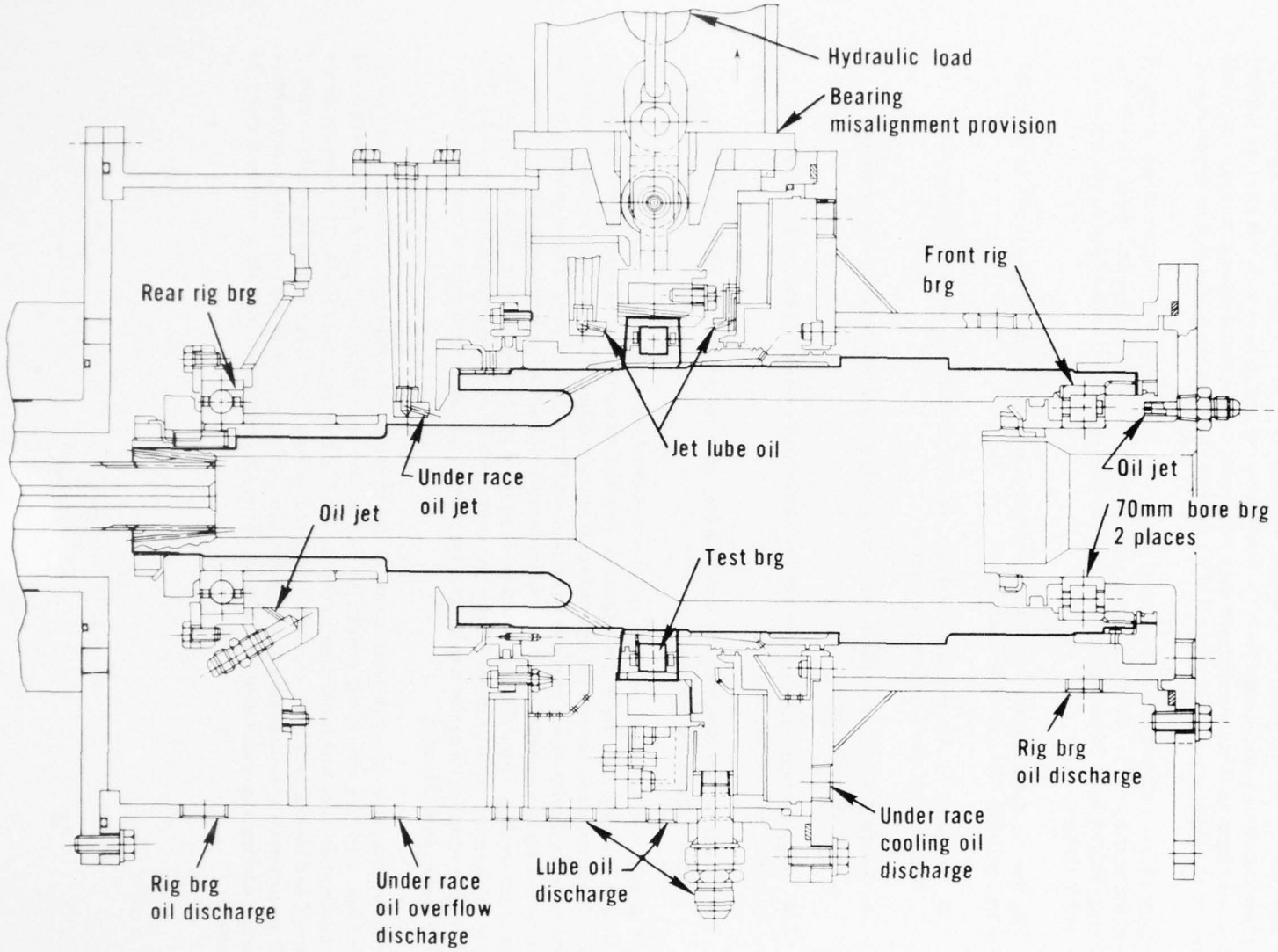

Figure 29. High Speed Roller Bearing Test Rig

Radial load, applied to the test bearing by the load cylinder, is transmitted through the shaft assembly to the end bearings and then through the end bearing carriers to the housing. These bearings are equally spaced from the center bearing and each carries half the load applied to the center bearing. This arrangement maximizes alignment control among the bearings. Axial location of the shaft assembly is controlled by the ball thrust bearing mounted at the drive end.

Lubrication and cooling oil is supplied to the test bearing by directing jet oiling into both sides of the bearing cavity. Oil is also supplied separately to axial slots located under the rotating inner ring. Radial holes intercepting a number of axial slots direct lubrication to the inner ring roller guide flanges.

The test rig itself is serviced by the lubrication system shown schematically in figure 30. This sytem provides the following functions:

- Supplies oil to the test bearings as well as the rig slave bearings for lubrication and temperature control
- Supplies oil to the speed increaser gearbox for lubrication of the gearbox bearings and gears
- Supplies pressurizing oil to the hydraulic load cylinder of the rig to radially load the test bearing
- Controls and monitors the temperature, pressure and flow of oil supplied to each part of the system.

The lubrication system includes an oil reservoir which supplies oil to two pressure pumps, one of high capacity and one of low capacity. The high-capacity pump supplies oil filtered to a level of 15μ absolute to the test rig internals and to the gearbox. The low-capacity pump supplies oil to the load cylinder which provides the radial load to the test bearing. The temperature of the oil to the test rig is controlled by a heat exchanger utilizing either high-pressure steam for heating or water for cooling. Three delivery branches supply oil to the test bearing. Two of the branches supply the bearing with primary lubrication and provide outer ring temperature control. The third branch supplies oil to the test bearing for inner ring temperature control and lubrication of the inner ring guide flanges.

Instrumentation is provided to measure the imposed test conditions, the bearing operating conditions, and the operating conditions of the test rig. This instrumentation consists of conventional devices which are maintained by the Contractor. Table 10 lists the measurements obtained and identifies the corresponding type of instrumentation employed. Manual recordings of all measurements are made every 10 minutes during the calibration portion of the experimental program. During the endurance test portion of the program recordings are made once every 20 minutes.

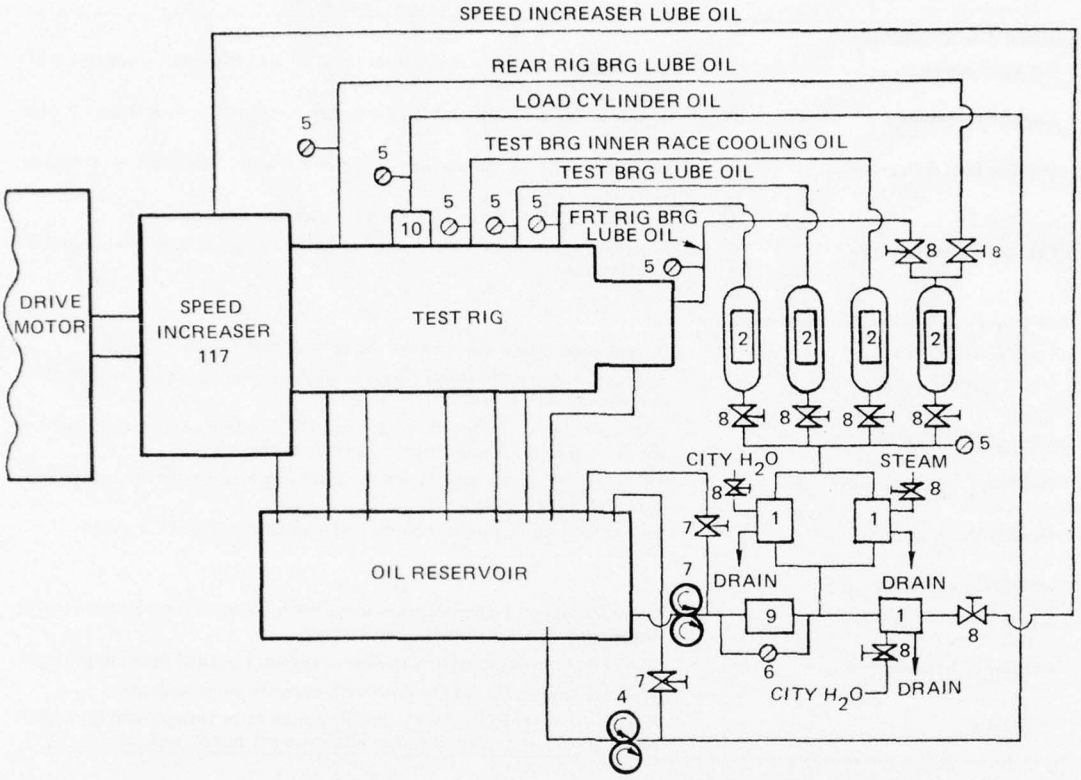

1. HEAT EXCHANGER
2. FLOWMETER
3. HIGH VOLUME PRESSURE PUMP
4. LOW VOLUME PRESSURE PUMP
5. PRESSURE GAGE
6. PRESSURE DIFFERENTIAL GAGE
7. PRESSURE CONTROL VALVE
8. FLOW CONTROL VALVE
9. STATIC FILTER
10. HYDRAULIC LOAD CYLINDER

Figure 30. Lubrication System for Test Rig

TABLE 10. TEST INSTRUMENTATION

Measurement	*Instrumentation*
Imposed Test Conditions:	
Rig shaft speed	Tachometer generator signal from input to 7:1 ratio speed increaser, with tachometer readout.
Applied radial load	Pressure tap at hydraulic load cylinder supply port, with pressure gage readout.
Oil flow to test bearing	Magnetic type oil flowmeters with direct readout, installed in oil supply lines.
	Pressure taps in oil supply lines with pressure gage readouts.
Oil supply temperature	Chromel-alumel thermocouples installed in oil supply lines, with potential type readout.
Test Bearing Operating Conditions:	
Cage speed or slip	Strain gage cemented to OD of outer ring, with digital readout.
Outer ring temperature	Chromel-alumel thermocouples installed in housing, contacting bearing outer ring, with potential type readout.
Inner ring temperature	Chromel-alumel thermocouples installed in shaft, contacting bearing inner ring, with potential type readout via slip-ring.
Discharge oil temperature	Chromel-alumel thermocouples installed in discharge oil rig sumps, with potential type readout.
Horsepower and torque	Direct reading voltmeter and current indicating digital voltmeter.
Rig Operating Conditions:	
Rig bearing temperatures	Chromel-alumel thermocouples installed in housing, contacting bearing outer rings, with potential type readout.
Oil flow to rig bearings	Magnetic type flowmeters with direct readout, installed in oil supply lines.
	Pressure taps in oil supply lines with pressure gage readouts.
Vibration	Accelerometers (ENDEVCO, 2233E) mounted in vertical and horizontal plane on test rig, with vibration displacement meter readout.

F. EXPERIMENTAL PROGRAM PLAN

A 10-hour test program to be followed during the rig evaluation of each of the Group-N and Group-AF parametric bearings was prepared. The program as shown in table 11 was designed to obtain both calibration and endurance test data for each of the bearings. The calibration section consists of 30 separate test combinations which were designed to obtain bearing operational data with variations of speed, oil flow, radial load, and oil temperature. The imposed conditions are maintained at each test combination for 10 minutes. From the operational test data obtained, the following performance parameters can then be determined for each bearing:

- Heat generation
- Horsepower and torque
- Roller skid
- Inner and outer ring thermal stability
- Outer to inner ring thermal gradient
- Axial and circumferential thermal gradients.

TABLE 11. TEST PROGRAM FOR GROUP-N PARAMETRIC BEARINGS

	SUPPLY OIL FLOW LB/MIN.					BEARING DN/TEST POINT NO.						
	UNDER RACE	PER SIDE JET*	TOTAL	°F	APPLIED BEARING LOAD, LBS.	1.0	2.0	2.5	2.75	2.9	3.0	TEST HRS.
CALIBRATION	10	5	20	225	250	1	4	7	10	13	16	3
					500	2	5	8	11	14	17	
					1000	3	6	9	12	15	18	
	5	4	13	225	500	19	20	21	22	23	24	1
	11	9	29	275	500	25	26	27	28	29	30	1
STEADY-STATE	5	4	13 OR 29	225	500	ENDURANCE AT 3M DN						4
CYCLIC SPEED	5 OR 11	4 OR 9	13 OR 29	225	250	2.0 ⇄ 2.75M DN ACCELS-DECELS						1

*TWO JETS, ONE DIRECTED AT EACH SIDE OF BEARING.

Once the calibration portion of the 10-hour program is completed, endurance testing will be conducted to assess the extended operating performance and roller wear durability of each bearing design. The first 4 hours of endurance testing will be conducted at the 3.0 MDN steady-state condition noted in table 11. For a specific bearing test within Group-N the level of the oil flow variable of either 13 or 29 lb/min will be determined from the Group-N bearing design chart shown in figure 27. The oil flow for the Group-AF bearings will be maintained at the baseline level of 20 lb/min since oil flow is not one of the variable parameters for this group. In the fifth hour of the endurance testing, the bearing speed will be cycled between the two speed levels indicated in table 11. A total of 30 acceleration-deceleration cycles will be completed on each bearing, simulating the type of transient operation found in gas turbine engines where accelerated bearing wear due to skidding and skewing may be encountered due to the rapid accelerations experienced by the roller elements.

At the completion of each 10-hour test on the Group-N and Group-AF bearings, the experimental data will be reduced to obtain the individual performance parameters. In addition, the overall condition of each bearing will be noted and any distress or unusual wear will be photographed. Each roller element will be weighed and also measured for the static angle of turn that is allowed within the inner ring guide flanges. Using the pre-test and post-test measurements, roller wear as determined by weight loss, and roller and guide flange wear as determined by change in static skew angle will be determined. Each bearing within either Group-N or Group-AF will then be ranked on the basis of wear. Then using statistical regression analysis techniques, the bearing parameters within each group will be ranked on the basis of wear. Modification to the analytical model, based on the experimental performance and wear results, will then be made.

G. BASELINE TESTING

Baseline experimental data is available on the TF30 engine No. 5 124.3 mm bearing for comparative use when analyzing the parametric test bearing results. The bearing was rig-evaluated following the test program outlined in table 11. Prior to testing, all of the roller ends were copper-flashed for the purpose of highlighting wear. In addition, pretest weight measurements of each roller were obtained and the resultant average value is that shown in table 8. The roller static skew inspection equipment used later in the program was not yet available to permit this measurement to be made on the baseline bearing. The bearing was installed into the test rig with zero outer raceway axial misalignment and the mounted internal radial clearance was measured to be 0.0025 inch.

The baseline bearing performed smoothly throughout the entire ten-hour parametric program. Performance was stable with no indication of thermal instability, roller element skid, or vibrational instability. The test results are shown in figures 31 through 33. Figure 31 shows the horsepower levels required to drive the rig system with the baseline bearing installed to speeds of 3.0 MDN. Also shown for comparative purposes is the data obtained earlier indicating the amount of horsepower required to drive the same rig system but without a bearing mounted in the center test position. Studying figure 31, it can be seen that the installation of the baseline bearing increases the rig system power requirements by an average of 7.5 hp in the speed range of 2.0 to 3.0 MDN. It is intended that the rig horsepower data be used to rank the relative performance of the various bearing designs. This data should not be considered as direct measurement of bearing power losses since the base for this data was obtained without applied radial loading and without normal lubrication. Roller bearing heat generation and cage-to-bearing speed ratio as a function of speed can be seen in figures 32 and 33. Figure 32 indicates that a variation in applied radial load in the range of 250 to 1000 lb has a negligible effect on bearing heat generation. Also, it can be seen in the same figure that the cage-to-bearing speed ratio, which provides a measure of skidding performance, is not significantly affected by radial load. In figure 33, bearing oil flow

rate is shown to have a direct effect on bearing heat generation. As expected, increasing the oil flow results in increased heat generation. The data in figure 33 further indicates that variation in oil flow rate has a very small impact on the cage-to-bearing speed ratio.

At post-test inspection, the flashed rollers from the baseline bearing were found to be free of any eccentric end wear. Several of the rollers were found to have some concentric end wear, providing an indication that these rollers had experienced the greatest amount of weight loss during test. It was determined that the average weight loss was 0.0004 gram per roller.

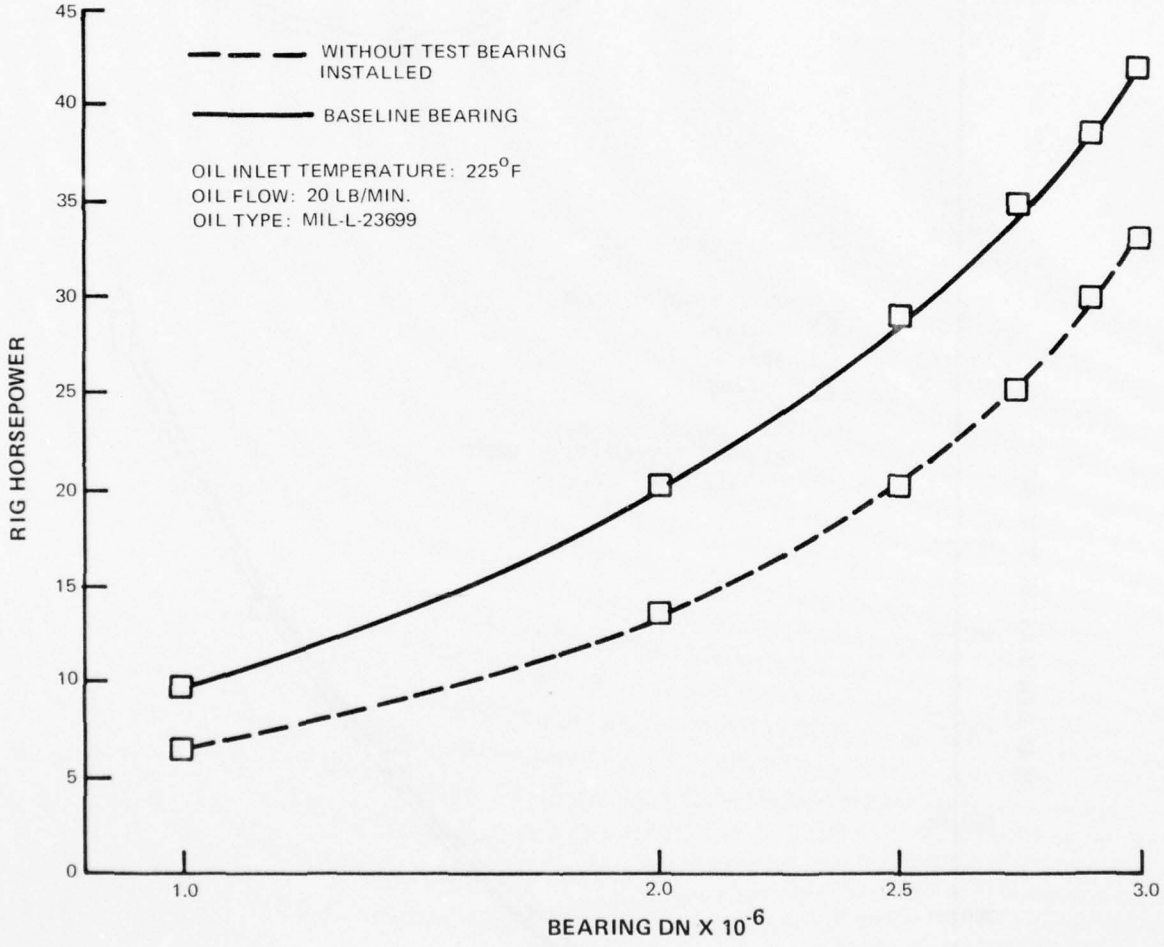

Figure 31. Experimental Evaluation of Baseline Bearing, Rig Horsepower vs Bearing Speed

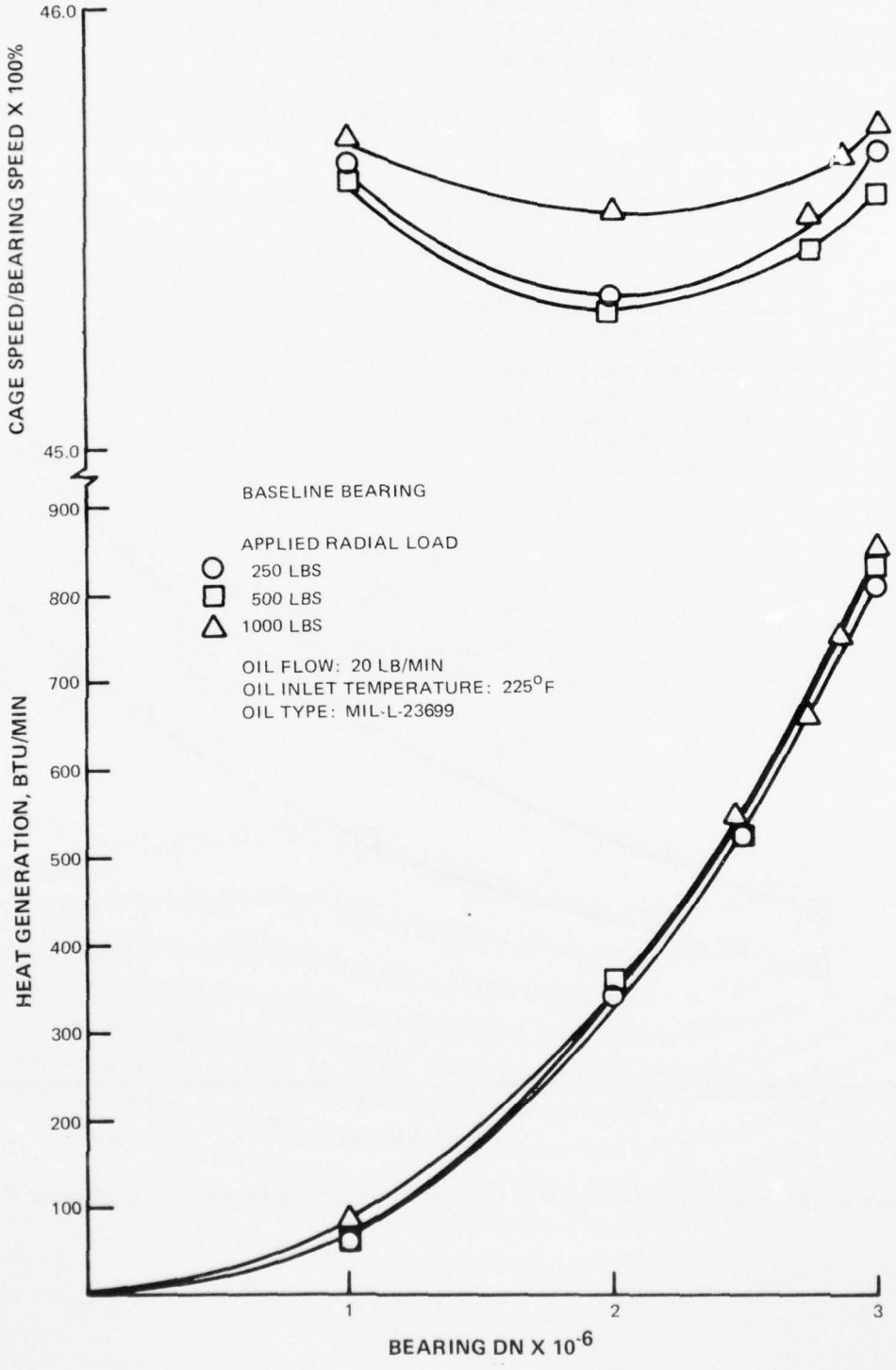

Figure 32. Experimental Evaluation of Baseline Bearing, Heat Generation and Cage Speed/Bearing Speed Ratio vs Bearing Speed with Variation in Bearing Radial Load

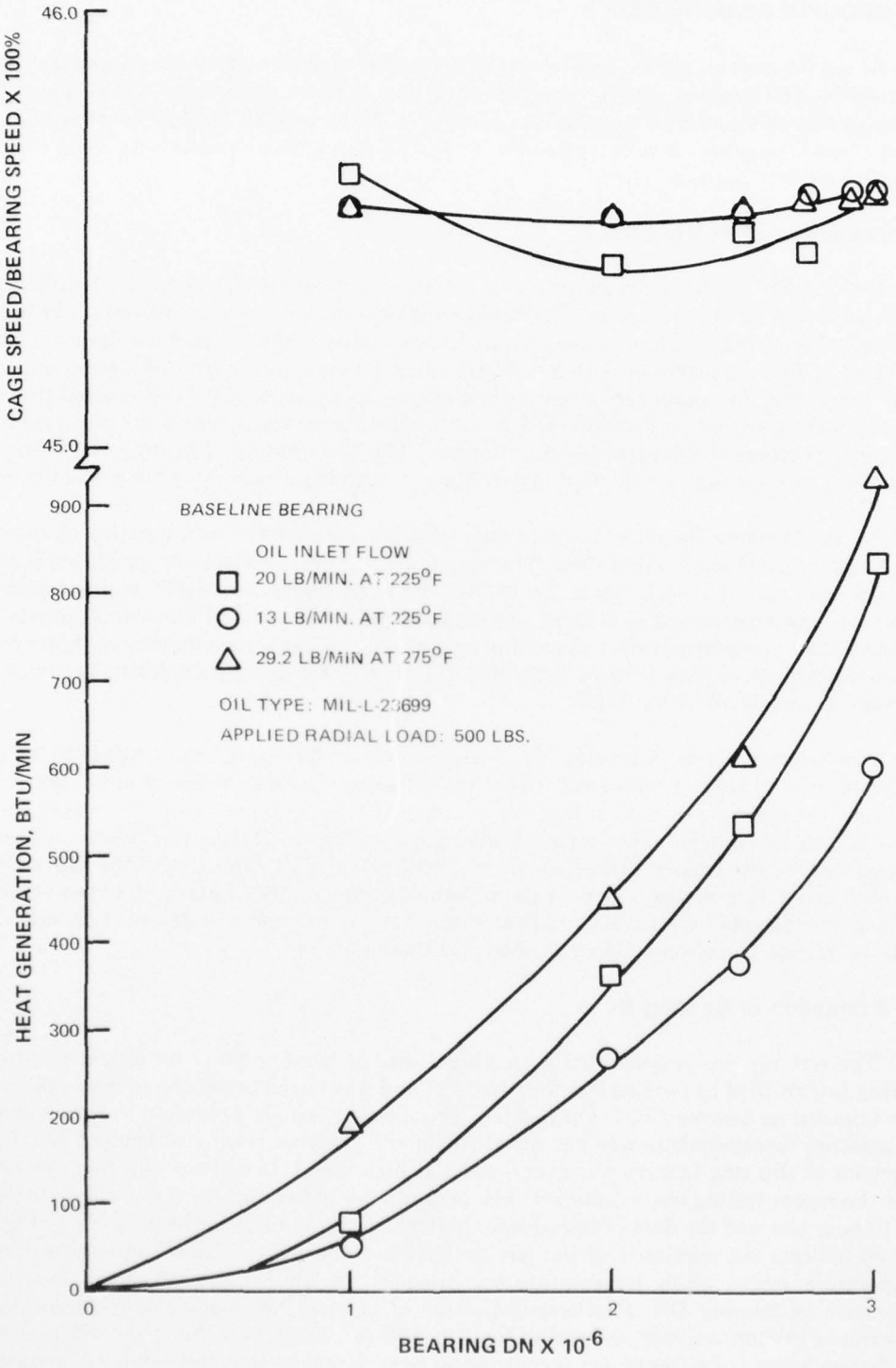

Figure 33. Experimental Evaluation of Baseline Bearing, Heat Generation and Cage Speed/Bearing Speed Ratio vs Bearing Speed with Variation in Oil Flow

H. GROUP-N BEARING TESTS

At the time of this report, testing had been completed on four of the ten parametric bearings of Group-N. The bearings tested were those identified in figure 27 as No's. 7, 9, 6, and 2. Stable operation was obtained with each bearing except No. 6 which failed during the calibration phase of the 10-hour program. A wide range of wear and performance was observed during the testing of these first four bearings.

1. Evaluation of Bearing No. 7

Bearing No. 7 was first selected for test since a duplicate of this bearing, identified as No. 9, was available for repeat testing. Thus, back-to-back tests of a similar design could be run at the beginning of the program so that testing repeatability could be assessed. Bearing No. 7 as indicated in figure 27 contained element preloading which is introduced by a two-point out-of-round outer ring. The outer race axial misalignment was adjusted to 0.4 degrees and the oil flow for this bearing design was maintained at 13 lb/min during the steady-state and cyclic speed endurance portions of the experimental program. The performance of bearing No. 7 was stable throughout the test with no thermal instabilities or significant raceway axial gradients noted.

Figure 34 shows the outer-to-inner race temperature gradient as a function of speed with variations in radial load and oil flow. The temperature gradients were not significantly affected by variations in radial load up to 2.5 MDN. However, above 2.5 MDN, higher temperature gradients were experienced as a result of increased radial loading. Oil flow variation was shown to have a more pronounced effect on bearing temperature gradient than loading as shown in figure 34. At the highest oil flow level of 29 lb/min, the bearing temperature gradient becomes nearly constant at speeds above 2.5 MDN.

Post-test inspection of bearing No. 7 revealed all of the bearing components to be in good condition with no distress indicated. All of the rollers were found to be free of any eccentric wear; however, they did exhibit moderate levels of concentric wear on both ends. This wear was most likely due to the applied outer ring misalignment. Roller weight measurements indicated an average loss for the copper-flashed rollers of 0.0005 gram. This compares to the average weight loss obtained earlier on the rollers of the baseline bearing of 0.0004 gram. Post-test static skew angle measurements on six rollers indicated an average increase of 0 degree, 1.26 minutes. Of these six rollers, three were copper-flashed and three were not.

2. Evaluation of Bearing No. 9

The test rig was reassembled with a duplicate of bearing No. 7 for repeat testing. This bearing is identified as bearing No. 9 in figure 27 and was tested under the same conditions that were imposed on bearing No. 7. For this test, the slip ring, which is required to obtain inner ring temperature measurements was not installed. In the previous testing of bearing No. 7 a high frequency of slip ring failures was experienced at high speed. Use of the slip ring was resumed after the repeat testing was conducted. The performance of bearing No. 9 was stable throughout the 10-hour test and the data obtained was similar to that obtained for bearing No. 7. Figures 35 and 36 indicate the similarity of the test data for both bearings. Figure 35 presents outer ring temperature minus oil-in temperature vs. bearing DN while figure 36 shows bearing heat generation vs bearing DN. Post-test inspection of bearing No. 9 indicated a similar overall appearance to that observed on bearing No. 7 at post-test inspection. All of the rollers of bearing No. 9 were found to be free of any eccentric end wear; however, they did exhibit moderate levels of concentric wear on both ends. Roller weight measurements indicated an average loss for the copper-flashed rollers of 0.0010 gram and 0.0004 gram for the unflashed rollers. This compares to an average weight loss of 0.0005 gram for the copper-flashed rollers and a maximum loss of 0.0002 gram for the unflashed rollers of bearing No. 7. A small increase in static skew angle was observed

with all roller elements. For the flashed rollers the average increase was 0 degree, 2.0 minutes while for the unflashed rollers the average increase was 0 degree, 1.5 minutes. This compares to an average skew angle increase of 0 degree, 1.26 minutes for six rollers measured in bearing No. 7.

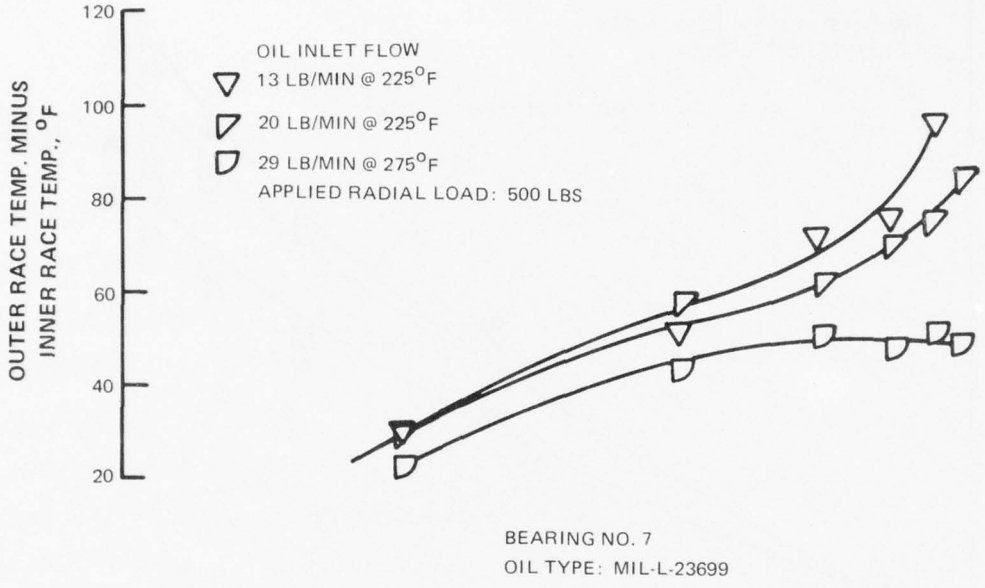

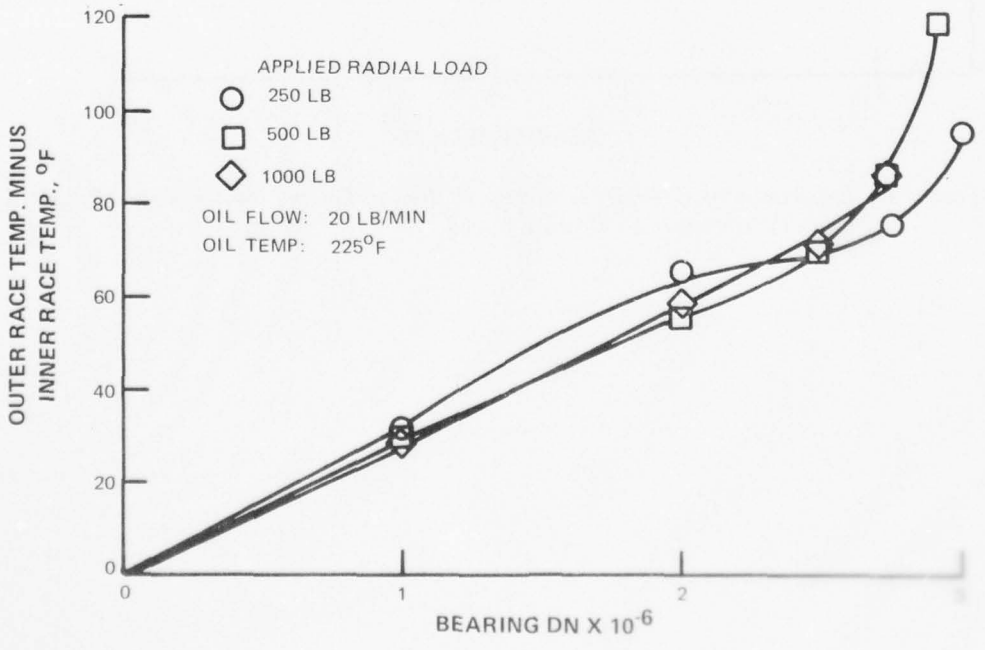

Figure 34. Experimental Evaluation, Group-N Bearing No. 7, Outer Race Minus Inner Race Temperatures vs Bearing Speed with Variation in Radial Load and Oil Flow

AD-A052 351 PRATT AND WHITNEY AIRCRAFT GROUP WEST PALM BEACH FL G--ETC F/G 21/5
DEVELOPMENT OF MAINSHAFT HIGH SPEED CYLINDRICAL ROLLER BEARINGS--ETC(U)
APR 77 P F BROWN, L J DOBEK, F C HSING N00140-76-C-0383
UNCLASSIFIED PWA-FR-8615 NL

2 OF 2
AD A052351

END
DATE FILMED
5-78
DDC

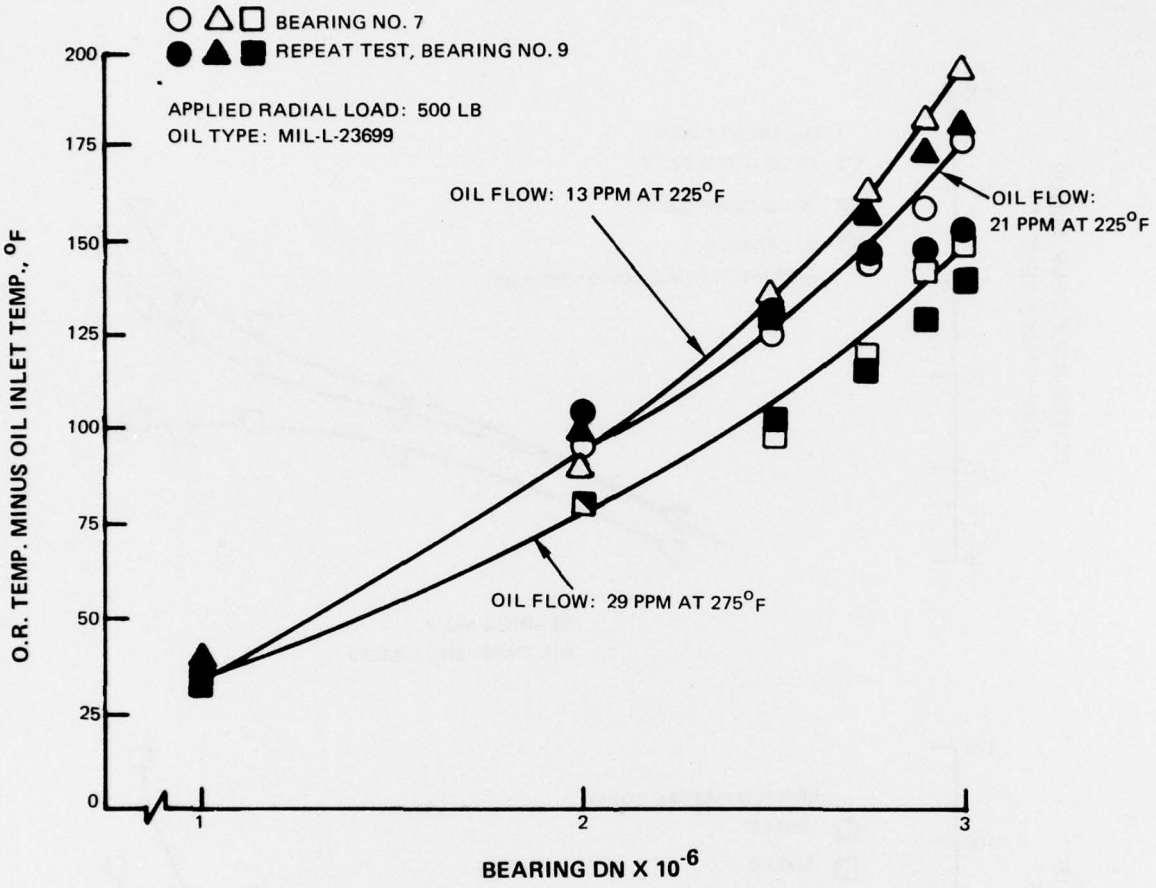

Figure 35. Experimental Evaluation, Group-N Repeat Testing, Outer Race Minus Oil Inlet Temperature vs Bearing Speed

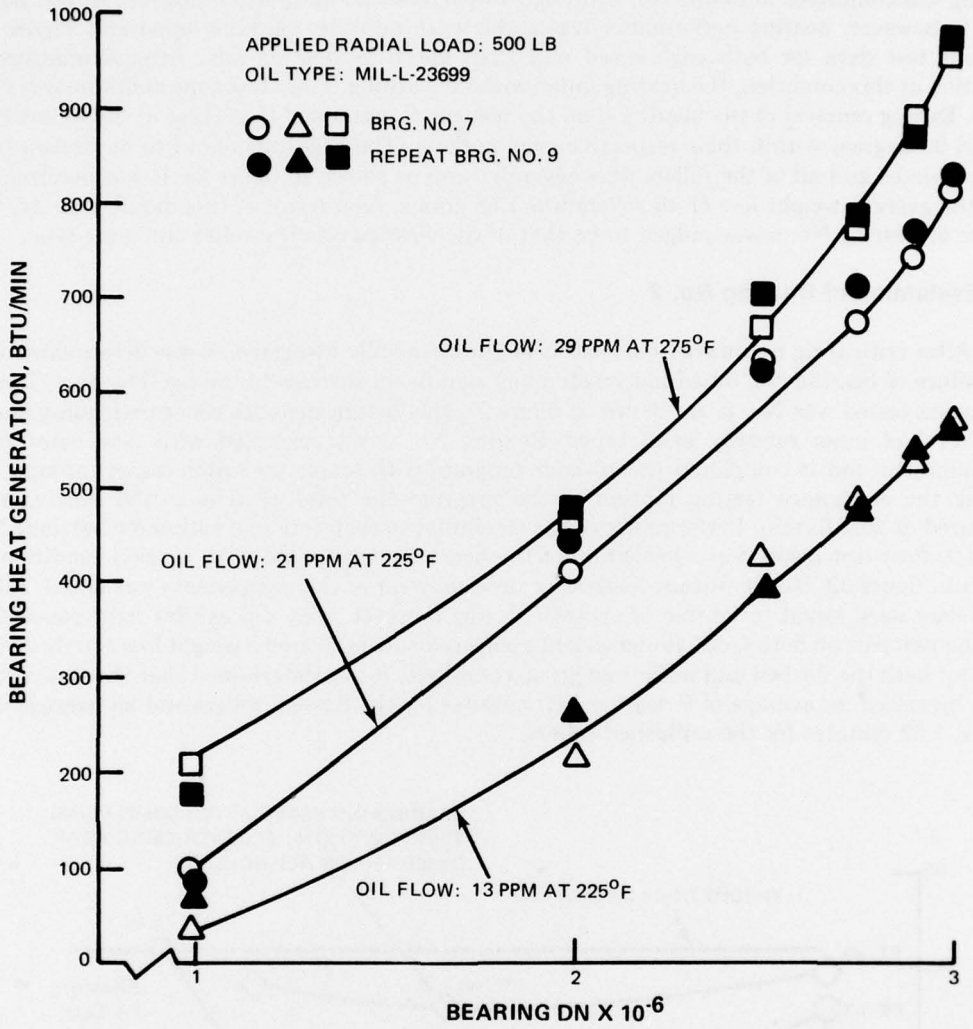

Figure 36. Experimental Evaluation, Group-N Repeat Testing, Bearing Heat Generation vs Bearing Speed

3. Evaluation of Bearing No. 6

With adequate test program repeatability having been demonstrated by the experimental results obtained from tests of bearings No.'s 7 and 9, testing of the Group-N bearings was resumed. The next bearing design tested was No. 6. As shown in figure 27, this design did not provide for roller element preloading and as shown in table 8, the maximum coupled roller end radius runout was determined to be approximately 0.00335 inch on all rollers. Testing was initiated following the program in table 11. From the onset, roller pass frequency measurements indicated that roller skid was occurring. Skid magnitude was the greatest at the lower applied loads and decreased somewhat as the load was increased. After completing the first six points of the calibration section, the test was interrupted and the bearing was visually inspected while it was still mounted on the rig shaft. At this point the total test time was 1.0 hour. Each roller was found to exhibit heavy eccentric wear on both ends. However, no skid damage to the bearing components was visible. The shaft was then reinstalled in the rig and the program was resumed.

Testing was completed at points No. 7 through 9 with roller skidding still indicated. At test point No. 10, however, bearing performance was stable with no roller skidding apparent. Figure 37 contains test data for both cage speed and shaft speed vs bearing DN. After 5 minutes of operation at this condition, the bearing failed without warning. Total test time at failure was 1.58 hours. During removal of the bearing from the test rig, it was noted that three of the rollers had turned 90 degrees within their respective cage pockets. The cage was found to be broken into several pieces and all of the rollers were severely worn as shown in figure 38. It was determined that the average weight loss of all rollers was 1.68 grams. As a result of this detailed study, the failure of bearing No. 6 was judged to be that of the classic eccentric roller end wear type.

4. Evaluation of Bearing No. 2

After critical rig hardware items had been dimensionally inspected, it was determined that the failure of bearing No. 6 had not created any significant distress to the rig. The next Group-N bearing tested was No. 2. As shown in figure 27, this design includes roller preloading and a high level of inner raceway axial taper. Bearing No. 2 was installed with zero outer race misalignment and it completed the 10-hour program with stable operation noted throughout. During the endurance testing portion of the program the total oil flow to the bearing was measured at 29.2 lb/min. Performance data was similar to that obtained earlier for bearings No. 7 and 9. Post-test inspection revealed all of the bearing components to be in good condition as shown in figure 39. No significant distress or unusual wear of the components was noted. All of the rollers were found to be free of eccentric wear; however, they did exhibit light concentric rubbing patterns on both faces. Roller weight measurements indicated a weight loss of only 0.0001 gram for both the flashed and unflashed groups of rollers. It was determined that the static skew angle increased an average of 0 degree, 1.09 minutes for the flashed rollers and an average of 0 degree, 1.32 minutes for the unflashed rollers.

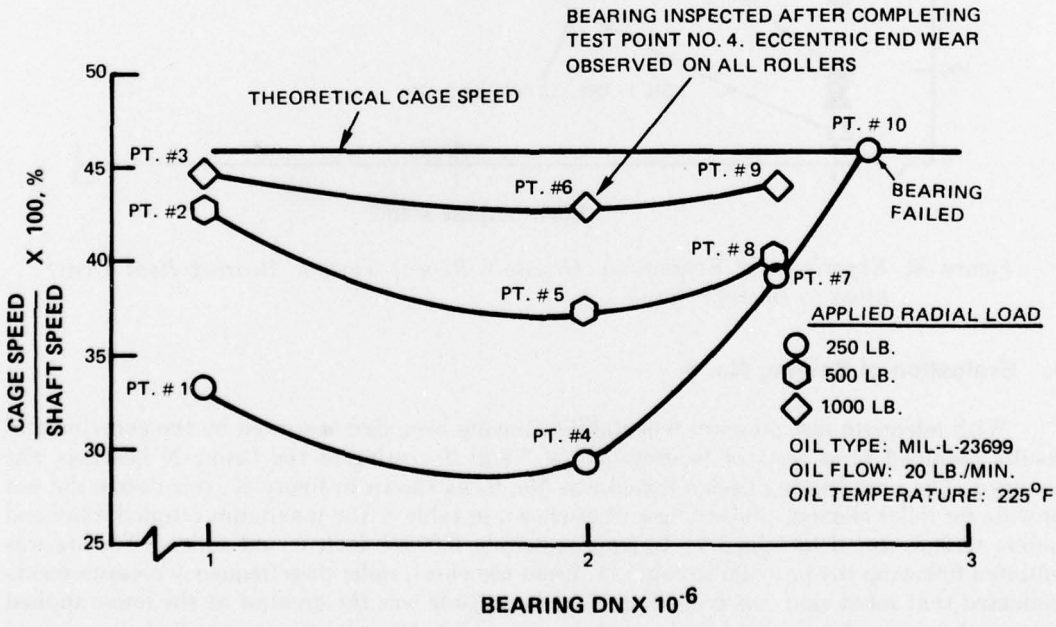

Figure 37. Experimental Evaluation, Group-N Bearing No. 6, Cage Speed/Bearing Speed Ratio vs Bearing Speed

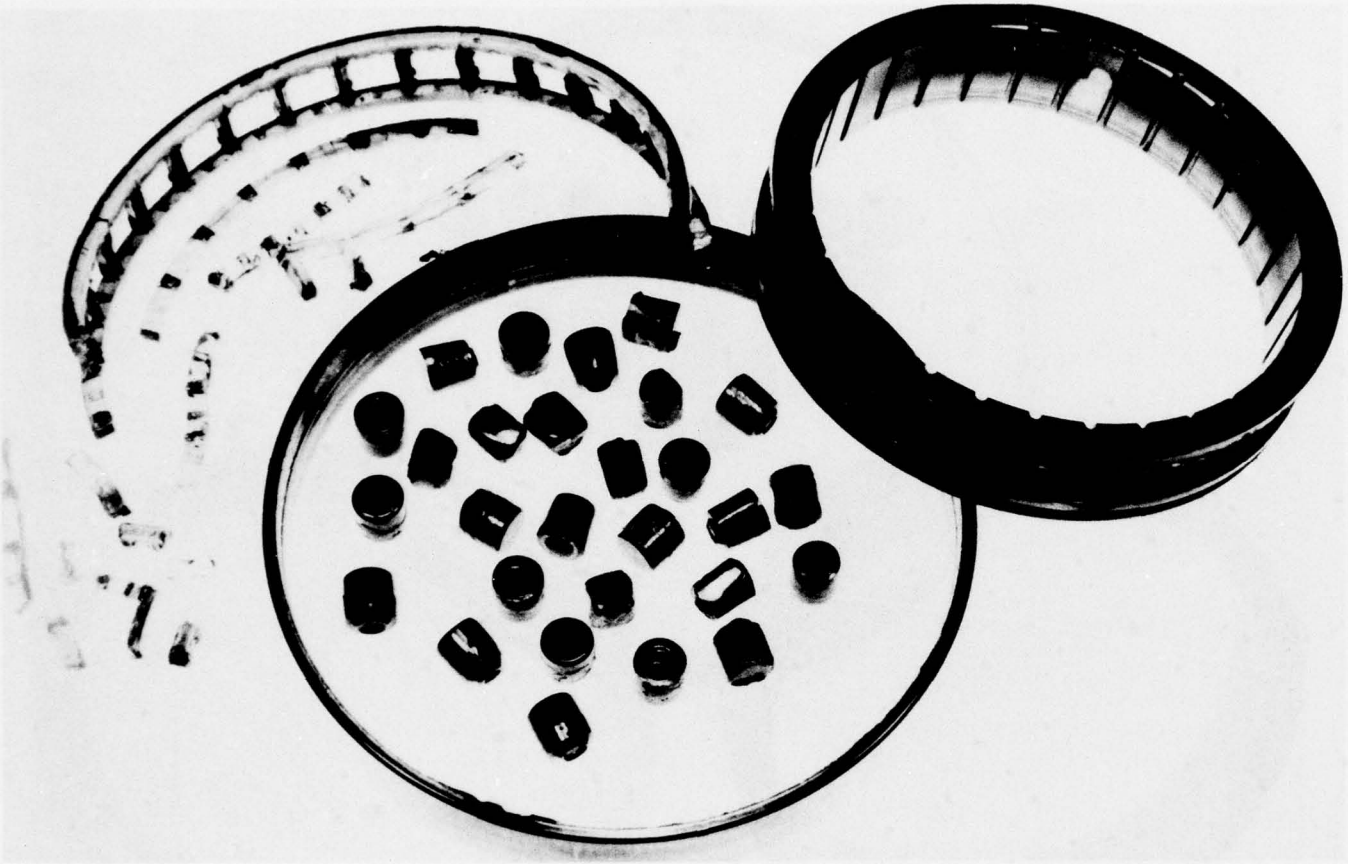

Figure 38. Group-N Bearing No. 6 Failure

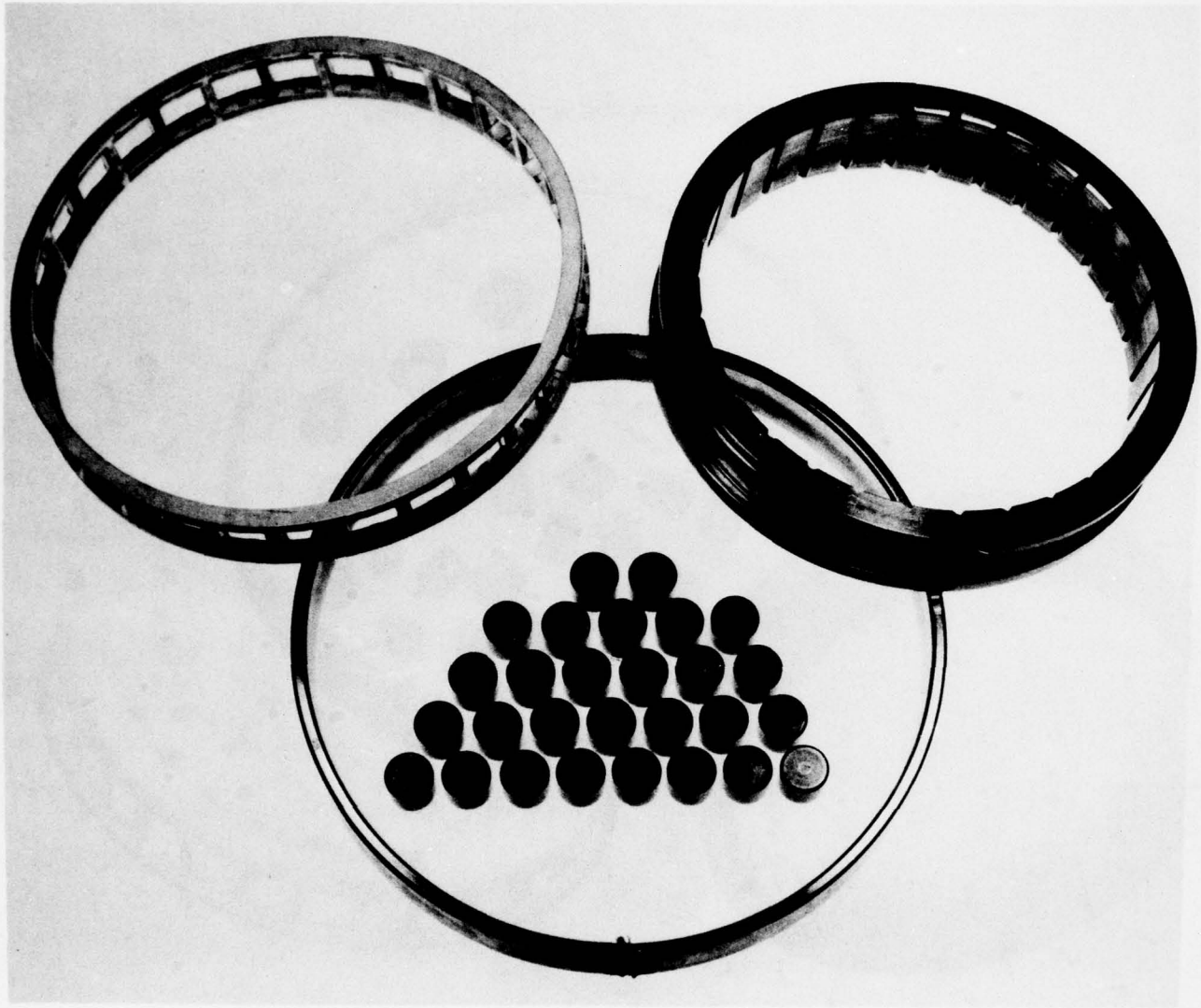

Figure 39. Group-N Bearing No. 2, at Completion of 10 Hour Parametric Test

I. SUMMARY OF GROUP-N TESTING

Composite curves representing operational data for the Group-N bearings tested to date as well as for the baseline bearing are found in figures 40 and 41. In general, similar thermal and horsepower results were indicated for each bearing. Although bearing No. 6 failed after only 1.58 hours of testing and exhibited heavy eccentric roller end wear, examination of the curves in these figures reveals no unusual thermal behavior. Only in the skid curve, shown as the ratio of cage speed to bearing speed vs. bearing DN, in figure 41 is there a significant difference in bearing operation indicated. Bearing No. 6, which is the only unpreloaded bearing tested thus far, shows continuous roller skidding for the conditions indicated, whereas, no significant element skidding is apparent for all of the other bearings tested.

A summary of the wear results obtained is shown in table 12. Average values of roller weight loss during test for both the flashed and unflashed rollers are presented. Also shown as a wear parameter is the average static skew angle change for the flashed as well as for the unflashed rollers of each bearing.

TABLE 12. GROUP-N BEARING TESTS — ROLLER WEIGHT AND SKEW ANGLE WEAR DATA

	Average Roller Weight Loss, Grams			*Average Skew Angle Increase, Minutes*		
Bearing No.	*Flashed*	*Unflashed*	*All Rollers*	*Flashed*	*Unflashed*	*All Rollers*
Baseline	0.0004	—	0.0004	—	—	—
7	0.0005	0	0.0003	0.98	1.53	1.26
9	0.0010	0.0004	0.0007	2.04	1.55	1.79
6	1.6145	1.7532	1.6838	—	—	—
2	0.0001	0.0001	0.0001	1.09	1.32	1.20

J. PLANNED EXPERIMENTAL PROGRAM

Parametric evaluation will continue on the remainder of the Group-N roller bearings. At the completion of testing, the wear data will be reduced and analyzed through statistical techniques. The seven roller bearing parameters will then be ranked in order, as to their effect on wear, and the results incorporated into the analytical model. The performance results obtained on each bearing design will also be correlated with the roller bearing analysis.

The wear and performance results from the Group-N bearing tests will be used along with the available roller bearing analysis and other test data to design a 3.0 MDN prototype bearing. In a subsequent task, this bearing design will be experimentally rig-evaluated to assess its durability for a period of 60 hours. Testing will be conducted over a speed range of 2.2 to 3.0 MDN, with a goal being to obtain at least 30 hours of operation at 3.0 MDN.

Future testing will also be conducted on the available Group-AF parametric bearings. The procedure used in the evaluation of the Group-N bearings will again be followed. The wear and performance results will be separately analyzed and then correlated with the analytical design system.

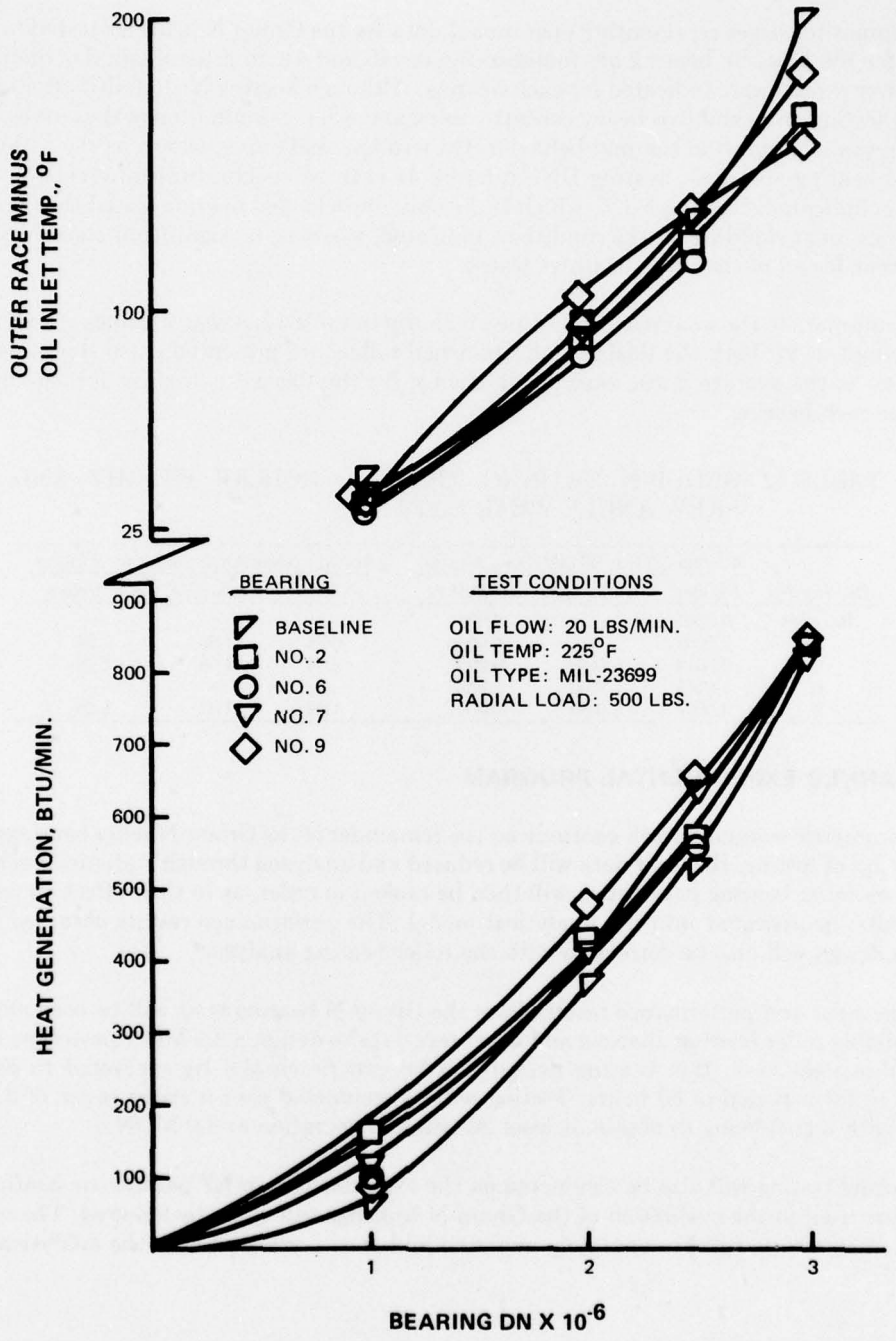

Figure 40. Experimental Evaluation, Group-N Bearings, Heat Generation and Outer Race Minus Oil Inlet Temperature vs Bearing Speed

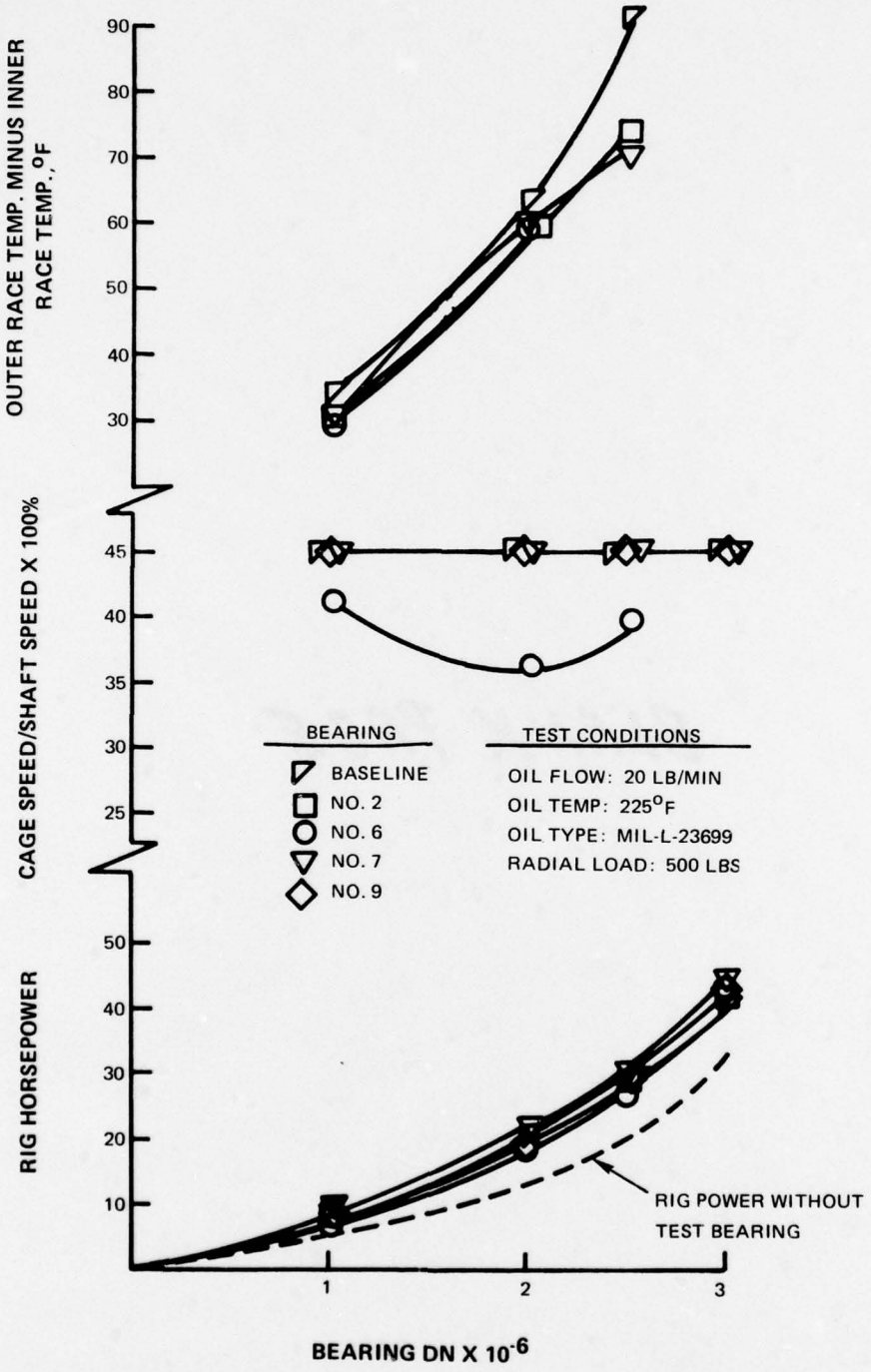

Figure 41. Experimental Evaluation, Group-N Bearings, Rig Horsepower, Cage Speed/Bearing Speed Ratio, and Outer Race Minus Inner Race Temperatures vs Bearing Speed

APPENDICES

LIST OF SYMBOLS

Nomenclature

A_{qj}, B_{qj}, C_{qj}, D_{qj}	influence coefficient matrices for the outer ring and housing
A'_{qj}, B'_{qj}, C'_{qj}, D'_{qj}	influence coefficient matrices for the inner ring and shaft
AA	arithmetic average, μ in.
a	smaller ring ID, in; coefficient domain of the finite element system or the element; Hertzian half-width, in.
b	smaller ring OD, in.; coefficient
C	clearance, in.; constant
C_a	roller axial clearance, in.
C_R	crown radius, in.
c	larger ring OD, in.; OOR constant
c_i	constant defined in Equation (38)
D	ring diameter, in.
D_H	crowned flange reference diameter, in.
d_i	ID of a hollow roller
d_o	OD of a hollow roller
d	roller diameter, in.
de	pitch diameter, in.
d_x	effective roller diameter, in.
E	Young's modulus, psi
e	Weibull slope
F	forces, lb_f
$\vec{F}$	force vector, lb_f
F_c	roller centrifugal load, lb_f
f_i	fatigue constant

LIST OF SYMBOLS (Continued)

Nomenclature

$\vec{f}$	diametral fit at outer ring OD, in.
g	gravitational constant
H, $\bar{H}$	dimensionless variables
h	inner ring shoulder height, in.; oil film thickness, in.; angular momentum
h_u	undercut height, in.
I_{Cj}	principal moment of inertia of cage, lbm-in.^{2}; j = x, y, or z
I_{rij}	principal moment of inertia of the i^{th} roller in the j^{th} direction, lbm-in.^{2}, coefficient defined by Equations (69) through (74)
$\vec{i}$, $\vec{j}$, $\vec{k}$; $\vec{I}$, $\vec{J}$, $\vec{K}$	unit vectors
K	spring rate, lb_f/in.; matrix; lubricant thermal conductivity, Btu/sec-in.-F
K_H	n-point spring rate of outer structure from *OROD* outward, lb_f/in.
K_i	spring rate defined by Equation (31)
K_j	empirical lubricant constant
K_S	n-point spring rate of inner structure from IRID inward, lb_f/in.
K_{1R}, K_{2R}	spring rate defined by Equation (30)
K_{1S}, K_{2S}	spring rate defined by Equations (28) and (29)
L	roller length, in.
L_{10}	90% survival life, hr
$\bar{L}$	composite bearing fatigue life, hr
L_F	lubricant factor
L_i	ring life, hr
L_m	material factor
L_p	preload, lb_f
l	cage land width, in.
l_e	effective roller length, in.

LIST OF SYMBOLS (Continued)

Nomenclature

l_F	roller flat length, in.
M	moment, in-$\mathfrak{lb}_f$; mass, $\mathfrak{lb}_m$
m_1, m_2	masses, $\mathfrak{lb}_m$
N	interpolation function, speed, rpm
n	number of rollers; number of OOR points
OOR	out-of-round, in.
P	dimensionless variable; load, $\mathfrak{lb}_f$
P_D	diametral play, in.
P_{ei}	equivalent ring load of the i^{th} component, $\mathfrak{lb}_f$
$\bar{P}_H$	normalized Hertzian pressure
P_q	q^{th} roller load, $\mathfrak{lb}_f$
P	pressure, $\mathfrak{lb}_f/in.^2$
$\bar{p}$	mean Herzian pressure, psi
Q	volumetric flowrate, $in.^3/sec$
Q_{ci}	dynamic capacity of the i^{th} component, $\mathfrak{lb}_f$
$\vec{R}$	position vector, in.
R, r	radius, in; position, in.
R_c	Rockwell hardness — C scale
R_F	radius of curvature of crowned guide flange, in.
S	skewing moment, in.-$\mathfrak{lb}_f$; boundary of solution domain; a variable defined by Equation (32)
T	torque, in.-$\mathfrak{lb}_f$; transformation matrix
t	time, sec
U	surface velocity, in./sec
$\bar{U}$	dimensionless variable; normalized speed
$\vec{U}$	surface velocity vector, in./sec

LIST OF SYMBOLS (Continued)

Nomenclature

V	surface velocity, in./sec
v_o	approach speed, in./sec
$\bar{V}$	dimensionless variable
W	line load, lb_f/in.; roller weight, lb_f; lubricant flowrate, ppm
w	width, in.
x,y,z; x′, y′,z′; X,Y,Z	coordinates
$\bar{x}$, $\bar{y}$	coordinates of center of pressure, in.
x_u, x_l	contact length extremities, in.
α	angular deflection, rad; angular acceleration, rad/sec^2
β	ring coning, rad
γ	constant defined in Equation (38)
Δ	linear contact deflection, in.; fit, in.; incremental change of a variable; area in^2
δ_k	deflection along kth bearing axis, in. or rad.
δ''_k	bearing misalignment about the kth axis, rad.
δ	dimensionless variable; lubricant temperature-viscosity coefficient; displacement, in.
$\vec{\nabla}$	gradient vector, in.$^{-1}$
ϵ	roller crown drop, in.; eccentricity ratio
η	dimensionless variable
θ	angle, deg
Λ	normalized film thickness = $\frac{h_{min}}{\sqrt{\sigma_1^2 \quad \sigma_2^2}}$; dimensionless parameter
λ_l	life reduction factor
μ	lubricant viscosity, lb_m-sec/in.^{2}
μ_s	coefficient of sliding friction

LIST OF SYMBOLS (Continued)

Nomenclature

ν	Poisson's ratio
σ_1, σ_2	surface finish or roller, raceway, μin.
τ	shearing stress lb$_f$/in^2
ϕ	angle, deg
ϕ_q	qth roller azimuth location
ϕ_s	stress factor
χ	anguiar location of the first pinch point, deg
ψ	angle, deg
Ω	angular velocity, rad/sec
ω	angular velocity, rad/sec
[ ] { }	matrices

Subscripts

A, a	ambient; axial
assembly	assembly condition
av	average
ci	cage, in the ith direction
c	crown; cage; cavitation
E	rolling element
e	effective; external
F, f	flange
flex	combined structural flexibility
H	horizontal component; housing
IR	inner ring
i	the ith element or node; i = 1, outer race; i = 2, inner race; impact; ID
ij	at the ith race due to the influence of the jth roller
i/o	ID of the outer ring

LIST OF SYMBOLS (Continued)

Nomenclature	
iq	the i^{th} race at the q^{th} roller location; i = 1, outer race; i = 2 inner race
j	shaft or j^{th} element or node; the j^{th} location
jE	externally applied load at the j^{th} race; j = 1, outer race; j = 2 inner race
k	the k^{th} element or node
m	maximum
min	minimum
N	normal
O	reference condition; center of mass
o	OD
o/i	OD of the inner ring
o/o	OD of the outer ring
OOR	out-of-roundness
operating	operating condition
OR	outer ring
P	pitch; pressure; pressure boundary
q	the q^{th} roller location; flow boundary
R	race
req	required
r	roller; radial
rk	the k^{th} roller
rkj	the k^{th} roller in the j^{th} direction
s	structural; shaft
T	tangential direction
u	unbalance; u-component
V	vertical component

LIST OF SYMBOLS (Continued)

Nomenclature

v	v-component
x	x-component
y	y-component
z	z-component
θ	tangential
τ	shear
1	outer ring; inner member of a compound cylinder; ID of a cyclinder
2	inner ring; outer member of a compound cylinder; OD of a cylinder

Superscripts

$(\cdot)$	first time derivative
$(\cdot\cdot)$	second time derivative
$(\vec{\ })$	vector quantities
$(\ )'$	outer race; equivalent
$(\ )^n$	n^{th} power
$(\ )^m$	m^{th} power
$*_\eta$	constant defined in Equation (37)

LIST OF ABBREVIATIONS

Avg	Average
BCL	Battelle Columbus Laboratories
B/L	Baseline
DN	Diameter (Millimeters) Times Speed (RPM)
EHD	Elastohydrodynamic
Gm- cm	Gram-Centimeter
ID	Inside Diameter (Inches)
in.	Inches
IR	Inner Race, Inner Ring
IRC	Internal Radial Clearance (Inches)
L	Loose (Inches)
lb	Pounds
L/D	Roller Length to Diameter Ratio
MDN	Million DN
Max	Maximum
Min	Minimum/Minutes or Arc/1/60 of Hour
mm	Millimeters
O/C	Operating Conditions
OD	Outside Diameter (Inches)
OOR	Outer Ring OD Out-of-Roundness
OR	Outer Race, Outer Ring
PPM	Pounds per Minute
psi	Pounds per Square Inch
Rad	Radians
RO	Run-Out
RPM	Revolutions per Minute
T	Tight (Inches)

REFERENCES

1. Loewenthal, S. H., Parker, R. J. and Zaretsky, E. V., "Elastohydrodynamic Film Thickness Model for Heavily Loaded Contacts," *Journal of Lubrication Technology*, Trans. ASME, July, 1974, pp. 472-481.

2. Jones, A. B., "A General Theory for Elastically Constrained Ball and Radial Roller Bearings Under Arbitrary Load and Speed Conditions," *Journal of Basic Engineering*, Trans. ASME, June, 1960, pp. 309-320. Also, private communications.

3. Lundberg, G. and Palmgren, A., "Dynamic Capacity of Rolling Bearing," *Acta Polytechnica, Mechanical Engineering Series*, Vol. 1, No. 3, Stockholm, 1947. Also, Vol. 2, No. 4, 1952.

4. Harris, T. A., *Rolling Bearing Analysis*, John Wiley and Sons, Inc., New York, 1966.

5. Skurka, J.C., "Elastohydrodynamic Lubrication of Roller Bearings," *Journal of Lubrication Technology*, Trans. ASME, April, 1970, pp. 281-291.

6. Roark, R. J. and Young, W. C., *Formulas for Stress and Strain*, 5th Edition, McGraw Hill Inc., 1975.

7. Ralston, A., and Wilf, H. S., *Mathematical Methods for Digital Computers*, John Wiley and Sons, New York, 1966.

8. Dowson, D. and Higginson, G. R., *Elastohydrodynamic Lubrication*, Pergamon Press, 1966.

9. Cheng, H. S., *Calculations of Elastohydrodynamic Film Thickness in High Speed Rolling and Sliding Contacts*, MTI-67TR24, Mechanical Technology Incorporated, 1967.

10. Murch, L. E. and Wilson, W. R. D., "A Thermal Elastohydrodynamic Inlet Zone Analysis," *Journal of Lubrication Technology*, Trans. ASME, April, 1975, pp. 212-216.

11. McGrew, J. M, Gu, A. Cheng, H. S. and Murray, S. F., *Elastohydrodynamic Lubrication*, AFAPL-TR-70-27, Air Force Aero Propulsion Laboratory, Air Force Systems Command, Wright-Patterson Air Force Base, Ohio, November, 1970.

12. Kannel, J. W. and Walowit, J. A., "Simplified Analysis for Tractions Between Rolling-Sliding Elastohydrodynamic Contacts," *Journal of Lubrication Technology*, Trans. ASME, January 1971, pp. 39-46.

13. Walowit, J. A. and Smith, R. L., "Traction Characteristics of a MIL-L-7808 Oil," *Journal of Lubrication Technology*, Trans. ASME, October 1976, pp. 607-612.

14. Akers, A., Michaelson, S., and Cameron, A., "Stability Contours for a Whirling Finite Journal Bearing," *Journal of Lubrication Technology*, Trans. ASME, January 1971, pp. 177-190.

15. Kirk, R. G. and Gunter, E. J., "Short Bearing Analysis Applied to Rotor Dynamics, pt. 1: Theory," *Journal of Lubrication Technology*, January, 1976, pp. 47-56.

BIBLIOGRAPHY

Barban, P., "Impact," *Mechanical Design and Systems Handbook*, Sec. 16, McGraw Hill Inc., New York, 1964.

Beer, F. P. and Johnston, Jr., E. R., *Vector Mechanics for Engineers — Statics and Dynamics*, McGraw-Hill Inc., New York, 1962.

Dubois, G. B. and Ocvirk, F. W., *Analytical Derivation and Experimental Evaluation of Short Bearing Approximation For Full Journal Bearing*, NACA TN-1157, 1955.

Etkin, B., *Dynamics of Atmosphere Flight*, John Wiley and Sons, Inc., New York, 1972.

McRuer, D., Ashkenas, I. and Graham, D., *Aircraft Dynamics and Automatic Control*, Princeton University Press, New Jersey, 1973.

Rumbarger, J. H., Filitti, E. G. and Gubernick, D., "Gas Turbine Engine Mainshaft Roller Bearing-System Analysis," *Journal of Lubrication Technology*, Trans. ASME, October, 1973, pp. 401-416.

Taylor, C. M., "Separation Cavitation in Lightly Loaded Fluid Film Bearing with Both Surfaces in Motion," *Journal of Mechanical Engineering Science*, Vol. 16, No. 3, 1974, pp. 147-155.

DISTRIBUTION LIST

	Copies
Commander, Naval Air Systems Command, Department of the Navy, Washington, DC 20361	14

Intra-Command Addressees

AIR-50174	(2)	AIR-52032	(1)
AIR-06	(1)	AIR-52031	(1)
AIR-536	(1)	AIR-330	(1)
AIR-5364	(1)	AIR-330A	(1)
AIR-5364C	(1)	AIR-310	(1)
AIR-53645	(1)	AIR-340E	(1)
		AIR-320A	(1)

Chief of Naval Material, (Code MAT 08T242 LCDR T. Hinton) Washington, DC 20360	1
Commander, Naval Air Development Center (Code 30212 — L. Stallings), Warminster, Pa. 18974	1
Commanding Officer, Naval Research Laboratory, (Code 6170 — H. Ravner), Department of the Navy, Washington, DC 20375	1
Chief of Naval Research, (Code 473 — R. S. Miller), Arlington, VA 22217	1
Commander, Naval Air Engineering Center, Naval Air Station Lakehurst, (Code 92724 — P. B. Senholzi), Lakehurst, N. J. 08733	1
Commanding Officer, Naval Air Rework Facility, Naval Air Station North Island (Code 341 — D. Stanley), San Diego, CA 92135	1
Superintendent, Naval Postgraduate School, Monterey, CA 93940	1
Commander, Naval Ship Engineering Center, (Code 6107 — D. C. Metcalf and G. F. Rester), Washington, DC 20362	2
Commander, David W. Taylor Naval Ship Research and Development Center, (Code 2832 — N. Glassman), Annapolis, MD 21402	1
Commander, Naval Weapons Support Center, (Code 70513 — J. A. Parkes), Crane, IN 47522	1
Commanding Officer, Naval Air Propulsion Center, P.O. Box 7176, Trenton, New Jersey 08628	
PE4	1
PE72	4
AD1	5
Defense Documentation Center for Scientific and Technical Information (DDC), Building No. 5, Cameron Station, Alexandria, Virginia 22314	12

DISTRIBUTION LIST (Continued)

	Copies
Commander, Robbins Air Force Base, (WRALC/MMIRDA — W. G. Webb) Robbins AFB, Georgia 31093	1
Commanding Officer, U. S. Army Aviation Systems Command, (Aircraft Power Plants Branch) (Code DRSAD-LEP, S. Chen), 12th and Spruce Sts., St. Louis, MO 63166	1
Director, Applied Technology Laboratory, U. S. Army Research and Technology Laboratories (AVRADCOM) (Code — DADL-E-TAP, D. Pauze), Ft. Eustis, VA 23604	1
Director, U.S. Army Ballistics Research Laboratories, (Code AMXBR-VL/W. Thompson), Aberdeen Proving Ground, MD 21005	1
Director, U. S. Army Air Mobility R&D Lab-Lewis, (Code MS-77-5 E. Bailey), 2100 Brookpark Rd., Cleveland, Ohio 44135	1
Commanding General, Corpus Christi Army Depot, (Code DRSAV-FESI H. Bull), Mail Stop 29, Corpus Christi, TX 78419	1
Commander, U. S. Army Aviation Systems Command, (Code DRSAD-LEP Stewart Chen), Box 209 Main Office, St. Louis, MO 63166	1
AFSC Liaison Office, NASA-Lewis Research Center, 21000 Bookpark Rd., MS-501-3, Cleveland, Ohio 44149	1
Administrator, NASA-Lewis Research Center, 21000 Brookpark Rd., Cleveland, Ohio 44135 (Attn Messrs R. Sliney, L. P. Ludwig and E. Zaretsky)	3
Ampex Corporation, Advanced Technology Division, Attn: Dr. W. A. Gross, MS 3-08 401 Broadway, Redwood City, Calif. 94063	1
Avco-Lycoming Division, Attn: Peter Lynwander, 550 S. Main Street, Stratford, Conn. 06497	1
The Barden Corporation, Attn: Harold R. Berglund, Dept. 76, 200 Park Ave., Danbury, Conn. 06810	1
Battelle's Columbus Labs, Engineering Systems Department, Attn: Mr. C. M. Allen, 505 King Ave., Columbus, Ohio 43201	1
Bell Aerospace Company, Technical Library, Attn: Mrs. Eunice P. Hazelton, P.O. Box 1, Buffalo, New York 14240	1
The Bendix Corporation, Research Laboratories, Attn: Dr. W. M. Spurgeon, 20008 Civic Center Dr., Southfield, Michigan 48076	1
The Boeing Company, Aerospace Group, Attn: Mr. Jan W. Vanwyk 205540, Box 3999, Seattle, Washington 98124	1

DISTRIBUTION LIST (Continued)

	Copies
The Boeing Company, Vertol Division, Attn: A. Lenski, Boeing Center, P.O. Box 16858, Philadelphia, Pa. 19142	1
Borg-Warner Corporation, Research Center, Attn: Research Library, Wolf and Algonquin Rds., Des Plaines, Ill. 60018	1
Catholic University of America, Attn: Prof. T. Litovitz, Department of Physics, Vitreous State Laboratory, Washington, D.C. 20017	1
CBS Laboratories, Attn: R. J. Roper, 227 High Ridge Rd., Stamford, Conn. 06905	1
Chevron Research Company, Attn: Mr. Neal W. Furby, P.O. Box 1627, Richmond, California 94804	1
Coordinating Research Council, Attn: Mr. N. K. McLeod, 30 Rockefeller Plaza, New York, N.Y. 10020	1
Curtiss-Wright Corporation, Wood-Ridge Facility, 1 Passaic Street, Woodridge, N.J. 07075	1
Detroit Diesel Allison, Div. of General Motors, Attn: Library (W. H. Richardson), P.O. Box 894, Indianapolis, Ind. 46206	1
Eastman Kodak Company, Engineering B-23 Attn: Mr. J. W. John, Kodak Park, Rochester, New York 14650	1
The Fafnir Bearing Co., Attn: H. B. Vandorn, New Britain, Conn. 06050	1
Fairchild Industries, Inc., Fairchild Republic Div., Attn: Henry W. Kleindienst, Conklin St., Farmingdale, New York 11735	1
Ford Motor Company, Scientific Research Labs, Attn: Mrs. L. B. Phillips, P.O. Box 2053, Dearborn, Michigan 48121	1
The Franklin Institute Research Labs, Attn: Mr. John Rumbarger, 20th and The Parkway, Philadelphia, Pa. 19006	1
The Garrett Corp., AiResearch Manufacturing Div., Attn: Peter Kamstra, 402 S. 36th Street, Phoenix, Arizona 85034	1
General Dynamics, Convair Aerospace Division, Attn: U. J. Swenney, CH Librarian, P.O. Box 80986, San Diego, Calif. 92112	1
General Dynamics, Convair Aerospace Div. Attn: Technical Library, P.O. Box 748, Fort Worth, Texas 76101	1
General Electric Co., Aircraft Engine Group, Attn: Mr. D. Hester, MS M87, Evendale, Ohio 45215	1

DISTRIBUTION LIST (Continued)

	Copies
General Electric Co., Aircraft Engine Group, Attn: Mr. John Clark, MS H62, Evendale, Ohio 45215	1
General Electric Co., Corporate Research and Development, Attn: G. R. Fox, Bldg. 37, RM 365, P.O. Box 43, Schenectady, New York 12301	1
General Motors Corporation, Research Laboratories, Attn: Mr. Fred Rounds, 12 Mile and Mound Rds., Warren, Michigan 48090	1
Georgia Institute of Technology, Attn: Mr. W. O. Winer, Department of Mechanical Engineering, Atlanta, Georgia 30332	1
Robert P. Grey Counsulting Engrs., Inc., Attn: M. R. Chasman, Vice President, 200 Grey Creek Drive, Athens, GA 30601	1
Hughes Aircraft Company, Attn: B. W. Campbell, Bldg. 6 MS E110, Centinela and Teale Street, Culver City, California 90034	1
IIT Research Institute, Attn: Document Library, 10 West 35th Street, Chicago, Ill. 60616	1
Industrial Tectonics, Inc., Bearings Division, Attn: H. Signer, Chief Engineer, 18301 S. Santa Fe, Compton, California 90224	1
International Harvester Company, Solar Division, Attn: Mr. P. A. Pitt, 2200 Pacific Highway, San Diego, California 92112	1
Jet Propulsion Laboratory, California Institute of Technology, Attn: Library Oper. Gr. (ACQUIS) 4800 Oak Grove Drive, Pasadena, Calif. 91103	1
Kaman Aerospace Corporation, Attn: R. B. Bossler, Old Windsor Road, Bloomfield, Conn. 06002	1
LTV Aerospace Corporation, Vought Aeronautics Co., Attn: Thomas P. McGinty, P.O. Box 5907, Dallas, TX 75222	1
LTV Missile and Space Division, Technical Information Center, Attn: T. M. Rozelle, MS B2, P.O. Box 909, Warren, Michigan 48090	1
Marlin-Rockwell Div. TRW, Attn: Mr. Arthur S. Irwin, 402 Chandler Street, Jamestown, N.Y. 14701	1
The Marquardt Corporation, Attn: Al Malek, MS 3-D8M 16555 Saticoy Street, Van Nuys, California 91409	1
Massachusetts Institute of Technology, Mechanical Engineering Department, Attn: Prof. B. G. Rightmire, 77 Massachusetts Ave., Cambridge, Mass. 02139	1
McDonnell Aircraft Co., Attn: Mr. J. M. Sinnett, MS 331, P.O. Box 516, St. Louis, MO 63166	1

DISTRIBUTION LIST (Continued)

	Copies
Mechanical Technology Inc., Attn: Leo Winn, 968 Albany-Shaker Rd., Latham, New York 12110	1
Midwest Research Institute, Attn: Mr. Vern Hopkins, 425 Volker Blvd., Kansas City, MO 64110	1
Miniature Precision Bearings, Inc., Product Engineering Attn: C. G. Beecher, Dept. 511, Keene, New Hampshire 03431	1
Monsanto Company, Attn: Richard Green, 800 North Lindberg Boulevard, St. Louis, Missouri 63166	1
MSA Research Corporation, Attn: J. W. Mausteller, Evana City, Pa. 16033	1
Northrup Corporation, Aircraft Division, Attn: Library — H. W. Jones, 3901 West Broadway, Hawthorne, Calif. 90250	1
North American Rockwell, Rocketdyne Division, Attn: Robert Spies, 6633 Canoga Ave., Canoga Park, Calif. 91303	1
North American Rockwell Corp., Attn: B. E. White, D/41-096 AJ01, 12214 Lakewood Blvd., Downey, Calif. 90241	1
North Carolina State University, Attn: Mr. N. W. Conner, P.O. Box 5356, 208 Daniels Hall, Raleigh, North Carolina 27607	1
Oak Ridge National Laboratory, Union Carbide Corporation Attn: A. G. Grindell, P.O. Box Y, Oak Ridge, Tenn. 37830	1
PPG Industries, Inc., Tribology Lab., Engineering Div., Attn: Mr. H. R. Gorman, P.O. Box 11472, Pittsburgh, Pa. 15238	1
Pratt & Whitney Aircraft, Attn: Library (L. T. Kress), 400 Main Street, E. Hartford, Conn. 06108	1
Rochester Institute of Technology, Department of Mechanical Engineering, Attn: Dr. Neville Rieger, Gleason Professor, Rochester, N.Y. 14623	1
Rensselaer Polytechnic Institute, Attn: Mr. F. F. Ling, Department of Mechanics, Troy, New York 12181	1
Rex Chainbelt, Inc., Bearing Division, Attn: W. G. Looft, P.O. Box F, Downers Grove, Ill. 60515	1
Rocketdyne Division, North American Rockwell, Attn: L. J. Rainey — Head Librarian, 6633 Canoga Ave., Canoga Park, California 91304	1
Rose-Hulman Institute of Technology, Attn: John J. Coy, Terre Haute, Indiana 47803	1

DISTRIBUTION LIST (Continued)

	Copies
Shaker Research Corp., Attn: J. M. McGrew, Northway 10 Executive Park, Ballston Lake, N.Y. 12019	1
SKF Industries, Inc., Attn: L. Sibley, Engineering and Research Center, 1100 First Ave., King of Prussia, Pa. 19406	1
Southwest Research Institute, Attn: Mr. P. M. Ku, 8500 Culebra Rd., San Antonio, Texas 78284	1
Sperry Rand Corporation, Vickers Division, Attn: Mr. Sam Jamieson, Engineering Library, Troy, Michigan 48084	1
Sundstrand Aviation, Attn: R. Allen, Dept. 759, 4747 Harrison Ave., Rockford, Ill. 61101	1
TRW, Inc., Engineering Library, Attn: Elizabeth Barrett, 23555 Euclid Ave., Cleveland, Ohio 44117	1
Technological Institute, Attn: H. S. Cheng, Department of Mechanical Engineering, 2145 Sheridan Rd., Evanston, Ill. 60201	1
Teledyne CAE, Attn: G. Hamburg, 1330 Laskey Rd., Toledo, Ohio 43697	1
The Timken Company, Physical Laboratories, Attn: Pete Orvis, 1835 Dueber Ave., S. W., Canton, Ohio 44706	1
Union Carbide Corporation, Attn: Tech. Librarian, P.O. Box 24166, 1500 Polco Street, Indianapolis, Ind. 46224	1
United Aircraft Corporation, Hamilton Standard Division, Attn: Library, Windsor Locks, Conn. 06069	1
University of Virginia, Department of Mechanical Engineering Attn: Dr. E. J. Gunter, Jr., Charlottesville, VA 22903	1
Westinghouse Electric Corp., R&D Laboratories, Attn: Research Library, Beulah Rd., Churchill Borough, Pittsburgh, PA 15235	1
Westinghouse Electric Corp., Aerospace Electrical Div., P.O. Box 989, Attn: A. E. King, Lima, Ohio 45802	1
Westinghouse R&D Center, Attn: Mr. D. J. Boes, Bldg. 501, Rm 3Y68, Beulah Rd., Churchill Boro, Pittsburgh, Pa. 15235	1
Williams Research Corporation, Attn: Lydia Johnstone (Librarian) 2280 West Maple Rd., Walled Lake, Michigan 48088	1

DISTRIBUTION LIST (Continued)

		Copies
Commanding General, Wright-Patterson Air Force Base, Dayton, Ohio 45433		
Code	AFAL/TSR	1
	AFAPL/CCN	1
	AFAPL/DOE (STINFO)	15
	AFAPL/DOY (Richard Motasney)	1
	AFAPL/POP-1 (Mr. B. L. McFadden, Jr.)	1
	AFAPL/POD-2 (Mr. K. E. Binns)	1
	AFAPL/SFL	35
	AFAPL/XP	1
	AFML/LAE/J. J. Sullivan	1
	AFML/LNE W. Johnson	1
	AFML/MBT R. Benzing	1
	AFML/MBT Maj. L. L. Fehrenbacher	1
	ASD/ENHEA Mr. Ray Bishop	1
	ASD/ENJZ Mr. Jim Barrett	1
	2750th ABW/SSL	1
	FTD/PDTA-4	1
AF Rocket Propulsion Lab., Attn: L. Tepe/LKDS, Edwards Air Force Base, CA 93523		1
HQ AFSC/INA Andrews Air Force Base, Washington, D.C. 20334		1
AFSC/DLF, Andrews Air Force Base Washington, D.C. 20334		1
HQ U. S. Air Force, RDPS/Mr. A. Eaffy, Washington, D.C. 20330		1
Chemical Propulsion Information Agency, The Johns Hopkins University, Attn: Dr. Peter L. Nichols, 8621 Georgia Ave., Silver Spring, MD 20910		1
Defense Supply Agency, Office of Technical Services, Dr. John A. Krynitsky, Director, Cameron Station, Alexandria, VA 22314		1
Department of Transportation, Library Service Div., FOB-10A, TAD-494/6, 800 Independence Ave., S. W. Washington, D.C. 20591		1
FAA HQ, GAO-1, H. Rochen, 800 Independence Ave., S. W. Washington, D.C. 20591		1
U. S. Atomic Energy Commission, Division of Reactor Development and Technology, Attn: Nicholas Grossman, F-309, Washington, D.C. 20545		1